DYNAMIC LOAD ENERGY DISSIPATION OF 3 STOREY REINFORCED CONCRETE BUILDING WITH INVERTED V-BRACED DAMPERS

CHEW WAI MENG

A project report submitted in partial fulfilment of the requirements for the award of Bachelor of Engineering (Honours) Civil Engineering

Lee Kong Chian Faculty of Engineering and Science
Universiti Tunku Abdul Rahman

April 2021

DECLARATION

I hereby declare that this project report is based on my original work except for citations and quotations which have been duly acknowledged. I also declare that it has not been previously and concurrently submitted for any other degree or award at UTAR or other institutions.

Signature : 

Name : Chew Wai Meng

ID No. : 1603488

Date : 5 May 2021

APPROVAL FOR SUBMISSION

I certify that this project report entitled **"DYNAMIC LOAD ENERGY DISSIPATION OF 3 STOREY REINFORCED CONCRETE BULDING WITH INVERTED V-BRACED DAMPERS"** was prepared by **CHEW WAI MENG** has met the required standard for submission in partial fulfilment of the requirements for the award of Bachelor of Engineering (Honours) Civil Engineering at Universiti Tunku Abdul Rahman.

Approved by,

Signature : 

Supervisor : Ts. Dr. Yip Chun Chieh

Date : 6.5.2021

ACKNOWLEDGEMENTS

I would like to thank everyone who had contributed to the successful completion of this project. I would like to express my gratitude to my research supervisor, Ts. Dr. Yip Chun Chieh for his invaluable advice, guidance and his enormous patience throughout the time of the research.

In addition, I would also like to express my gratitude to my loving parents and friends who had helped and given me encouragement, support and love during the time of research.

Lastly, I would like to thank my group mate for their assistance and guidance during the construction of reinforced concrete building and thank to lab officer for the support to undergo experiment test safely.

ABSTRACT

Earthquake is a natural disaster that leads to uncountable life sacrificed and people are losing their family and houses in the blink of eye. The earthquake event that happens in East Malaysia had brought the attention of the people especially seismic and structural engineer. However, most of the existing reinforced concrete buildings in Malaysia does not include the structure earthquake resistance design. Therefore, this research is focusing on the seismic energy dissipation of low-rise reinforced concrete building with and without inverted V-braced dampers under various dynamic loadings and important for the development of construction industry in future. A 1 bay 1 frame 3 storey reinforced concrete model is constructed with a scale factor 1:8. The scaled model with and without inverted V-braced dampers are analysed through the shaking table test under eleven different sets of peak ground acceleration. The results and discussion show the spectral acceleration at each floor increases as the PGA increases and roof floor has the highest spectral acceleration. Besides, maximum inter-storey drift happens at first storey indicates first storey is more vulnerable to earthquake. The seismic energy dissipation by the model with inverted V-braced damper at later stage is the highest with an increment of 5.34 kNmm and 5.60 kNmm as compared to bare frame. The output of the structural damage reliability analysis of reinforced concrete shows no damage to model under PGA of 0.1 g and 0.16 g; minor damage to model under PGA of 0.2 g, 0.3 g and 0.4 g; extensive damage to model under PGA of 0.5 g, 0.6 g, 0.7 g, 0.8 g and 0.9 g; model collapse under PGA 1.0 g. In conclusion, the novelty of this research is the inverted V-braced damper improved the seismic dissipation energy through reducing the base shear and lateral displacement from the building.

TABLE OF CONTENTS

LIST OF TABLES

LIST OF FIGURES

LIST OF SYMBOLS / ABBREVIATIONS

F	force, N
K,	stiffness, N/m
M	mass, kg
N	random sample
N_f	simulation number
P_f	failure possibility
R	load-carrying capacity
R(t)	reliability index
S	applied loading
x	displacement, mm
α	scale parameter
β	slope parameter
Δ_i	inter-storey displacement, mm
Δ_{roof}	roof displacement, mm
Φ	mode shape

C&S	civil & structure
CP	Collapse Prevention
EC8	Eurocode 8
FEMA	Federal Emergency Management Agency
IDR	inter-storey drift ratio
IO	Immediate Occupancy
LS	Life Safety
LVDT	linear variable differential transformers
L-waves	Love waves
MDOF	multiple degree of freedom
MRF	moment resisting frame
OPC	Ordinary Portland Cement
PGA	peak ground acceleration
P-waves	Primary waves
RC	reinforced concrete
R-waves	Rayliegh waves

SDOF	single degree of freedom
SSD	saturated surface dry
S-waves	Secondary waves

LIST OF APPENDICES

CHAPTER 1

INTRODUCTION

1.1 General Introduction

Earthquake is a terrible natural disaster that arises from the past causing countless life is sacrificed, damages of property and economy to deteriorate in a country. For examples, San Francisco in 1906, Tokyo in 1923, Alaska in 1964, Iran in 1968, Mexico in 1985, Kobe in 1995 and Turkey in 1998. In May of 2008, an 8.0 magnitude of earthquake strike to the Sichuan Province in China silently that lead almost 5 million of people turn into homeless and 87,000 of people raise to the skies that astonish the people all around the world. (Sen, 2009). The occurring of earthquakes is due to the seismic wave as strain energy that radiates from the epicentre towards the Earth's surface induce a sudden displacement across a fracture within the Earth. The ground motion whereas ground shaking is the dominant cause to the collapse of the building structure. (National Research Council, 2003).

For a building to sustain itself without collapse over the design period, the building is required to overcome a wide array of static and dynamic loading. Dynamic loading which means load reacts carrying with the time. The structural engineer needs to consider dynamic loading towards the structure of building. One of the dynamic loads contribute the critical impact to the building structure is the load from nature such as winds, waves and earthquake. The structure will experience an acceleration motion due to the dynamic load of earthquake due to ground motion at the base (Anderson and Naiem, 2012).

As an earthquake is a type of dynamic loads, the load can be resolved into 3 direction usually taken as the lateral and longitudinal direction. However, the superstructure of the building does not make much response to the vertical load from earthquake, but the horizontal load does as the building is weaker in resisting horizontal forces. There are some of structural failures when response to the earthquake motion. For example, the ground motion is causing the reservoirs or dam failure lead to floods due to additional lateral force other than water is pressured on the wall. Besides, pile or raft foundation will be failed and

damaged due to liquefaction of soil or huge ground displacement leads to the collapse of the building structure (Sen, 2009). Apart from that, shear force will generally raise at the column and beam joint due to the lateral force from earthquake. This creates damages and failure on the column and beam of the reinforced concrete building (Yön, Sain and Onat, 2017).

Inevitably, earthquake will occur anytime. The building is design to its maximum limit to withstand the tremendous vibration and motion of earthquake with some permanent deformation of the building structure. The hysteretic behaviour of the material is the causes of structure deformation during the dissipation of energy from an earthquake. Then, an energy damping device is developed since 1970s and introduced to dissipate the earthquake-induced energy in the new and existing buildings. The devices are to lower the inelastic yielding of the material during earthquake load-receiving. Before the structural drift to the limit, the energy dissipation must be accomplished. There are some other dampers available nowadays such as hysteretic dampers, viscous damper and mass-effect dampers (Sen, 2009).

1.2 Importance of the Study

The outcome of this research will exhibit the behaviour of the low-rise reinforced concrete building during the earthquake experimental test. This study also shows how important an inverted V-braced member and dampers to be placed in the existing or newly built reinforced concrete structure to resist the dynamic load and dissipate the energy from earthquake. This study will show the young engineer to understand the importance of seismic resistance in the reinforced concrete structure in order to prepare and protect our homeland for future unforeseen circumstance.

1.3 Problem Statement

Malaysia is a country that stays in the comfort zone all-time without experience any earthquake because the country located within relatively stable Sunderland plate which can be categorised as a low-seismicity country. However, Sabah which located at the East of Malaysia is categorised under a moderate seismicity group (Sarruddin and Nazri, 2015). This had led the Malaysian in trembling nowadays due to most of the building design in Malaysia without the use of Eurocode 8 which is the earthquake resistance in structure design. This might cause the building tends to be failed and collapsed when an abrupt hit of a seismic wave to the homeland. Reinforced concrete is a type of materials that being widely used in Malaysia's building structure as it is economical and durable. Hence, an understanding of new or future reinforced concrete building effect towards the seismic wave from earthquake is important in order to keep our beloved safe. A low-rise reinforced concrete building model is significant to be constructed like most of the research nowadays tend to focus on low-rise building which allows this research to compare and improve the after-effect of low-rise building structure towards the seismic wave impact.

In Malaysia, most of the structural engineers when designing the building structure are using the assumption of applied load. Structural engineers are considering the dead and live load inside the building but without considering the seismic action. Therefore, dynamic load which act as earthquake loading applied to the building structure during the experiment test by shaking table is required to study the structural performance.

As mentioned earlier, most of the low rise and governmental building in Malaysia does not possess an earthquake-resistant device for structure. Besides, some of the building are built with soft storey configuration, especially at the ground floor level. Soft storey tends to be used in Malaysia for commercial purpose. Ground soft storey drift may become a major problem during an earthquake event. Therefore, the research study by installing the inverted V-braced damper is vital to determine their effectiveness towards the dynamic characteristic of building structure.

1.4 Aim and Objectives

This research aims to construct and analyse the reinforced concrete structure with and without inverted V-braced damping device under dynamic loads. The objectives are as follow:

1. To construct a 1 bay 1 frame 3 storey reinforced concrete structure in laboratory.

2. To apply suitable levels of dynamic loads for the structure with and without inverted V-bracing dampers.

3. To assess structural reliability based on the structural behaviour, spectral accelerations and seismic energy dissipation curve for both with and without inverted V-braced dampers structure.

1.5 Scope and Limitation of the Study

The scope of the study includes the experimental test by the shaking table to stimulate the earthquake ground movement on the model. The study includes the construction of 1:8 scale downsizes of 1 bay 1 frame 3 storey reinforced concrete building model based on the design drawing and proper design concrete mix. This study also applies different levels of dynamic loading in shaking table test to obtain the behaviour of the scaled model through mode shape and obtain the spectral acceleration and displacement in each floor of the model. Two experimental tests will be undergone which is the model with and without the inverted V-braced damper to obtain the seismic energy dissipation. Structural reliability analysis also performs to identify the structural performance level.

The limitation of the study is implementing a one-dimensional earthquake simulation on the shaking table towards the model due to the lack of advanced earthquake simulation equipment to stimulate three-dimensional earthquake.

1.6 Contribution of the Study

The outcome of the study shows the behaviour of low-rise reinforced concrete building with and without inverted V-braced damper under various ground acceleration of earthquake. The findings are important to the existing or newly-built low-rise building in Malaysia to cope with the increasing number of earthquake event recently. The results of the research can serve to improve the seismic performance of low-rise RC building in earthquake event and to minimize the failure or damage in reinforce concrete building by installing seismic energy dissipation device such as inverted V-braced damper.

1.7 Outline of the Report

Chapter 1 Introduction discusses the general introduction, the importance of the study, the problem statement, the aim and objective and the scope and limitation of study and contribution of the study.

Chapter 2 Literature Review discusses the formation of earthquake and seismic issue all around the world. The characteristic of reinforced concrete under seismic loads such as ductility, damages and seismic structural performance are discussed. The characteristic of dynamic load and earthquake load are discussed. Besides, building response towards seismic is also discussed in this chapter. Moreover, the earthquake resistance structures and damper are discussed to differentiate their function in term on earthquake resistance design. Lastly, Chapter 2 end with the result analysis discussion by various researchers.

Chapter 3 Methodology describes the workflow of the study. The procedure of the workflow includes an overview of building detailing, construction of model, installation of damping devices, experimental test with eleven different sets of peak ground acceleration (PGA) and analysis of results .

Chapter 4 Results and Discussion discussed and compare the spectral acceleration, inter-storey drift, seismic energy dissipation and structural damage reliability of the model with and without inverted V-braced dampers under eleven different sets of PGA. This chapter also presents the experiment results in data, table and figure for discussion and comparison.

Chapter 5 Conclusion and Recommendation conclude the research with the related result and recommendation for future work.

CHAPTER 2

LITERATURE REVIEW

2.1 Introduction

This chapter reviews the seismic activity and the effect on the building structure all around the world. The discussion of earthquake characteristic and formation is important before understanding the consequence and prevention of earthquake. Besides, reinforced concrete is the construction material that commonly used in the Malaysia building because of economic. Reinforced concrete structure is vulnerable to the earthquake when a higher earthquake load exceeds its capacity lead to damages and collapse. Apart from that, earthquake load is a dynamic load in which the load varies with the time. The characteristic of earthquake loads such as amplitude, frequency and period will affect various responses in the building. The type of responses in structure will be discussed for understanding the building behaviour. As Malaysia is classified as the low seismic activity group, most of the building fails to install a proper earthquake-resistance system. This chapter will highlight the various earthquake-resistance structure and system in modern day to suits the existing and future building in Malaysia.

2.2 Issue About Seismic Around the World

Earthquake is a destructive natural disaster in the world. There is uncountable life sacrificed and people lose their homeland after a huge earthquake impact in their city. The situation of a country can be deteriorated such as economic recession, depopulation and infrastructure demolition.

Table 2.1: Largest Earthquake Magnitude in the World (USGS, 2020).

Year	Earthquake	Magnitude
1960	Valdivia Earthquake	9.5
1964	1964 Great Alaska Earthquake	9.2
2004	Sumatra-Andaman Islands Earthquake	9.1
2011	Tohoku Earthquake	9.1
1952	Kamchatka, Russia	9
2010	Maule Earthquake	8.8
1906	Ecuador-Colombia Earthquake	8.8
1965	Rat Island Earthquake	8.7
1950	Assam, Tibet	8.6
2005	Nias Earthquake	8.6

Table 2.1 shows the history of the largest earthquake magnitude in the world. Valdivia Earthquake happened at Bio-Bio, Chile. According to Bichell in 2016, the earthquake experienced by Sergio Barrientos that stay in Valdivia, Chile is intensive. This leads to him unable to stand about 10 minutes during the ground shaking by earthquake. This is the most powerful earthquake ever recorded. The country stretched itself about 30 feet from the coast towards the west. This event causes about 2 million of people to become homeless and about 1 655 people deaths through this earthquake. Besides, the earthquake from Chile also triggered numerous of further destruction to other countries. Hawaii faces a tsunami after twelve hours of ground shaking in Chile. Therefore, earthquake has brought up the attention to the researcher as the Earth can vibrate itself like a guitar string. The vibration caused by seismic waves able to travel to every part of the Earth. At that point, research started to agree with earthquake is caused by the collision of the plate and folding into each other

Earthquake will create many disasters not merely on ground shaking effects. (Daniell, Schaefer and Wenzel, 2017) had mentioned that secondary effects of earthquake event are vital for understanding and investigating. The summary of primary, secondary and tertiary effects shows in Table 2.2.

Table 2.2: Primary, Secondary, Tertiary Effects of Earthquakes. (Daniell, Schaefer And Wenzel, 2017).

Type of effect	Name	Key elements
Primary effects	Ground shaking	Source effects, Path effects, Site effects
Secondary effects	Tsunami	Wave height, size of fault rupture and proximity to coastline
	Landslide	Geological map, soil typologies
	Liquefaction	Sand or soil type, water table location
	Ground level changes	Ground loading
	Fire	Flammability Index
	Surface breaks	hypocenter depth, lateral spreading
	Floods, dam breaking	shaking location to the water bodies
Tertiary effects	Economical	economic status
	Environmental	environmental susceptibility of the region
	Epidemics	Susceptibility of population and climate

(Daniell, Schaefer and Wenzel, 2017) defined primary effect of earthquake is the ground shaking effects by the energy release from earthquake due to the surface rupture along the fault. Landslide, tsunamic wave, liquefaction, ground rupture, fire, epidemic diseases and others are the secondary effects or later effects caused by the direct ground shaking from earthquake as shown in Table 2.2. For an example, the intensity of tsunami is affected by the height of seismic wave, fault rupture size below ground and proximity to coastline. Besides, they also mentioned tertiary effects such as earthquake cause tsunami waves that destroy nuclear power plant, then nuclear disaster occurs. The destruction of power plant will cause economic downturn, global environmental deterioration and depopulation. The cascading effect can be used to define the effects of secondary and tertiary effect.

(Daniell, Schaefer and Wenzel, 2017) article shows the secondary effects of earthquakes are greatly pertinent to the history for the damages and losses. Their study shows that shaking effects cause 60% to 75% of economic fatalities and deaths where secondary effects have taken up 25% to 40% globally.

Therefore, secondary effects caused by the earthquake has brought significant effects conformity with primary ground shake effects such as building damages, economic losses and deaths.

2.2.1 Seismic Activity

The impact of earthquake has caused catastrophic damages to the planet. Therefore, it is important to understand what earthquake is and how earthquake often happens around the Earth. (Rajasekaran, 2009) stated earthquake is produced by the waves emitting from a source of disturbance inside the Earth that vibrate the Earth's surface. Energy released in the Earth's crust will cause the abrupt movement of the Earth's surface. He also stated the only dependable source about the interior of the Earth is generated by seismic waves. However, Earth composes of the different layer that makes seismic waves travel at various velocity.

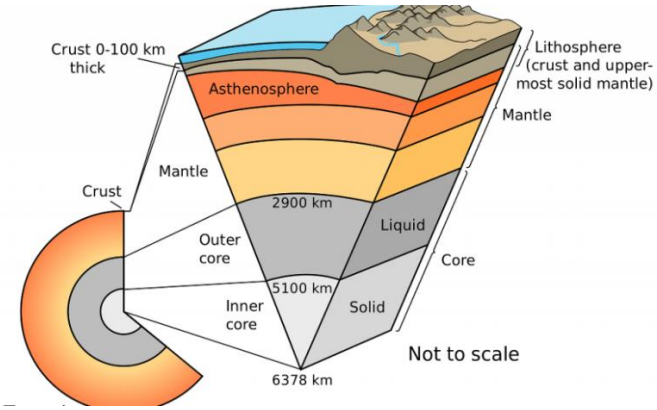

Figure 2.1: Section of Earth (Wahab, 2020).

Figure 2.1 shows the section of Earth which consist of main three layers such as core, mantle and crust. The different composition and thickness of layer caused the seismic waves to travel at a different velocity. *Lithosphere* is the layer composed of crust and upper mantle. The lithosphere is made up of mainland plates consist of land mass and oceanic plates that under water. When the lithosphere moved aerially with the asthenosphere layer, this known as tectonic plates movement. The crust and the core is having a popular high temperature and pressure gradient that formed convection in the viscous mantle.

The convective flow will slide the crust and mantle in the hot molten outer core. Therefore, the sliding is said to be tectonic plates (Rajasekaran, 2009).

(Rajasekaran, 2009) mentioned that there are seven major and smalls tectonic plates on the surface of the Earth. (British Geological Survey, 2020) stated various kind of tectonic plates interaction around the boundaries would produce different types of seismic activity. The boundaries between the tectonic plates are constituted from a *fault* system. Faults can be defined as the crustal rocks bed slip relative to each other. Each kind of boundary interaction will be associated with one fault system such as normal, reverse and strike-slip fault. First, the plates that move away from each other at the boundary is known as *divergent boundary*. Normal faulting will be the dominant faults at this boundary interaction as shown in Figure 2.2a. This is due to the hot magma from the mantle that makes the plates move apart. The earthquake produced at this boundary tends to be small and associated with volcanic activity. Then, *convergent boundary* is the boundary in which the plates move towards each other to create reverse faulting as shown inFigure 2.2b. The best scenario to describe this case is the continental collision. The collision forced rocks upward and created a mountain in nature. This fault tends to produce an earthquake magnitude that bigger than 6.0. Next, the plates slide across each other in the opposite direction at boundary can be categorised *as transform boundary* with strike-slip faulting as shown in Figure 2.2c. Large and shallow-focus earthquake tends to be produced during this plate interaction. Despite there are various type of tectonic plates interaction at the boundary, the tectonic plate's movement tends to be small in which few centimetres per year (British Geological Survey, 2020).

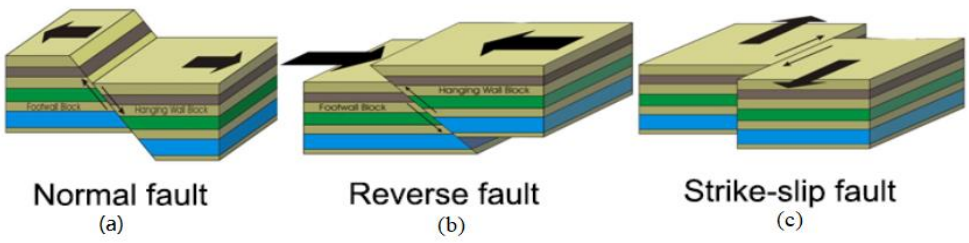

Figure 2.2: (a) Normal Fault (b) Reverse Fault (c) Strike-slip Fault (GeologyPage, 2017).

The tectonic plate's movement at boundary will cause the formation of tectonic force to the crust and produce straining in crustal rocks. Strain is accumulated at the rocks with the slowly sliding of tectonic plates. The rock will continue to accommodate the stress until exceeding its capacity. When the stress is exceeded, crust will break and the shape of Earth returned to its unstrained position. This scenario can be defined as 'elastic rebound theory'. A huge energy will be released from the break of rocks that produce seismic wave travel to the Earth's crust which cause vibration. This vibration is said to be an earthquake (Rajasekaran, 2009).

2.2.2 Seismic Activity in Malaysia

Natural disasters include forests fire, floods, tsunamic, cyclonic storms, landslide, haze and seismic activity. As Malaysia is located outside the Pacific Rim of Fire, the country is fairly encountering the effects and devastation triggered by natural disasters. (Center For Excellence in Disaster Management & Humanitarian Assistance, 2020).

Table 2.3: Frequency of Disaster Hazards in Malaysia (Center For Excellence in Disaster Management & Humanitarian Assistance, 2020).

High	Medium	Low
Flood	Forest Fire	Earthquake
	Landslide	Tsunami
		Drought
		Storm
		Haze

Table 2.3 shows there is still possessing low frequency of Earthquake incident occurring in Malaysia. On 26 December in 2004, west coast of Malaysia such as Perlis, Penang and Kedah facing a severe Tsunami as a horrendous earthquake strike in Indian Ocean which near to the Indonesian of Sumatra. Despite there is no direct ground shaking effect on peninsular Malaysia, Malaysia is now categorised into an earthquake zone. However, no safety measures are being taken earnestly by Malaysia although there are numerous research and professional opinion of scholars have carried out

through many years. The lack of environmental alertness is also made it tough to encourage earthquake safety awareness (kukuplaut.com, 2018).

Apart from that, the greatest impact of earthquake in Malaysia history happened at Ranau, Sabah, Malaysia on 5 June 2015. A magnitude of 6.0 that last for 30 seconds had caused 18 deaths due to the rockfalls on Mount Kinabalu. This incident has attracted the attention of other country as there are 5 foreigner's deaths during this earthquake. Besides, the vertical and horizontal ground shaking movement have also caused structural damages to the infrastructure and private building such as school, hostel, hospital, bank, shops and houses. (Tongkul, 2016). Figure 2.3 shows the damages of structural building.

Figure 2.3: Building Collapse (left) (Center For Excellence in Disaster Management & Humanitarian Assistance, 2020) and Cracked Column at SMK Ranau Teacher's Flat (right) (Tongkul, 2016).

Figure 2.3 shows the private building collapse and column damages at the infrastructure may lead to a sudden collapse of that building structure. Fortunately, there are no injuries and deaths through the collapse of building. However, the broken down of infrastructure has affected the daily life of the community. As prevention is better than cure, local authorities must look into deep to formulate some guidelines and manual to develop the building structure in future especially in high-risk area. This action is to lower the damages experienced by building that might lead to collapse. The Ranau earthquake has cause a destructive impact on social, building, economic and natural environment.

(Yuen, 2017) mention that Malaysia's local authorities are working to prepare a Malaysia National Annex of Eurocode 8 (EC8) which applies for the low-seismic zone new building structure in Malaysia. The code is used to enhance the earthquake resistance in building structure rather than earthquake-proof. Despite the building in peninsula and Sarawak is safe based on the past 100 years record of earthquake, no one can forecast the arrival of earthquake in anytime. Therefore, other than new design earthquake-resistance building structure, most of the existing building in Malaysia should retrofit or renovate to meet the standards of the code.

2.3 Reinforced Concrete Structure Against Seismic

Reinforced concrete (RC) has been widely used in the construction industry. The combination of concrete and reinforcement steel bar give satisfactory in both compressive and tensile strength to resist the external force such as loading, wind, or earthquake. Building structure builds with reinforced concrete tends to possess a longer life of service. During an intensive of earthquake event, RC structure will receive the seismic or vibration energy from seismic wave. The RC structure has a satisfactory ductility in resisting earthquake as compare to other brittle building materials such as concrete and masonry. (FHWA,2010) state that the steel bar inside the concrete will yield and distort in tension under earthquake loading to prevent concrete cracking that leads to abrupt failure.

(Kappos, 2014) mentioned ductility of RC structure is the structure that has the ability in absorbing and dissipating the seismic energy through the hysteresis loops and the structure able to maintain its structural integrity without massive strength lessening. (Saatcioglu, 2013) study shows when the seismic force exceeds the force capacities in the structure (ultimate region), structure drifts and do not deform in the inelastic region where fracture of material inside structure take place. The seismic energy inside the structure will not be dissipated consequence leading to building failure. Figure 2.4 show lateral load–drift graph typical structure member and damages stage.

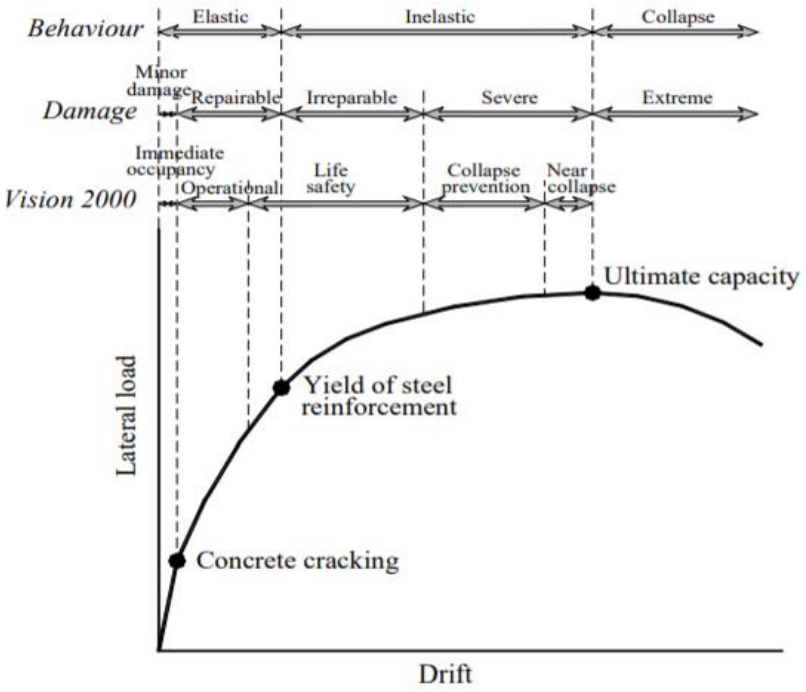

Figure 2.4: Lateral Load – Drift Graph for Structural Performance and Associated Damages States (Ghobarah, 2004).

2.3.1 Performance-Based of Reinforced Concrete Design in Seismic Structure

The objective of performance-based seismic is to forecast the recognizable terms of any building system with predicted ground shaking motion of earthquake that may afford on to the building site over its design life. The structural seismic performance possesses different level of performance in term of the damage that relatively associated with the earthquake hazard level (Matthew, 2000).

According to Saatcioglu in 2013, the structural need to be assessed on the accepted performance criteria founded by the Federal Emergency Management Agency (FEMA) of the USA such as FEMA 273 in 1997, FEMA 356 in 2000 and ASCE 41-06 in 2007. FEMA 273 had introduced four different levels of structural seismic performance levels which are Operational, Immediate Occupancy (IO), Life Safety (LS) and Collapse Prevention (CP) as shown in Figure 2.4. The structural seismic performance levels are used to assess the post-earthquake building for reoccupation or retrofitting. Besides, the level of performance helps to identify and quantify the damages in a structural system.

In operation level of performance, the structure has very light overall damage with some minor hairline crack. The structure component such as beams, columns, slabs and walls did not undergo permanent drift which strength and stiffness has remained. The reinforce concrete structural element still remains in their elastic zone. Building such as hospital, police and fire station can operate as usual during and after an earthquake event (Saatcioglu, 2013). Besides, negligible damage for non-structural component might occurs such as broken glass from window. The power supply and other utilities is still obtainable from the emergency power generators (FEMA 273, 1997).

In Immediate Occupancy (IO) performance level, the building is safe to be reoccupied. However, the earthquake resisting system for lateral force and gravity load functions as pre-earthquake design strength with light damage. Repairing work for minor structural can be undergoing while building is occupied (Saatcioglu, 2013). Besides, the structure did not undergo permanent drift and retains original strength and stiffness with some minor cracks. Lift and escalator are functioning but may be shut down due to the safety issue. The facilities are restarting once the earthquake event stop (FEMA 273, 1997).

Life Safety (LS) level indicates the structure have significant damage in the post-earthquake damage stage. The structure has some residual of margin safety against the partial or total structural collapse. Part of stiffness and strength is left in all stories. The gravity-load-carrying elements are functioning to serve its purpose. The structural elements such as beam are experiencing servery damage with hinge formation at joint. The structure experiences some permanent drift. Extensive crack is noticed at unreinforced masonry infill walls and masonry crushing is noticeable. The structure needs a structural evaluation and assessment to decide for repairing or reusing. However, the risk for threatening life is still low in this level of performance (Saatcioglu, 2013).

Collapse prevention (CP) level shows the building experience massive earthquake damage that come close to partial or total collapse. The strength and stiffness of structural element are deteriorating. Large permanent lateral drifts occur and limited function of vertical load-bearing elements (columns and walls). The structure is extensively damaged and at high risk for life-threatening (Saatcioglu, 2013).

2.3.2 Reinforced Concrete Structure Damages

RC structure will suffer structural damage and non-structural damage during the impact of earthquake. Column, beam, wall, slab and roof which is the main structural component to constitute a building structure received the damages during earthquake. The lack of strength in structure will cause critical damages with various type of stress. This might occur due to the inadequate of material strength and number of reinforcements inside the structure or at the connection of structure. Damages tend to form at the end of flexural members, connection of beam-column and shear deficient regions of the column. For instance, the lack of confinement reinforcement will cause the lateral expansion and buckle of column due to large moment induced at column ends by the lateral movement of earthquake shown in Figure 2.5a. Plastic hinge will form at the end of column due to the column is less ductile to resist lateral load and dissipate seismic energy. Plastic hinge will also form at the soft storey of the building. Furthermore, brittle shear failure will occur at the inclined shear plane of column as shown in Figure 2.5b. This is due to the lack of transverse reinforcement steel bar that causes weak in shear transfer mechanism. Short column shear distress will happen due to amplify of shear stress over a short span as shown in Figure 2.5c. (Saatcioglu, 2013).

(a) (b) (c)

Figure 2.5: (a) Column Buckle At End (b) Shear Failure (c) Short Column Failure (Saatcioglu, 2013).

Apart from that, shear failure tends to occur at the beam to column joint at RC frame. The lack of shear reinforcement tends to cause failure at the joint due to the flexural shear from beam and shear from column as shown in Figure 2.6a. Strong column weak beam concept is commonly used in designing seismic resistant structure. Figure 2.6b shows strong column-weak beam creates local failure (structure member failure) than global failure (structure failure). This concept helps to form flexural hinge at the beam to dissipate seismic energy. This will prevent column failure that leads to abrupt collapse of building (Saatcioglu, 2013).

(a) (b)

Figure 2.6: (a) Beam-Column Joint Failure and (b) Strong Beam-Weak Column Failure (Saatcioglu, 2013).

Besides, soft storey in building structure is one of the damage creators during an event of earthquake. Soft storey is an open space area in a storey that support by the column only (Figure 2.7a). (Ozturk and Ogutcu, 2018) study shows the soft storey tends to build at the ground floor level for commercial purpose. The height of the ground level is increased as compared to other storey levels for the construction of mezzanine floors. The infill wall such as bricks wall and shear wall are removed to create a bigger activity area. Thus, these factors had cause low rigidity at the ground floor to resist horizontal load by earthquake. During an earthquake event, the column at ground floor is drifted due to the lateral ground motion. This will cause the formation of plastic hinge at its both ends as shown in Figure 2.7b. Fracture will occur once inelastic deformation is exceeded. Column then will fail lead to building collapse at ground floor level.

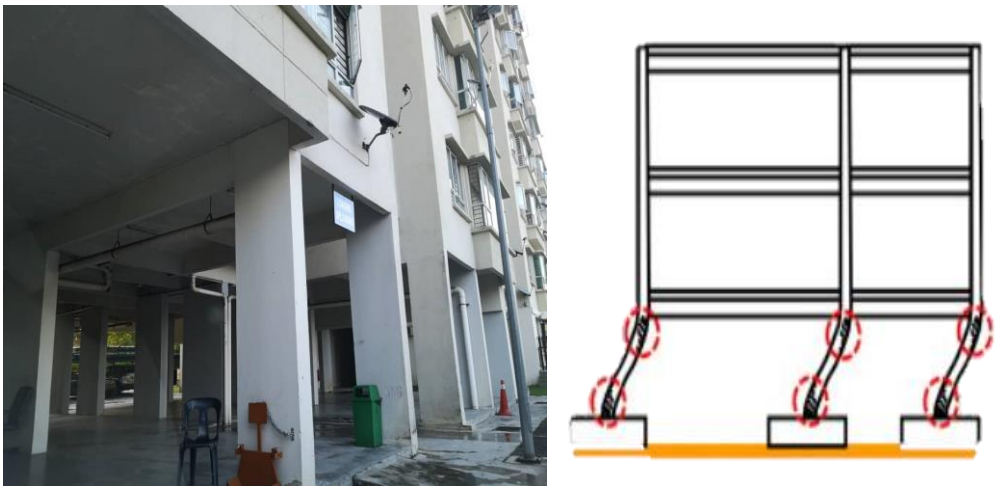

(a) (b)

Figure 2.7: (a) Ground Soft Storey at Alpha Villa Apartment, Malaysia and (b) Plastic Hinge Formed at Soft Storey's Columns (Gazetas, 2015).

2.3.3 High-Rise Building

According to Australian Bureau of Statistics in 2019, high-rise building consists of 9- 19 storey height. (Kappos, 2014) mentioned higher building will have low natural period. When an earthquake event occurs, the period of the building might be altered. The RC structure starts cracking and 'softening' due to the strong ground motion that increases the structure's period. This action will cause RC structure to reach the same period as ground motion or *resonance* lead to high vibration and collapse. In short, high-rise building tends to attract low frequency ground motion that will lead to building collapse.

Besides, the high-rise building is flexible due to the high number of storey. There is a combination of two translation mode shape that occurs at the high-rise building when ground motion moves at the base. Flexure mode shape tends to occur at the lower storey due to the axial deformation of column. Shear mode shape is happened at the higher storey due to lower axial load compression (Murty, et al., 2020). Tall building tends to have different mode of oscillation, but fundamental period or 1st mode will be important for seismic design purpose. The lateral and roof displacement is the highest as compare to low-rise and mid-rise building structure.

2.3.4 Mid-Rise Building

Mid-rise building is built with 4 to 8 storey height with concrete frame and use for apartment. The natural period is in between low-rise and high-rise building. (Arnold, 2006) mentioned the rule of thumb could be used to determine the building period by diving the storey number with 10. The natural period of building can be assumed in between 0.4 to 0.6 s.

Moreover, the translation mode of oscillation of medium-rise building is shear type which has the same design as low-rise building. Besides, the lateral deformation (drift) of building for mid-rise will be smaller as compared to high-rise building. Figure 2.8 illustrates lateral deformation profile for 5, 10, 15, 20 and 25 storey buildings.

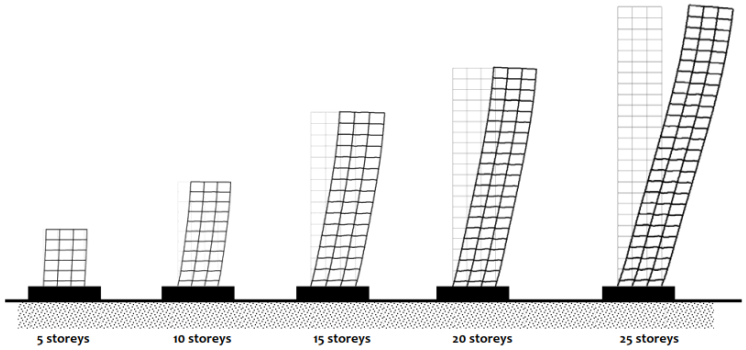

Figure 2.8: Lateral Deformation Profile or 5, 10, 15, 20 and 25 Storey Buildings (Murty, et al., 2020).

2.3.5 Low-Rise Building

Low-rise building is classified as 1 to 3 storey height (Australian Bureau of Statistics, 2019). Low-rise building structure tends to be built for shop lot or living unit. (Saatcioglu, 2013) mentioned that low-rise building tends to receive high frequency of ground motion. (Murty, et al., 2020) study shows low-rise building has a lower mass lead to structure stiffness increase. The natural period of the low-rise building will decrease with the attraction of high-frequency ground motion. Their study shows 5 storey building has 0.45 s of natural period as compare to 25 storey building have 3.14 s of natural period. The low natural period of low-rise building will lead to higher base shear formation at the ground of the building. Figure 2.9 illustrates natural period effects on the design horizontal seismic load.

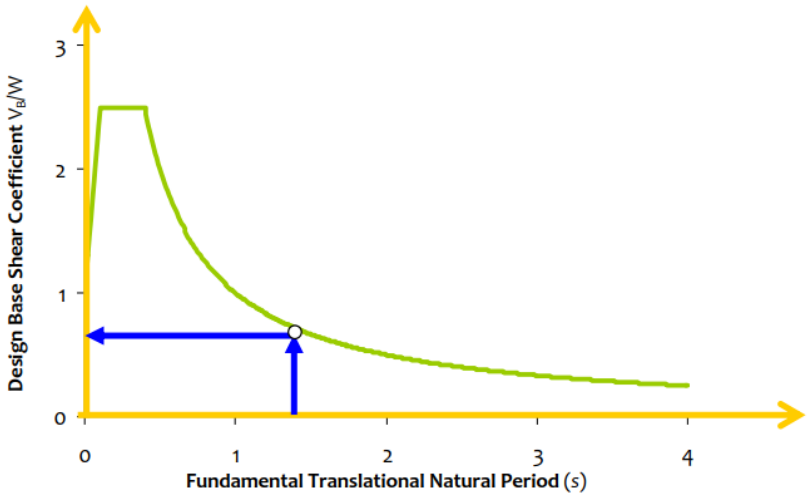

Figure 2.9: Natural Period effects on design horizontal seismic load (Murty, et al., 2020).

Besides, the idealized translation mode of oscillation in low-rise building is shear type. Both column and beam will bend in double curvature because of the finite ratio of beam to column flexural stiffness. It is not desired column flexural stiffness exceed the beam which forms flexural type. Besides, it is not desired increase of beam flexural stiffness which cause its strength over the column. Therefore, limit ratio of beam to column flexural stiffness is required as stated in the code (Murty, et al., 2020).

(Murty, et al., 2020) study shows the roof displacement or drift will decrease when the slenderness ratio is decreased. The 2 storeys building roof drift is 0.1% where 25 storeys building is 0.6%. This result concludes low-rise building will roof drifting is less as compare to mid-rise and high-rise building.

2.4 Dynamic Load

Dynamic loads are the time-dependent load also known as time-varying load. The load application and load removal are also varied with time. Dynamic loads can define as a load which fluctuate in magnitude, direction and position with respect to the time. Dynamic loads can be differentiated into periodic and non-periodic loadings. The load recur itself in an equal time interval throughout the motion is said to be periodic loading. For example, rotating mass is inducing a vibration is a type of periodic motion. Figure 2.10 shows the periodic loading in simple harmonic motion. In contrast, any load does not fall under period loading is referred as non-period loading. The vibration induced by the blast loading and seismic wave is non-periodic. Figure 2.10 illustrates the non-periodic graph of earthquake motion. (Rajasekaran, 2009).

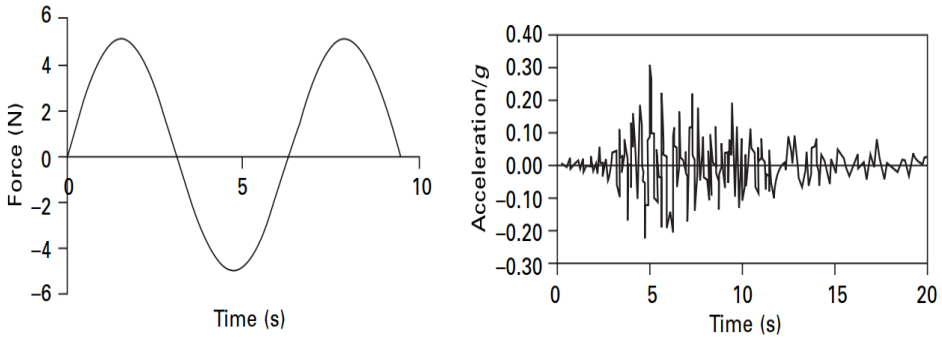

Figure 2.10: (a) Simple Harmonic Motion of Period Loading and (b) Non-Periodic Earthquake Motion (Rajasekaran, 2009).

(Hilti, 2020) stated dynamic action can generally be categorised into three groups such as fatigue loads, seismic loads and shock loads. Fatigue load is the load repeated cyclically and is frequently occurs during the service time of structure such as winds and traffic loads. Seismic loads also known as earthquake load is a type of dynamic load caused by the seismic wave propagation to the Earth crust then to the building. Shock loads are the special load happen in sometimes during the service time of the structure such as explosion which high impact loads over a short time. This study will mainly focus on the seismic or earthquake load impact on the building structures.

2.4.1 Seismic Wave

An earthquake event will occur when the tectonic plate faults that generate seismic wave propagate through the Earth's crust. (Rajasekaran, 2009) mentioned that *hypo-centre* or focus is the fault plane that generates the seismic waves. He also mentioned *epicentre* is the point perpendicular above the hypo-centre. The focus distance which will be the distance between focus and observed ground motion on the Earth's surface. The focal depth less than 60 km, earthquake is normal or shallow earthquake. Intermediate earthquake is focal depth in between 60 and 180 km. Deep focus earthquake occurs when focal depth 185 and 300 km.

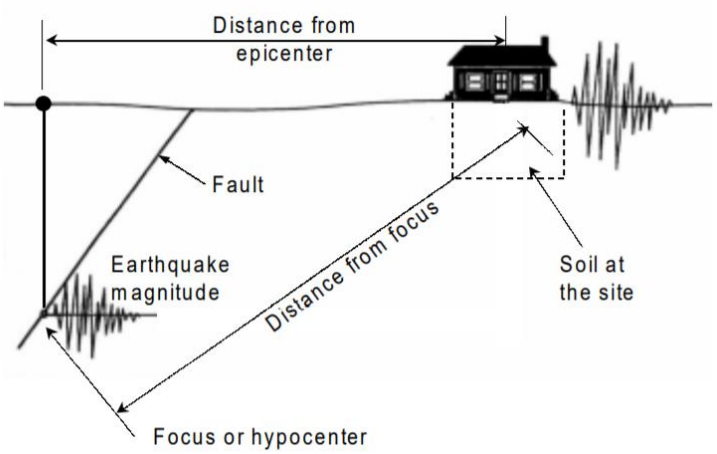

Figure 2.11: Location of Focus and Epicentre (ATC, 2020).

Figure 2.11 illustrates the source which is focus to the epicentre and surface ground motion. Seismic wave generates from focus will propagate to the Earth's surface in any direction that causes ground motion. If the focus distance is shorter, the seismic wave can reach the surface in a shorter time to cause greater ground motion.

There are two types of seismic waves that generated to cause ground shaking that can be felt. There are *body waves* and *surface waves.* Body waves consist of *Primary wave (P-wave)* and *Secondary wave (S-wave)* that propagate the rock body to reach the surface. P-waves motion act as a sound wave. The particles move in the direction of propagation by push (compresses) and pull (dilates) each other. The P-waves is less destructive than S-waves due to the lower amplitude. S-waves can be known as shear wave. Its motion travel in

perpendicular to the direction of propagation (vibration). Therefore, S-waves have both vertical and horizontal motion at the ground surface. S-waves is disadvantages moving in liquid as the amplitude will decrease. Besides, both waves are reflected into crust once they reach the ground surface, the surface will be affected by moving upward and downward instantaneously. This may cause amplification of ground motion to occur at the surface (Rajasekaran, 2009). In most cases, S-waves will late arrive than P-waves. S-waves arriving will cause the horizontal and vertical motion that cause ground shaking. Most of the structure is damaged due to the S-waves.

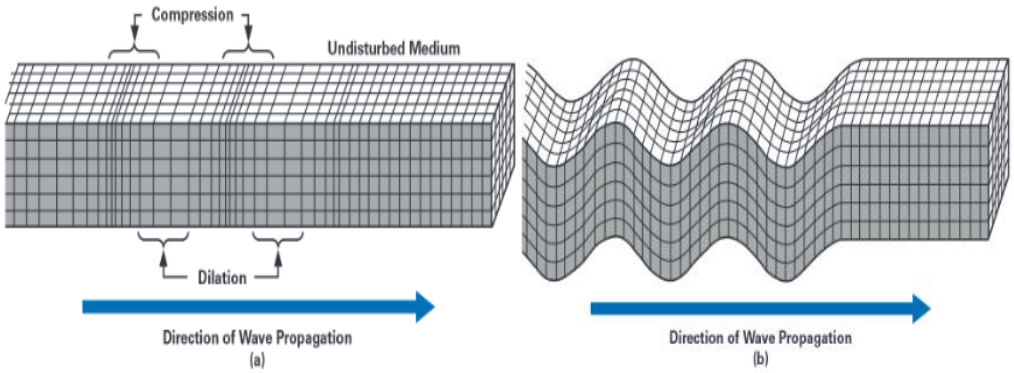

Figure 2.12: Movement of P-wave (left) and S-wave (right) (Santos, Catapang and Reyta, 2019).

Another type of seismic wave is the surface waves. Surface waves can be categorised into *Love waves (L-waves)* and *Rayliegh waves (R-waves)*. (Rajasekaran, 2009) mentioned this type of waves name surface wave due to their waves is constrained when near to the ground surface. L-waves has the same motion as S-waves which only move in horizontal displacement. L-waves move the side to side parallel to the Earth's surface but in right angle to the propagation direction. R-waves have the lateral and longitudinal movement in a vertical plane to the direction of propagation. Its motion tends to in elliptical and retrograde due to a combination of P and S waves. Both of this wave will result in the foundation and building structure in serious damage.

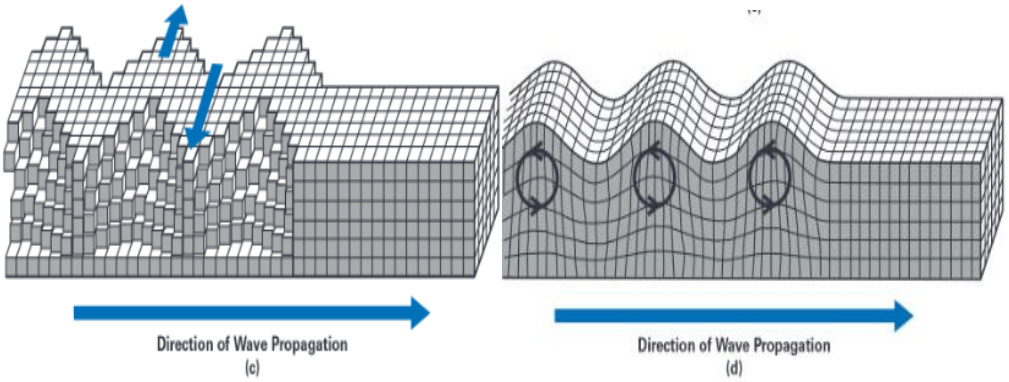

Figure 2.13: Movement of L-wave (left) and R-wave (right). (Santos, Catapang and Reyta, 2019).

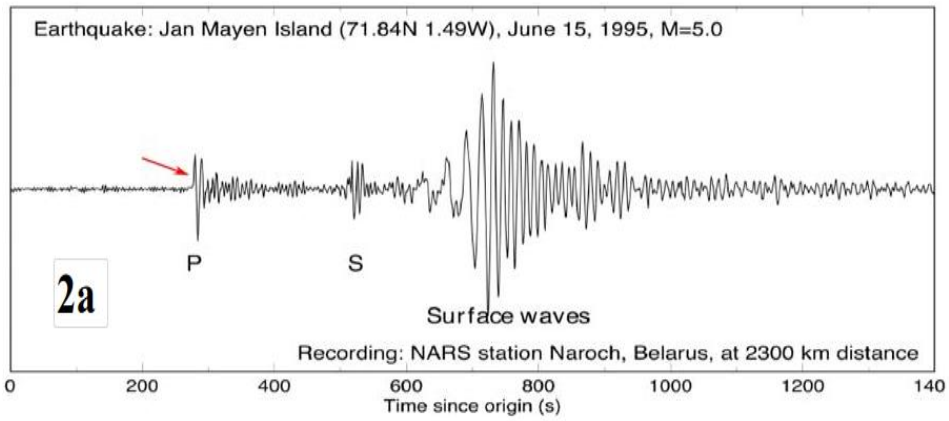

Figure 2.14: Seismograph of Different Waves (Kayal, 2020).

Figure 2.14 illustrates the seismograph of different waves when an earthquake event happened. It noticed S waves come after P waves which prove (Rajasekaran, 2009) statement is correct. People will feel the short vibration from P waves whenever an event of earthquake happened. Then, surface waves (L-waves and R-waves) will come after the body waves that make a huge ground motion impact. This is because surface waves have larger amplitude and smaller frequency as compared to body waves. This high amplitude and low frequency of the waves can cause a building structure to receive high earthquake load slow vibration.

2.4.2 Earthquake Load

Earthquake load is one type of dynamic loading. Earthquake load can be repeated itself but in an irregular manner or known as non-period motion. Earthquake loads have uncertainty characteristics such as amplitude, duration, period and frequency content. (Patil and Sonar, 2018). First, the amplitude is the measure of wave size. Amplitude can express in term of displacement, velocity and acceleration. Higher amplitude of incoming waves caused stronger ground motion. The duration of seismic wave can be said unknown. Another characteristic of cyclic load is the period. This is the measurement of one complete wave in a time interval. Frequency also tends to use to characterise seismic wave in earthquake which is the number of cycles in one second. Body waves give higher frequency that causes ground motion faster. Besides, the impacts of earthquakes can from any direction but earthquake loads are mainly striking in the horizontal direction. The earthquake loads are higher when faster and stronger ground shaking to the heavyweight building induces inertial load in building. (Szakats, 2006).

(Lin and Yoda, 2017) mentioned that seismic loading is the loads that a structure received from seismic oscillation. It occurs where seismic wave in contact to the surface of structure whether is adjacent structure or ground. The level of the earthquake loading is dependent on the seismic magnitude and intensity, geotechnical parameter at the site, and structure's natural frequency.

2.4.3 Earthquake towards building

The ground motion induced by the earthquake will create various forced that act on a building structure. The translation of ground motion to forces at the building will be the criteria for designing earthquake-resistance building structure. Building structure is affected by the lateral force from earthquake rather than vertical force due to the self-weight of the building tends to provide adequate resistance (ATC, 2020).

In the earthquake design for building, inertia force is induced in a building structure as the ground motion is shaking at the base of the structure. Figure 2.15 shows ground motion cause vibration within building. The inertia force will lead to stresses in the building which known as displacement-type loading. The ground motion recurs about the neutral position of the building structure. Therefore, the stress in the building will experience numerous complete counterturns during the small duration of earthquake. (Murty, et al., 2020).

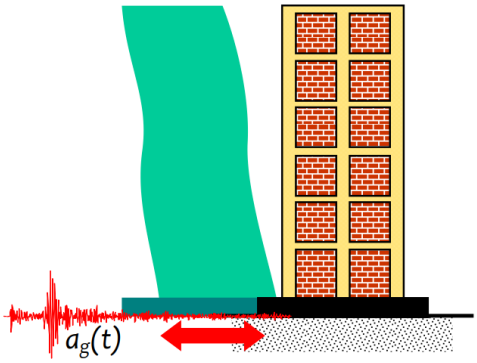

Figure 2.15: Ground Motion Cause Building Vibration (Murty, et al., 2020).

As earthquake is predominant in the lateral direction, it will create in-plane and out-of-plane forces on to the building. The horizontal forces of earthquake will divert into orthogonal component and act parallel to these directions on either regular or irregular shape buildings. The internal force which is inertia force of building produced during earthquake will be transfer along the orthogonal axes as well. Figure 2.16 shows the in-plane and out-of-plane forces from the earthquake (ACT, 2020). In-plane forces is the force act long one axis of building structure lead to wall or frames resist in parallel direction where force perpendicular to in-plane force is the out-of-plane force. Therefore, building design needs to resist both forces at the same time.

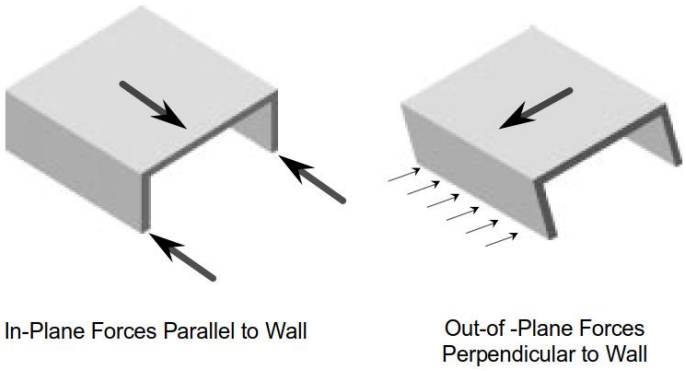

Figure 2.16: In-Plane Forces (Left) And Out-of-Plane Forces (right) (ACT, 2020).

2.5 Structure Response

When earthquake load across the building, the deformation of building can be known as structure response. (Patil and Sonar, 2018) mentioned earthquake load is a type of dynamic load that can constitute various mode of response in different building. The response of *single degree of freedom* (SDOF) and *multiple degree of freedom* (MDOF) structures tend to be observed during ground motion. Besides, (Miranda, 1996) explained displacement (drift) parameter is used to express the structure response in an earthquake event. (Ghobarah,2004) also mentioned the displacement is related to the ductility of the structure where its ability to deform. Inter-storey drift or peak roof drift is the common parameter to express the displacement of the building structure in different storey. Soft storey drift also tends to be investigated during soft storey formation. Figure 2.17 illustrates the roof displacement, Δ_{roof} and inter-storey displacement, Δ_i under earthquake ground motion.

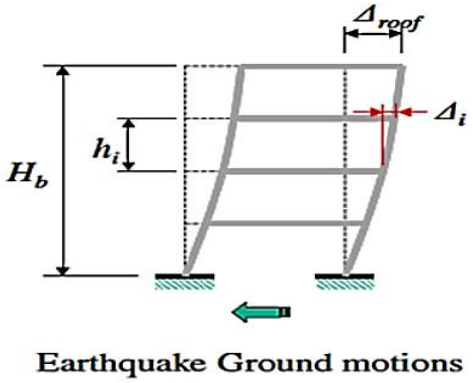

Figure 2.17: Roof Displacement and Inter-storey Displacement Under Earthquake Ground Motion (Jabeen, Mythili And Mohiuddin, 2014).

2.5.1 Soft Storey Drift

Soft storey drift represents the displacement or deflection of soft storey. As mention earlier, soft storey formation is due to the wide-open storey supported by column for commercial purpose, especially at ground level (open ground storey). This cause irregular vertical member at the structure (Miranda,1996). The irregularities cause the strength and stiffness at soft storey are decreased and drift at that floor level generally maximum throughout the building. (Ghobarah,2004) also mentioned the maximum inter-storey drift at soft storey indicates as the collapse of building structure.

2.5.2 Inter-Storey Drift

Inter-storey drift (local deformation) defined as the different lateral displacement or deflection of the top and bottom storey. The strength and stiffness of structural member are the significant characteristics for reducing inter-storey drift (Arnold, 2006). Besides, the inter-storey drift is associated with floor level damage. The maximum inter-storey drift undergoes the greatest deformation change and damage due to the lack of stiffness and discontinuity in structural member. Inter-storey drift can be controlled by earthquake resistance structure design to dissipate the seismic energy induced by earthquake. For instance, Moment Resisting Frame (MRF) designed in the structure provided a consistent inter-storey drift distribution along the height of building (Ghobarah,2004). Therefore, deflection movement is acceptable during earthquake without causing any failure of structural and non-structural component.

2.5.3 Roof Drift

Roof drift or global deformation is the roof displacement relative to the ground. (Ghobarah,2004) mentioned root drift is useful to determine the damage of structure and to represent the overall structure displacement under earthquake. The roof drift also can be represented by the response spectrum based on the SDOF. Generally, the maximum displacement occurs at the roof drift of building.

2.5.4 Single Degree of Freedom (SDOF)

In the structure of SDOF, the mass concentrate at a single point (usually at the top) and moves on one axis. The single mass is located above the cantilevered column of the building. For example, an elevated water tank with a concentrated mass located at the top of the structure. Figure 2.18 shows the elevated water tank and the model of SDOF.

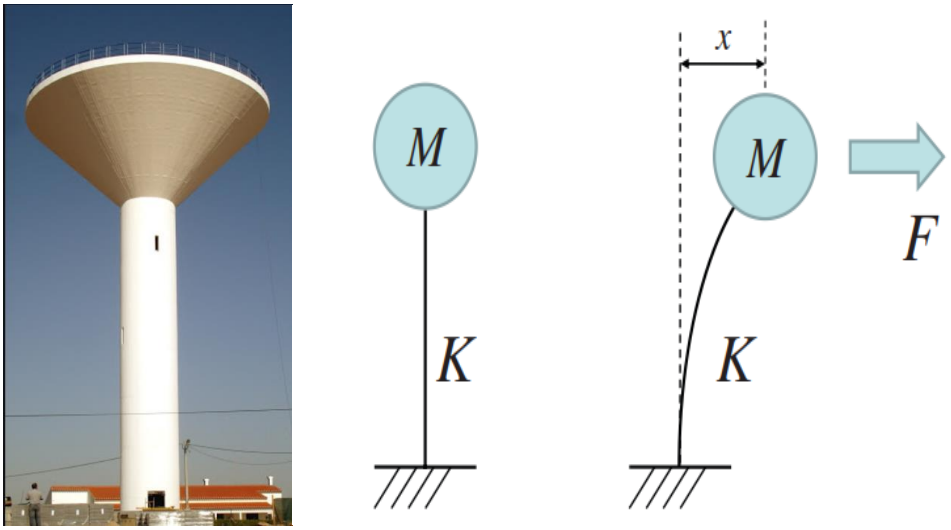

Figure 2.18: Elevated Water Tank with SDOF Model (Hamburger and Gumpertz, 2009).

As in Figure 2.18, when force, F applied to the mass, M, the column will displace horizontally with displacement, x. The K represents the stiffness of column to restrain its lateral movement. The applied force will cause shear force in the column and inertia in the mass through the structure. The shear force and inertia bring the vibration movement of the structure in back-and-forth in a single direction. Besides, single storey consists of 2 series of SODF model. This is due to the horizontal translation degree of freedom in 2 direction. The mass of roof or suspended ceiling can represent the concentrated load at the centre of the roof. (Hamburger and Gumpertz, 2009).

2.5.5 Multiple Degree of Freedom (MDOF)

Building has more than one storey is known as multiple degree of freedom structure. This kind of structure has the same degree of freedom as single storey building. However, the torsional degree of freedom may be neglected in multi-storey building if the stiffness and mass are coincident and align at the centre of each level. Stick model is used to represent the MDOF structure respond during ground motion of earthquake. Figure 2.19 shows the MDOF of 3 storey building in different mode shape.

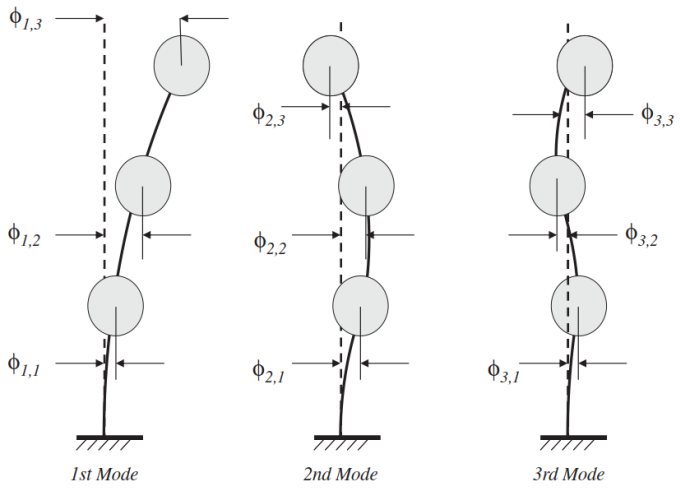

Figure 2.19: MDOF of 3 Storey Building in Different Mode Shape (Hamburger And Gumpertz, 2009).

As shown in Figure 2.19, each degree of freedom consists of one natural mode of vibration through MDOF structure. Each different mode will possess a natural period and a deform shape (mode shape), Φ. $\Phi_{i,j}$ =where i is the mode shape number and j is the degree of freedom. The 1st mode has the longest period or known as the fundamental natural period (Hamburger and Gumpertz, 2009). As the natural period is highest, the structure offers higher motion as compare to other mode shapes.

2.6 Earthquake Resistance Structure

Earthquake resistance structure is the structure that has the ability and capacity to withstand the lateral load from earthquake. There are some of the systems such as building configuration, frame, wall and bracing to resist earthquake load by dissipating the seismic energy induced from earthquake.

2.6.1 Building Configuration

According to Lorant in 2012, building configuration defined as the design shape of building in structural and non-structural element to deal with the seismic load of various magnitude. The building configuration will affect the seismic load distribution within the building. Figure 2.20 shows the example of regular and irregular building configuration.

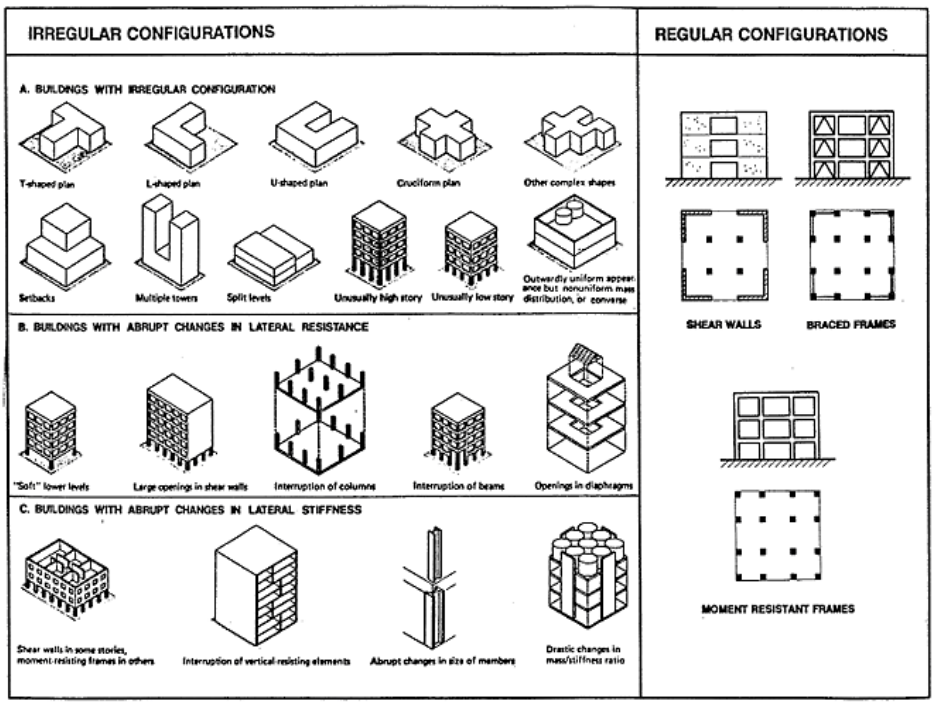

Figure 2.20: Examples of Irregular and Regular Building Configuration (Lorant, 2012).

Regular building configuration tends to have symmetrical plans, identical floor height, continuous load path and more. Shear wall, Moment-Resisting Frame or braced system will be the examples for the regular building configuration. Irregular building configuration tends to cause concentration of stress and torsional effect within the building. This is due to the discontinuity of strength and stiffness of the members (Lorant,2012). For examples, irregular plan of the building, open ground storey and discontinuous of vertical member. Regular building configuration commonly used in the design of earthquake-resistance structure.

2.6.2 Moment Resisting Frame

Moment Resisting Frame in Figure 2.21 composed of a grid of two members which are columns and beams. The beam connects rigidly to the column provide a good lateral stiffness and strength to the moment resisting frame. The frame provides resistance to seismic overturning moment through axial forces, bending moment and shear force generated from columns and beams. The ductility behaviour of beam and column under reinforced concrete design provides a good resistance to the seismic force. During the design stage of moment resisting frame, brittle shear failure must be taken into consideration. The building with moment resisting frame has a good seismic resistance due to the predominant flexural behaviour of columns and beam. The structural configuration of building tends to design with relatively long frame members, short beam and short columns. The design will attract huge forces and able to fail in a brittle manner (Murty, et al., 2020). According to Dhande, Suryawanshi and Patil in 2015, moment resisting frame is less stiff than other earthquake-resistance system. However, moment resisting frame is economically suits for low-rose building.

2.6.3 Shear Wall System

Structural wall or shear wall provides a strong lateral stiffness of building to reduce overall building displacement. Building with moment resisting frame only may offer large swinging during low intensity of earthquake. Therefore, structural wall tends to build with the moment resisting frame to lower down the large lateral displacement of the building. Figure 2.21 shows the frame-wall system. The shear wall resists the horizontal force through combined axial-flexure-shear action. The shear wall may reduce the moment and shear demand on the vertical and horizontal member of moment frames. The shear wall should construct continuous along the height of building to obtain the efficient earthquake resistance design (Murty, et al., 2020). Besides, the shear wall is designed parallel to the lateral load direction such as wind or earthquake. However, the construction of shear wall required longer time in low and mid-rise building. Shear wall also weak ductility which does not suit severe earthquake (Dhande, Suryawanshi and Patil, 2015).

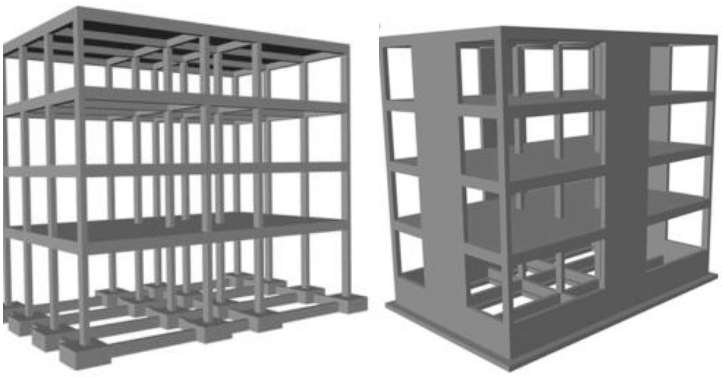

Figure 2.21: Moment Resisting Frame (Left) and Frame-Wall System (Right)(Fardis,2021).

2.6.4 Bracing

Bracing is another type of earthquake-resistance system provided in the entire structure. Brace commonly made by steel is performing well in earthquake resistance structure due to the ductility of steel is high. Building with braces able to dissipate seismic energy without damage the structure. Bracing is easy and cost-effective to be replaced after an earthquake event (Dhande, Suryawanshi and Patil, 2015). Figure 2.22 show different type of bracing install in the

moment resisting frame building. In general, the braces are provided for the entire height of the building. Braces help irregular building configuration with unsymmetrical stiffness in plan to avoid twisting effect. Braces need to be installed in both plan directions. The function of installing braces is to reduce overall structure drift of building and reduce shear and bending moment demand in both vertical and horizontal member of building. The seismic force that strikes to the building will be transferred into axial compressive and tensile force through the braces in the building. Chevron, K-bracing and X- are the common bracing that uses in the mid-rise building (Murty, et al., 2020). In some situation, dampers are connected to bracing to dissipate the seismic energy more efficiently.

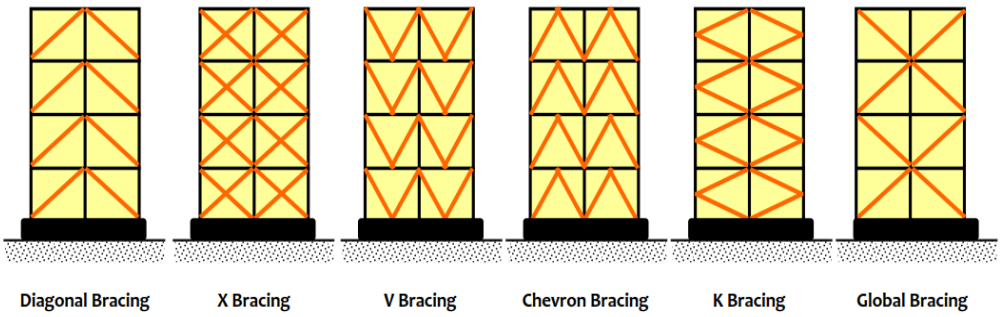

Figure 2.22: Types of Bracing in Buildings (Murty, et al., 2020).

2.7 Damper

Damper is a type of seismic protective devices that protect the structure during an extensive of earthquake event. The devices will absorb or dissipate the induced seismic energy from shaking motion of earthquake (Agrawal and Amjadian, 2016). Besides, the damping and flexibility characteristic of damper installed in the building helps to control the seismic response. Damper installed in building can be damped alone or connect to the braces (Dhande, Suryawanshi and Patil, 2015). The common seismic component devices used in the structure are base isolation (elastomeric and sliding isolators) and dampers (friction damper, fluid viscous damper, viscous-elastic damper and yielding damper). The seismic component devices change the dynamic behaviour (natural period, damping or energy dissipation behaviour) of the structure to provide safety and stability.

2.7.1 Base Isolation

Base isolation helps to reduce seismic force and displacement demands in a building. Base isolation is installed at the base of a building to prevent the ground motion transfer from foundation to the superstructure as shown in Figure 2.23. The building with base isolation will almost remain as rigid body with deformation happen at the isolator during earthquake. Base isolation system is recommended to the structure with rigid body and non-ductile characteristic (Saaticioglu, 2013).

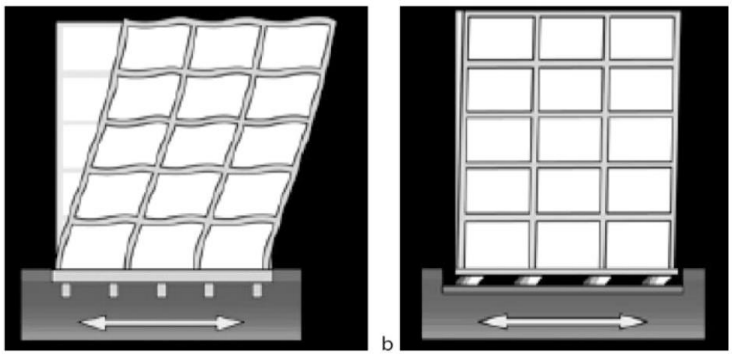

Figure 2.23 Schematic View of Base Isolation in A Building (Saaticioglu, 2013).

Base isolators can generally differentiate into two categories which are elastomeric and sliding isolators. *Elastomeric isolators* possess a laminated rubber bearing to support the structure vertical load and earthquake lateral load simultaneously in a flexible manner. Elastomeric isolators tend to equip with passive damper or energy dissipation capabilities to isolate ground motion on superstructure in excessive displacement. Figure 2.24 (a) and (b) shows the low and high damping rubber bearings for base isolation. A damper is installed in between two steel plate to provide a satisfactory level of damping. Figure 2.24 (c) illustrate lead rubber bearings. Lead rubber bearings have one or few lead core insert at the centre of rubber. The lead plug will dissipate the seismic energy from earthquake through yielding. The movement of steel plate will yield the lead plug through pushing during an earthquake event. Figure 2.24 (d) exhibits the *sliding isolators*. The sliding isolator possesses a concave surface to provide horizontal flexibility. Concave surfaces provide a slippage between support and sliding surface. The friction motion in slipping will dissipate seismic energy through damping effect. Sliding isolator has a strong stiffness that proficient to

carry large vertical load in the range of large horizontal displacement. (Agrawal and Amjadian, 2016).

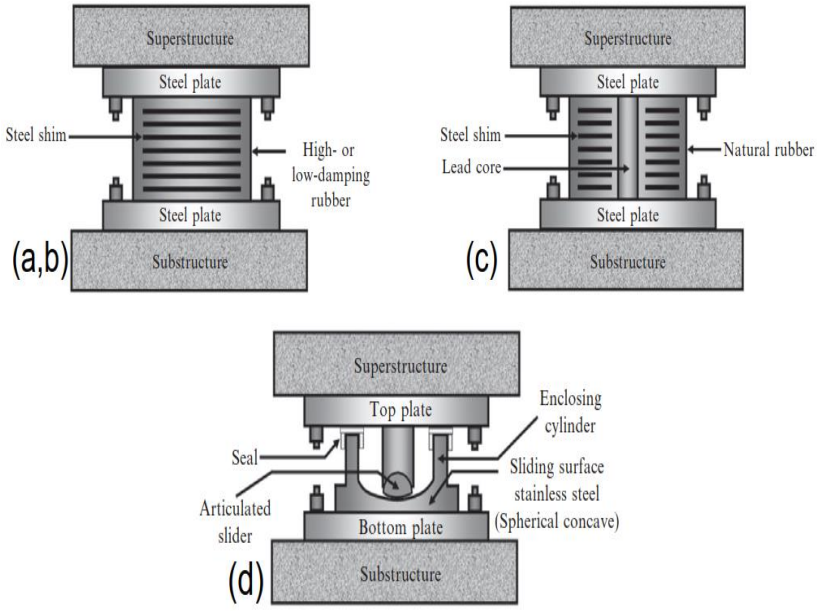

Figure 2.24: Base Isolation (Agrawal and Amjadian, 2016).

2.7.2 Fluid Viscous Damper

Fluid viscous damper dissipates the seismic energy through the moving piston in the cylinder. As compare to other dampers such as viscoelastic damper and friction damper, fluid viscous damper using viscous fluid flowing through the orifices inside the damper to dissipate energy. The type of viscous fluid is silicon oil and oil is compressible. The fluid viscous damper possesses a stainless-steel piston, compressible oil, steel cylinder with two chambers split by a piston and an accumulator for fluid circulate smoothly. The working principle of fluid viscous damper to dissipate seismic energy is the fluid movement from one chamber to the other chamber through orifice. The fluid will be compressed from a larger area into a small area of orifice. The movement of fluid will cause head loss in the damper due to the disperse of energy. Figure 2.25 illustrates a fluid viscous damper (Agrawal and Amjadian, 2016).

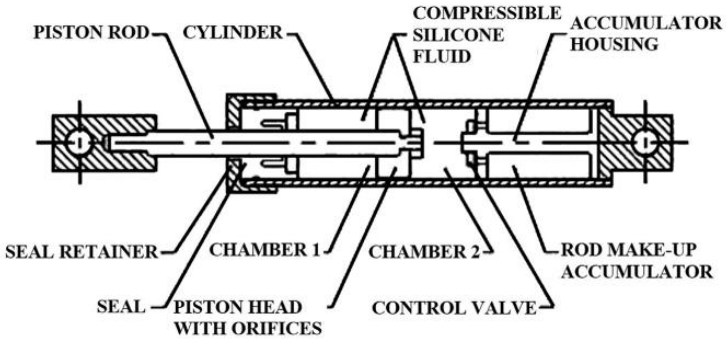

Figure 2.25: Fluid Viscous Damper (Agrawal and Amjadian, 2016).

Besides, fluid viscous damper often connects with braces in a structure. The damper built with braces increase damping effect in a building, contribute higher strength and stiffness of structure, decrease lateral deformation and reduce damages of structural and non-structural component during seismic event (Saaticioglu, 2013). The efficiency of damper will depend on the brace damper arrangement and type of damper-brace system. Different fluid viscous damper arrangement will also provide various protection for the building from seismic events. Figure 2.26 show the fluid viscous damper installed with different type of bracing such as diagonal, chevron, scissor and toggle.

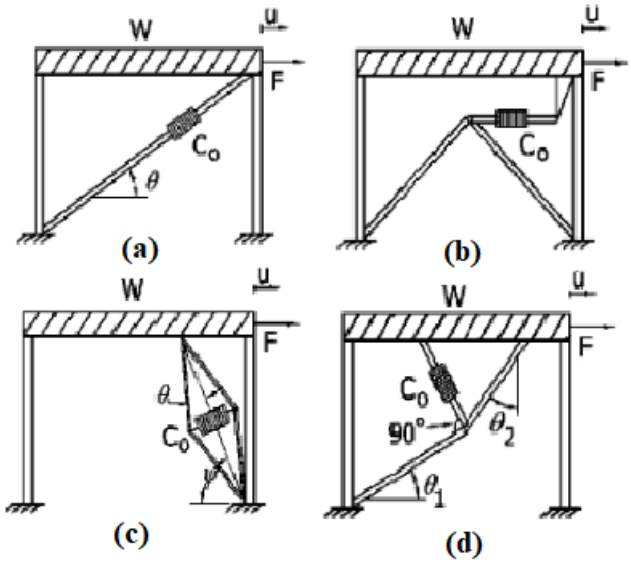

Figure 2.26: Different Type of Brace Damper System: (a) Diagonal; (b) Chevron; (c) Scissor; (d) Toggle (Sigaher and Constantinou, 2003).

Chevron bracing installed with damper suits the needs of an opening size such as windows and doors. Chevron provides more spacing for the architectural elements (Dhande, Suryawanshi and Patil, 2015). Next, toggle brace damper is the original design that dissipates seismic energy with damping. The installation process is easy and toggle design always installed at the corner. of a frame (Damptech, 2015). Scissor-jack-damper system is the latest among the four braces damper system shown in Figure 2.25. However, diagonal and chevron brace damper is favourable by the people installed in a structure contemporarily.

2.8 Results Analysis

Peak ground acceleration and seismic response of the building such as spectral acceleration, displacement, seismic energy dissipation need to be analysed during or post-earthquake event.

2.8.1 Peak Ground Acceleration (PGA)

Ground motion induced by the earthquake must be recorded for the use of earthquake engineering. A strong-motion accelerograph tends to place at different location to capture the strong ground motion of earthquake. The recorded acceleration of earthquake possesses two lateral components and one vertical component. The two lateral components are equal magnitude where the vertical component is slightly smaller. On the other hand, peak ground acceleration (PGA) is the maximum ground acceleration that happened during earthquake and equal to the amplitude of the largest acceleration recorded in the accelerogram. PGA is useful in scaling earthquake design spectra and acceleration time forces. Figure 2.27 illustrates the accelerogram of Northridge earthquakes. The PGA of the Northridge earthquake shown in Figure 2.27 is 0.30g after 5 seconds of commencement of ground motion (Rajasekaran, 2009).

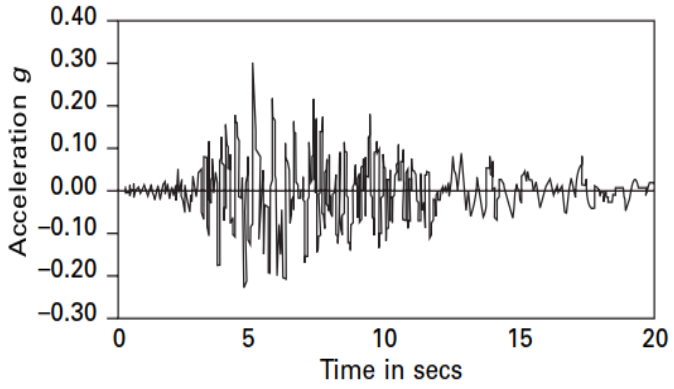

Figure 2.27: Accelerogram of Northridge Earthquakes (Rajasekaran, 2009).

2.8.2 Spectral Acceleration

Spectral acceleration is the acceleration that experienced by a building which differs from PGA where acceleration experienced by particle on the ground. Spectral acceleration is a response spectrum that reflects the response of building during different intensity of earthquake. Figure 2.28 shows response spectrum graph of the maximum acceleration response value. The graph shows responded maximum acceleration located at the period of about 0.3 seconds which is the mid-rise building. Shorter period building (low-rise building) will have greater acceleration but lesser horizontal displacements. Spectral acceleration is useful to determine the resonant frequencies at which structure will experience peak acceleration (Arnold, 2006).

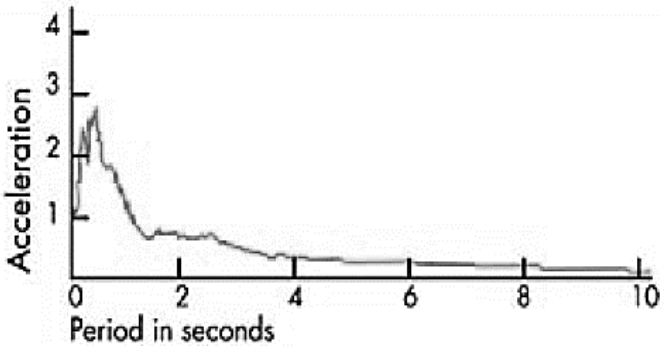

Figure 2.28: Response Spectrum of Spectral Acceleration (Arnold, 2006).

Besides, the distributing base shear is attributed to the spectral acceleration at each floor of the building. Base shear is the horizontal earthquake forces applied to a building that can be calculated by the equation $F = ma$. It relates to the Force (F) with the building mass (m) and horizontal acceleration (a). A portion of total base shear is applied as the horizontal force at each floor level and at the roof level when designing multi-storey building. The horizontal force at each floor is based on both tributary mass at that floor and the height of the level above the base of the building. This result in the seismic base shear distribution over the building height is larger at the roof level than bottom level. Moreover, additional horizontal load on the roof level of tall and flexible building due to the extra stresses from "whisplash" effect at roof level (ACT, 2020).

2.8.3 Displacement

According to (ACT, 2020), drift is the total amount of horizontal displacement occurs at the building or floor level. Drift will cause the building into deformed shape due to the stress formed in structural elements and non-structural elements. Maximum drift tends to happen at the roof level of the building but each storey is subjected to drift known as storey drift. Besides, Uniform Building Codes (UBS) in 1997 mentioned the spectral acceleration and drift will elevate towards the top of the building. Roof level should resist seismic forces four times greater than on ground floor.

Zhou el al. (2018) performed a shaking table test for tall, multitower reinforced concrete buildings with large bottom podiums. The maximum floor displacement is obtained through the highest value of the time history data. The displacement in time history data is the relative displacements between storey and shaking table. Besides, maximum storey drift is obtained through the subtraction of time history data between adjacent floors. Model A has lower maximum displacement than model B under minor, moderate and major earthquake in both X and Y directions. The different of maximum displacement between model A and model B is due to the large podium level of model A that provides higher stiffness and strong restraining effect at the bottom of structure.

(Adiyanto and Majid, 2014) performed the seismic design of two storey reinforced concrete building in Malaysia with low class ductility. The inter-storey drift ratio (IDR) of the building increase as the intensity of PGA value increase. Besides, the IDR at the same PGA value of seismic design building is lesser than those non-seismic frame building.

2.8.4 Seismic Energy Dissipation

(Ozturk and Ogutcu, 2018) study the different types of steel diagonals on the soft storey irregularities RC frames. In this study, a one bay one frame storey building with ground soft storey was tested under simulation earthquake with reverse cyclic loading. The soft storey then strengthening by brick infill walls, central X-braced and inverted V-braced for simulation. The results of the study mainly show the seismic energy dissipation by each type of building configuration. The study shows dissipated energy is calculated by areas under hysteresis curves in each cycle with the test results data. Figure 2.29 depicts the seismic energy dissipation of each specimen. The results show brick infill wall building (EXP1-F) consume 54% more energy than soft storey building (EXP2-SS) at the last cycle. Soft storey formation greatly reduced the energy dissipation capacity of the building. Besides, the building with inverted V-braced (EXP3-SV) and X-braced (EXP4-SX) consume 22% and 8% more energy than bricks infill wall building respectively. Therefore, building with inverted V-braced shows the best solution for strengthening RC frames as it gives higher load-carrying capacity for better seismic energy dissipation than X-braced.

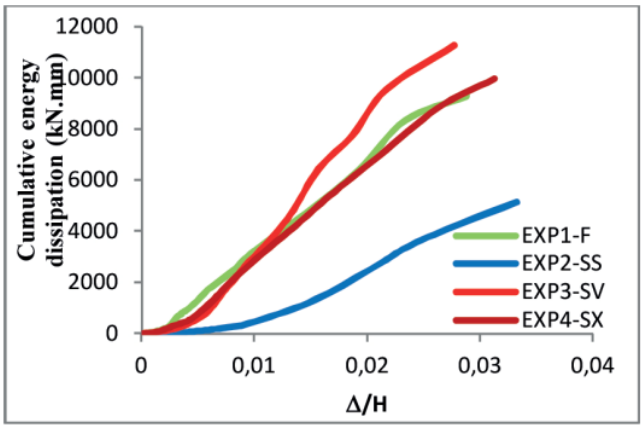

Figure 2.29: Comparison of Energy Dissipation Characteristic of Specimens (Ozturk and Ogutcu, 2018).

2.9 Structural Damage Reliability

The formula of structural reliability analysis is based on the happening of structural failure. The loading demand exceeds the load-carrying capacity of structure.

2.9.1 Structural Reliability Analysis

Earthquake is a destructive event that interrupts the society life which causes numerous damage and losses. Despite the characteristic of earthquake such as ground motion and frequency cannot be estimated, an assessment of the structure in seismic performance is required. R denotes as the load-carrying capacity of structure or resistance offered by structure. S denotes as the loads applied on structure. Equation 2.1 shows the conventional reliability analysis formula (Sankararaman, 2014).

$$G \equiv R - S \tag{2.1}$$

G= R – S >0 indicate the structure is safe which load apply is smaller than load-carrying capacity. Conversely, the structure is mean to be failed. If the applied loading (S) can be identified accurately and load-carrying capacity (R) can be calculated correctly, the design structure will not be failed due to loads problem. However, earthquake engineering has a challenge to determine the safety level of structure due to the uncertainty of R and S (Sankararaman, 2014).

2.9.2 Monte Carlo Sampling

Monte Carlo sampling (MCS) is the simplest measure to assess failure possibility P_f. N random samples of X need to be generated then function G required to be assessed for every random sample X. G<0 indicates the structural failure. N_f is defined as simulation number of G<0. Equation 2.2 shows the failure probability (Sankararaman, 2014).

$$P_f = \frac{N_f}{N} \tag{2.2}$$

Generally, probability of failure can be calculated precisely with an infinity samples number. However, the estimated value of P_f is uncertain due to only finite number is available. The uncertainty of P_f is calculated in variance as shown in equation 2.3 (Sankararaman, 2014).

$$Variance\ of\ P_f = \sqrt{\frac{P_f(1-P_f)}{N}} \quad (2.3)$$

Therefore, the accuracy of the estimated P_f value will increase proportional to the square root of samples number with number of samples is provided. The N value from equation 2.3 is important because the P_f value is depending on N. Besides, the probability of failure might be smaller than 10^{-5} in engineering application. Only 1 out if 100, 000 samples will cause failure on average. Therefore, 100,000 number of samples is required to detect the failure. N value should be at least tenfold in order to estimate accurate P_f value(Sankararaman, 2014).

2.9.3 Weibull Reliability Method

Weibull reliability method also known as life data analysis. Weibull reliability analysis tries to estimate the lifespan of all products in population by matching a statistical distribution to life result from a specific set of groups. The analysis capable to predict the vital life characteristic such as failure reliability or failure probability of a product at a certain time, mean life and failure rate (Corporation, 2015). The Weibull reliability analysis can be done through this few procedures:

a) Collect the life statistic for the product
b) Choose a lifetime distribution will match the data and model of product life.
c) Evaluate the parameter will match the distribution to data.
d) Produce results of life characteristic product estimation such as reliability or mean life.

The variety of Weibull distribution helps to analyse the reliability and life data. Weibull distribution also can model a variety of life behaviour depends on parameter values. Beta, β denotes as shape or slope parameter while alpha, α denotes as scale parameter. The two parameters will be examined to determine their effect on distribution characteristic such as curve shape, reliability and failure rate (Corporation, 2015).

The slope parameter, β in a probability plot is the gradient of the regression line. The value of β will affect the distribution behaviour. The value β has a failure rate effect on Weibull analysis. β can be categorised into 3 ranges as shown in Figure 2.30. The value of f(t) denotes as the reliability of Weibull analysis. β <1 indicates failure rate decrease with time in the same time reliability also decrease. When β =1, the regression line indicates constant failure at exponential distribution with reliability decreasing. For β >1, the failure rate is increase with the time (Corporation, 2015)..

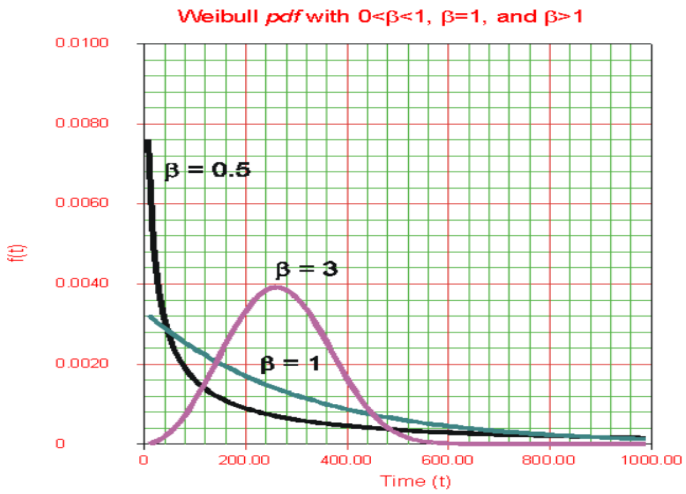

Figure 2.30: Weibull Reliability Plot with Shape Parameter, β (Weibull,com, 2021).

Besides, different value of α will have effect on the Weibull distribution due to changes of abscissa scale. The scale parameter, α can be categorized into three different distribution curve shape in the reliability graph as shown in Figure 2.31. The distribution curve will be stretched out to the right and decrease in height when η (scale parameter, α) value increase from 100 to 200 with the constant beta β value 3. The distribution curve will push to the left and increase

in height when α value decrease from 100 to 50 with constant β. The α unit can denote as the same unit with time such as miles, cycles, hours or actuations (Corporation, 2015).

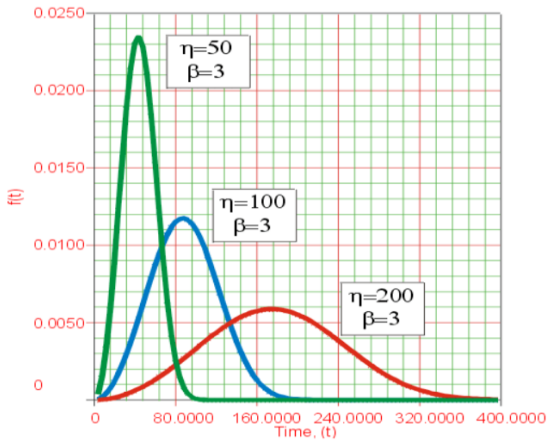

Figure 2.31: Weibull Reliability Plot with Scale Parameter, eta η (Weibull,com, 2021).

Few equations need to be used to determine reliability from Weibull reliability analysis. Firstly, equation 2.4 shows Median Ranks formula for a total number of samples. An approximation of unreliability of every failure is obtained through Median Ranks formulation. Next, equation 2.5 refer to the equation to obtain scale parameter alpha, α. The intercept coefficient needs to calculate based on regression line. Equation 2.6 show the Weibull reliability analysis formulation with the value of α and β (Corporation, 2015).

$$MR = \frac{(rank-0.3)}{(\sum rank+0.4)} \tag{2.1}$$

$$\alpha = EXP\left(\frac{-\,Intercept\ Coefficient\ t}{In\ (Design\ A\ Coeffiecint\ t)}\right) \tag{2.2}$$

$$R(t) = e^{-\left(\frac{x}{\alpha}\right)^{\beta}} \tag{2.3}$$

2.10 Summary

In short, the literature review highlights the seismic issue around the world includes seismic activity in Malaysia such as Ranau Earthquake in 2015. This shows that Malaysia has to alert for future earthquake event occurrence. Next, reinforced concrete is one of the ductile construction materials in earthquake structure design. The literature review also highlights the possible damages of the reinforced concrete structure during earthquake. There are 3 class of building can be categorised such as low-rise, mid-rise and high-rise building. The height of the building will affect its response to the earthquake. Besides, the literature review illustrates how the seismic waves turn into the earthquake load that cause ground motion on building. The structure response such as drift and degree of freedom is significant in earthquake structure design. Furthermore, regular building configuration such as shear wall, moment-resisting frame and braced system are important in earthquake-resistance structure. Base isolation and viscous damper also discussed in this chapter to illustrate their mechanism to dissipate the seismic energy from the earthquake. The result analysis such as PGA, spectral acceleration, displacement and seismic energy dissipation by different researchers also discussed in this chapter. Lastly, structural reliability analysis can be determined by using different method such as Monte Carlo sampling and Weibull's reliability analysis. Structural reliability analysis determines the functional level and safety level of building after an earthquake event.

CHAPTER 3

METHODOLOGY AND WORK PLAN

3.1 Introduction

This chapter will cover the methodology of scale down model construction and test method used in the experiment to obtain the desire results.

3.2 Overview of Work Plan

Figure 3.1 shows the flowchart of the work plan. First, the structural detailing of the low-rise reinforced concrete building was reviewed. The building consists of a 1 bay 1 frame 3 storey reinforced concrete structure. A scale factor of 1:8 is used in structural detailing to scale down the model size. Next, the reinforcement steel bar was tied to form the footing, column, beam and slab reinforcement. Plywood was cut and used as the formwork to construct the model during concrete casting. The entire structural model will use the same concrete mixture for concrete casting obtained through the three different trial mix. The concrete grade used will be 30N/mm^2. Three concrete cylinders were cast before each casting work to ensure the desire concrete grade is achievable. Then, the model was moved and placed on the shaking table for the experimental test. Measuring instruments such as linear variable differential transformers (LVDT) and accelerometer were installed at the model and shaking table. The test then will input different levels of dynamic load or seismic load in harmonic action ranging from PGA of 0.1g to 1.0g. The measuring instruments were recording the data into the data logger and digitally stored in a computer. Acceleration and horizontal displacement were obtained from the experiment. Next, the model will equip with the inverted V-braced damper and the shaking table test will start over again. The bracing used is the steel plate and the damper used is the viscous damper. Besides, structural damage reliability analysis was performed by Microsoft Excel software to compute the reliability plot. Lastly, the data and result for the model with and without inverted V-braced damper are discussed and compared.

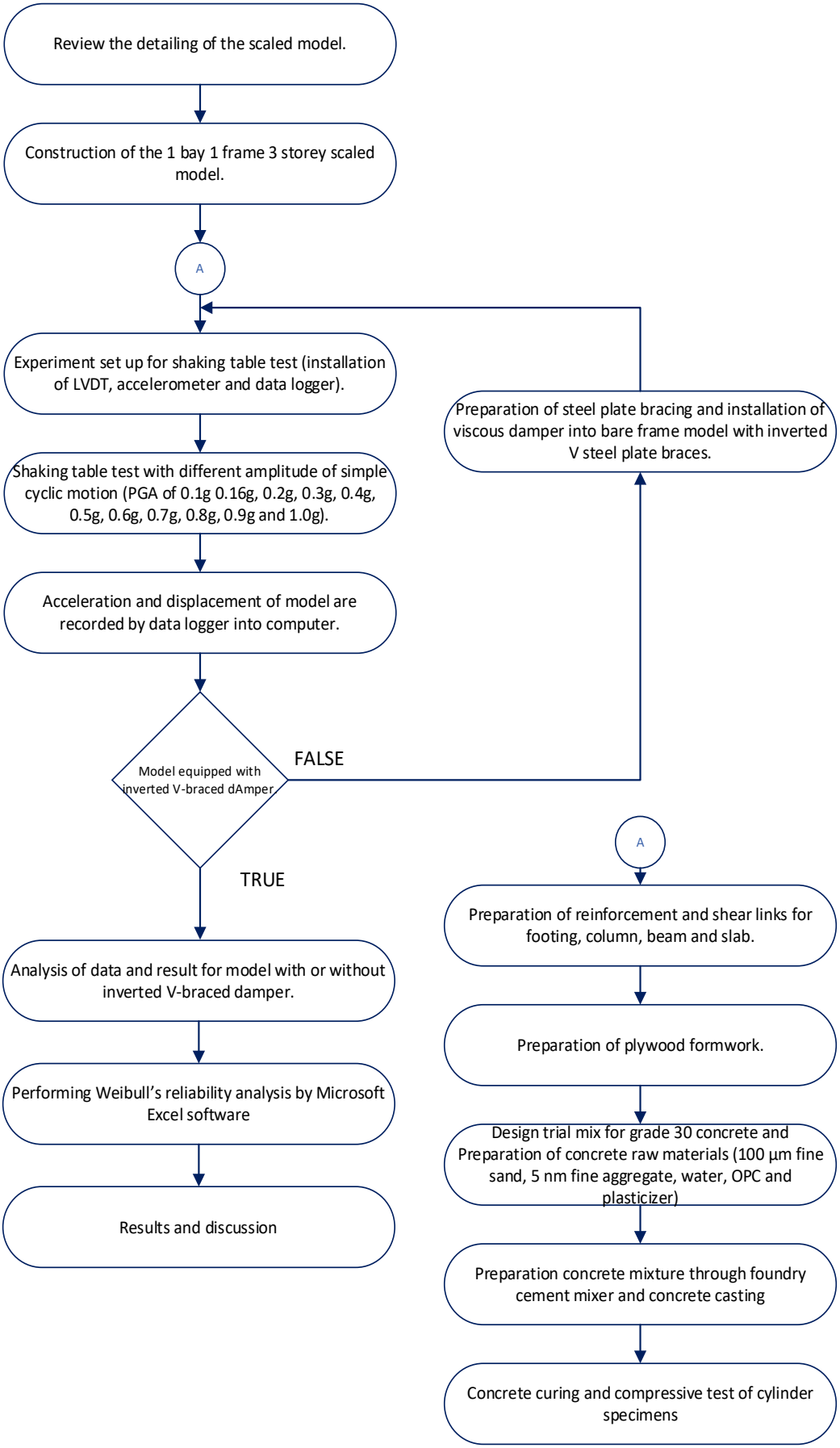

Figure 3.1: Flowchart of Work Plan.

3.3 Overview of Model Detailing

The civil and structure (C&S) drawing and architecture drawing of low-rise reinforced concrete building are obtained from the author's thesis supervisor. The structural model that built has to scale down due to the limited size of the shaking table. A 1 bay 1 frame 3 storey building is scaled down with a factor 1:8 according to the C&S and architecture drawings. Table 3.1 shows the properties of the scaled model. Figure 3.2 shows the detailing and 3D view of the scaled model.

Table 3.1: Properties of Scaled Model.

Properties	Height	Length	Width	Volume	Mass
	1500 mm	790 mm	790 mm	0.0697 m^3	175 kg

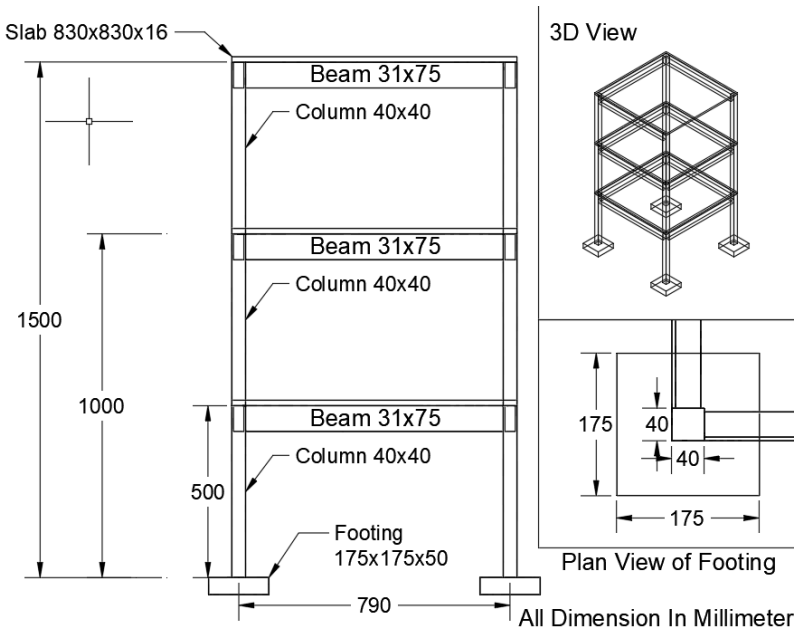

Figure 3.2: Detailing and 3D View of 2 Bay 1 Fame 3 Storey Scaled Model.

3.4 Construction of Model

This sub-section covers the procedure in the construction of a scaled model, including the preparation of reinforcement and formwork, concrete casting, and inverted V-braced dampers.

3.4.1 Reinforcement Steel Bar

The material used for the model was reinforced concrete. Hence, 3 mm steel bar was used for the reinforcement and 1 mm steel bar was used for the shear links. In order reinforcement can be built in shape, steel wire was used to tie up the reinforcement tightly. According to the detailing, there were total 6 footings, 18 columns, 6 slabs and 21 beams reinforcement need to be prepared. The beam and slab reinforcement will possess starter bar that connects the first and second bay. Figure 3.3 (a) shows the steel bar for 3mm and 1.5mm and Figure 3.3(b) shows the steel wire.

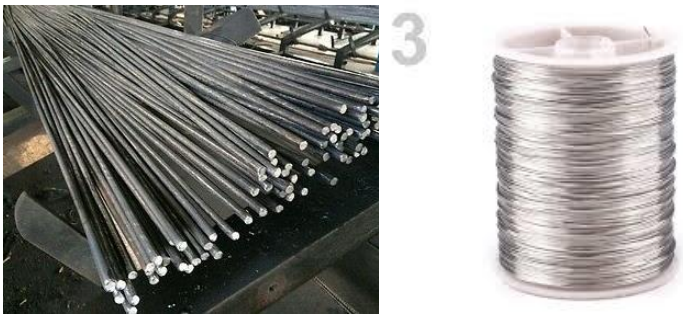

(a) (b)

Figure 3.3: (a) Steel Bar and (b) Steel Wire

3.4.2 Plywood Formwork

Plywood was a type of building material that commonly used in the construction industry. Plywood was made by glueing few thin sheets of wood together to form a thicker wood. Plywood tends to be used in construction because of economical and flexible. Plywood was able to cut into desire size according to the drawings. However, plywood does not suit in mass construction. Therefore, plywood was used as the formwork to construct the scaled model during concrete casting in this study. Figure 3.4 shows the slab and beam reinforcement is placed in the cut to size plywood formwork.

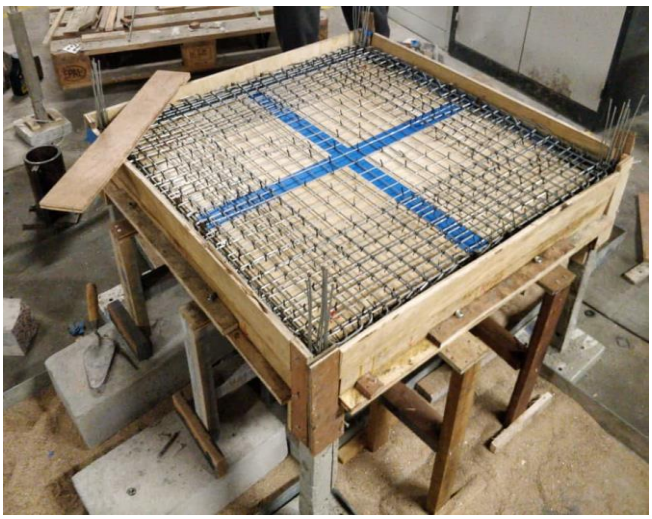

Figure 3.4: Installation of Slab and Beam Reinforcement into Plywood Formwork.

3.4.3 Raw Materials

The concrete mixture consists of 5 raw materials which were fine sand, fine aggregate, water, Ordinary Portland Cement (OPC) and plasticiser. The fine sand that used was 100% sieved through 100 μm sieve. The fine sand used should also in saturated surface dry (SSD) condition which avoids additional free water into the concrete mixture. Besides, the aggregate used must crush by aggregate crusher to obtain the fine aggregate that can pass through the spacing in between reinforcement. The fine aggregate that sieved through 100% of 5mm sieve was rejected and fine aggregate that trapped on the sieve was collected. The water used was from the municipal water supply tap. The water should have free impurities which provide a good quality of the concrete mix. The OPC that used was Orang Kuat branded which compliance with the Malaysian Standard of MS 522: Part 1: 2003 and certified by MS ISO 14001 and OHSAS 18001. After the OPC package was opened, the OPC need to be stored in the tight container to avoid additional moisture in contact with OPC that occur the hydration process. Last but not least, the plasticiser was used in the mixture to enhance workability and reduce water content required. Figure 3.5 shows the raw materials of concrete mixture.

(a) Fine Sand

(b) Fine Aggregate

(c) OPC

(d) Water

(e) Plasticizer

Figure 3.5: Raw Materials of Concrete Mixture.

3.4.4 Trial Mix Proportions

Before the construction of the model can be started, trial mix is a crucial step to determine the suitable concrete mixture to achieve the desired concrete strength. The proportion of the fine sand, fine aggregate, water, OPC and superplasticiser need to be designed to grade 30 (30N/mm^2) of concrete compressive strength in 28 days. Three designed trial mix proportions are prepared in this experiment as shown in Table 3.2, Table 3.3 and Table 3.4.

Table 3.2: Trial Mix Design 1

	Trial Mix 1					
Grade 30	Water (ml)	Cement (g)	Sand (g)	Coarse (g)	Plasticiser (ml)	Density ($\frac{g}{mm^3}$)
w/c 0.42	233.00	550.00	511.00	1086.00	5.50	2380
Per cylinder	0.37	0.86	0.80	1.71	0.01	
9 cylinders	3.29	7.77	7.22	15.35	0.08	
+20% wastage	3.95	9.33	8.66	18.41	0.09	

Table 3.3: Trial Mix Design 2

	Trial Mix 2					
Grade 35	Water (ml)	Cement (g)	Sand (g)	Coarse (g)	Plasticiser (ml)	Density $(\frac{g}{mm^3})$
w/c 0.46	225.0	489.13	749.60	916.23	4.89	2379.96
Per cylinder	0.35	0.77	1.18	1.44	0.01	
9 cylinders	3.18	6.91	10.59	12.95	0.07	
+20% wastage	3.82	8.29	12.71	15.54	0.08	

Table 3.4: Trial Mix Design 3

	Trial Mix 3					
Grade 35	Water (ml)	Cement (g)	Sand (g)	Coarse (g)	Plasticiser (ml)	Density $(\frac{g}{mm^3})$
w/c 0.60	205.00	342.00	701.00	1052.00	0.00	2300
Per cylinder	0.32	0.54	1.10	1.65	0.01	
9 cylinders	2.90	4.83	9.91	14.86	0.05	
+20% wastage	3.48	5.80	11.89	17.84	0.06	

Then, each trial concrete mix was cast into 3-cylinder moulds and cured in the tank. The concrete cylinder then was tested under compressive strength test for the 7 days strength. The 7 days strength of the concrete was two-third of the 30 days strength of concrete. Hence, 20N/mm^2 strength was targeted for the concrete. Table 3.5 illustrate the results of 7 days compressive strength test of each trial mix design. Only trial mix 1 passed for the target strength of 20N/mm^2. Therefore, trial mix 1 was used for the concrete mix proportion.

Table 3.5: Trial Mix 7-days Concrete Compression Test

Trial Mix	**Weight (kg)**	**Maximum Strength (N/mm^2)**	**Target Strength at 7-days (N/mm^2)**	**Status**
Trial Mix 1	3.74	34.20	20	Pass
	3.47	30.29		Pass
	3.49	32.89		Pass
Trial Mix 2	3.45	6.21	20	Fail
	3.32	7.53		Fail
	3.39	6.47		Fail
Trial Mix 3	3.79	22.37	20	Pass
	3.52	18.92		Fail
	3.53	17.87		Fail

3.4.5 Concrete Mixture

The proportion of fine sand, fine aggregate, water, OPC and plasticiser is obtained according to the trial mix. The mass of concrete mixture needs to include 15% of wastage and the mass for 3 cylinders. First, dry raw materials such as fine sand, fine aggregates and OPC are mixed well by the foundry cement mixer as shown in Figure 3.6. One-third of water and plasticiser then added to turn the mixture become moisture. The remaining water is slowly adding in by observing the humidity and workability of the mixture is suits for concrete casting.

Figure 3.6: Foundry Cement Mixer.

3.4.6 Concrete Casting

After installation of reinforcement into plywood formwork and preparation of the concrete mixture, concrete casting work is commenced. The formwork needs to be oil to before casting work start. During the pouring of concrete into the formwork, the action needs to be slow in order concrete can fill in the spacing between the reinforcement. Damping rod is used to compact the concrete to avoid the formation of honeycomb inside the concrete. However, over compaction need to be avoided as it will cause segregation and non-homogenous of concrete. Figure 3.7 illustrates the concrete casting of slab and beam at second floor

Figure 3.7: Concrete Casting of Second Level Slab and Beam.

Besides, three concrete cylinders with the same mixture for model concrete casting is cast into the cylinder mould with 100 mm diameter and 200 mm height. This step is to obtain the compressive strength of concrete to ensure the quality of the mixture. Figure 3.8 shows the cylinder mould.

Figure 3.8: Cylinder Mould.

In this study, the model consists of 1 bay 1 frame 3 storey. The concrete casting starts from the footings to first storey column, beam and slab. The second and third storey will follow the sequence of first storey.

3.4.7 Curing of Concrete

Curing provides the optimum condition for the hydration of the concrete specimens. It is crucial to obtain the compressive strength of the cylinder. According to the ASTM C192, the concrete cylinder is cured in the water tank with the temperature in between 25ºC and 28ºC. The period of the curing will be 28 days. Figure 3.9 shows the water curing process.

Figure 3.9: Water Curing Process.

3.4.8 Compressive Strength Test

After 28 days of curing, the cylinders are dried inside the oven for 24 hours with temperature 105ºC. It is vital for all cylinders are free from moisture content on their surface. ASTM C39 is used as the standard for testing the concrete cylinder in the compressive strength test. The properties of the cylinder such as dimension and weight are written into the machine before the test started. The top and bottom surface of the concrete cylinder are locked by the Unit Test Machine. By preventing the abrupt failure of cylinder, the load rate is pre-set inside the machine. The maximum axial load is recorded based on the machine screen and average compressive strength is computed. Compressive strength is essential to carry out during the trial mix and every stage of the concrete mixture during casting. Figure 3.10 shows the compressive strength test for concrete cylinder.

Figure 3.10: Compressive Strength Test.

3.5 Inverted V-braced Damper Installation

After obtaining control data for the 1 bay 1 frame 3 storey model during shaking simulation, the model will only equip with the inverted V-braced damper. The damper used in this study is the shock absorber to dissipate the dynamic energy caused by the shaking table. The damper was connected with 2 steel plate in inverted V-braced shape. Then, inverted V-braced damper is locked at both ends by the welded steel plate to avoid its movement during shaking simulation. The procedure from the experiment set up and shaking table test was repeated. Figure 3.11 shows the inverted V-braced dampers at the first bay first storey.

Figure 3.11: Inverted V-Braced Dampers.

3.6 Experiment Set-Up

An accelerometer is a transducer that can measure the acceleration motion of the ground and building. Linear variable differential transformer (LVDT) is another type of transducer that measures the displacement of an object. There is 1 accelerometer sensor to measure the ground acceleration induced by the shaking table. There were 4 accelerometers and 4 LVDT displacement sensors installed at each storey to measure the movement of the building. Figure 3.12 shows the position of LVDT and accelerometer sensor at model with and without inverted V-braced damper. Besides, data logger is required to connect with the transducer in order the data of acceleration and displacement sensed by the transducer can be transmitted into computer. Figure 3.13 shows the data logger. All the wire and transducer need to check for functionality before the experiment test commenced.

Figure 3.12: Position LVDTs (Left) and Accelerometers (Right) at Model.

Figure 3.13: Data Logger

3.7 Shaking Table Test

Advanced Civil Lab in UTAR campus is equipped with the shaking table. The 1 bay 1 frame 3 storey model will be brought to the advanced civil lab and mounted onto the shaking table. The dimension of the shaking table is 2 X 2 m square area as shown in Figure 3.14. Figure 3.15 illustrates 3 layers of the shaking table platform. The bottom layer consists of a steel frame that is welded and bolted with angular and rectangular sections to support the shaking table. The second layer of the platform consists of an aluminium plate with foam. The holes inside the aluminium plate will connect with the air compressor in order the air pressure lift up the shaking table. The top layer of the platform is the shaking table. The movement of shaking table is controlled by a torque motor with a software, namely MotCtProg (3DA-GateCtrl). The shaking table can sustain with the maximum load of 4000kg.

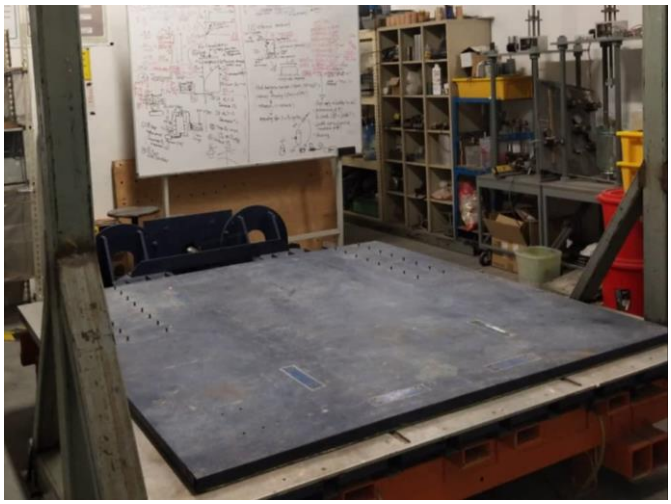

Figure 3.14: Shaking Table with 2 X 2m.

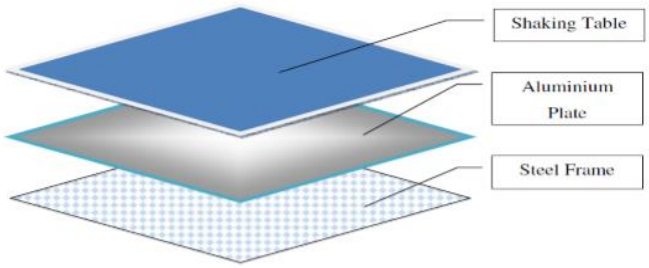

Figure 3.15: Layers of Shaking Table Platform.

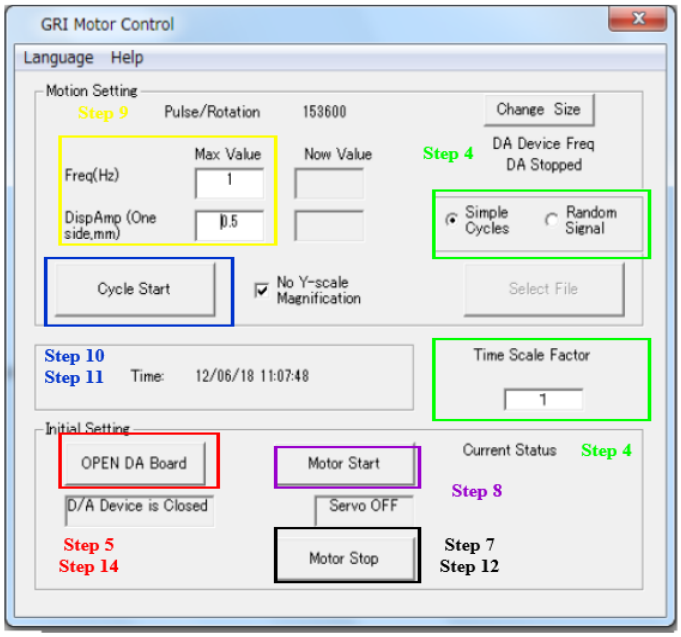

Figure 3.16: Control Panel of the MotCtProg (3DA-GateCtrl).

Figure 3.16 shows the control panel of the MotCtProg (3DA-GateCtrl) to adjust the motion of shaking table. Simple Cyclic Motion is chosen in this study. The value of frequency and amplitude of the cyclic motion can be entered into the software by the user. Higher frequency gives a lower period of cyclic motion and higher amplitude give higher horizontal displacement motion of shaking table. The shaking motion can be commenced once the “Motor Start” button is selected. The data of acceleration and horizontal displacement received by the transducer will be transmitted into the data logger then into the DA board of this software. The reinforced concrete building with or without inverted V-braced damper will be tested under shaking simulation.

3.8 Analysis of Result

The 1 bay 1 frame 3 storey reinforced concrete structure will undergo shaking table test with eleven different sets of Peak Ground Acceleration (PGA). The PGA ranging from 0.1g to 1.0g. However, the MotCtProg programme from shaking table which requires only frequency and displacement value to be entered. Calibration test was undergone to determine the correct frequency and displacement value corresponding to each value of peak ground acceleration for shaking table test. The analysis results such as displacement and spectral acceleration in each floor is obtained from the shaking table with the LVDTs and Accelerometer equipment. The value of displacement and spectral acceleration with different PGA at each storey are compared from model with and without inverted V- bracing damper. Besides, the acceleration and displacement obtained can be converted into hysteresis curve which is the force-displacement curve. The force is computed by multiplying the spectral acceleration and mass of the model. Then, the seismic energy dissipation by the model is calculated from the area of the hysteresis loop with the use of Autocad software. The seismic energy dissipation by model with and without inverted V-braced damper is compared to determine the seismic energy dissipation increment by the inverted V-braced damper. Three stages such as early stage (PGA of 0.1g and 0.2g), mid stage (PGA of 0.5g and 0.6g) and later stage (PGA of 0.8g and 0.9g) are categorised for comparison the energy dissipation at each stage.

3.9 Analysis of Structural Damage Reliability

The reliability analysis is analysed using Weibull's Reliability Method to obtain the structural damage reliability. Base shear is selected for the damage reliability analysis. Eleven different sets of base shear are calculated by the production of overall structure mass and their roof spectral acceleration. The eleven data of base shear are entered into Microsoft Excel software to perform Weibull Analysis.

Two of Weibull's parameters are determined before reliability analysis can be performed. The two parameters are shape parameter beta, β and, scale parameter alpha, α. The ground storey base shear data is important to plot regression function graph in Microsoft Excel. Figure 3.17 illustrates the base shear data was assigned into sample according to the eleven sets of PGA value. The base shear for sample 1 was calculated by the formula: =A16*C3. Copy the cell B3 down through cell B13 for other sample base shear data.

	A	B	C
1	Design A	IBS	Spectral
2	Sample	Base Shear (N)	Accleration
3	1	210.32	1.2018132
4	2	233.69	1.335348
5	3	437.33	2.4990084
6	4	544.15	3.1094532
7	5	597.57	3.4146756
8	6	827.92	4.7309472
9	7	794.53	4.5401832
10	8	911.38	5.2078572
11	9	1171.77	6.6958164
12	10	1165.09	6.6576636
13	11	1415.47	8.0883936
14			
15	Mass of Model		
16	175	kg	

Figure 3.17: Sample of Base Shear Data.

Figure 3.18 show the preparing data from Design A for Weibull's Analysis. First, base shear data was assigned to Design A from sheet 1. Each of Design A was assigned with a rank in ascending order from cell B2 to B12 with integers 1-10. In Column C, the median rank for rank 1 was calculated with the formula: ((B2-0.3)/(11+0.4)). The 11 in the denominator is the total number of base shear data tested in the analysis. In Column D, the formula for cell D2 is =1/(1-C2). In Column E, the formula for cell E2 is =LN(LN(D2)). Lastly, enter the formula =LN(A2) for cell F2 in Column F. Copy the value at row 2 down to row 12 for each column to complete the table.

	A	B	C	D	E	F
1	Design A	Rank	Median Ranks	1/(1-Median Rank)	ln(ln(1/(1-Median Rank)))	ln(Design A)
2	210.32	1	0.061	1.065	-2.759	5.349
3	233.69	2	0.149	1.175	-1.823	5.454
4	437.33	3	0.237	1.310	-1.308	6.081
5	544.15	4	0.325	1.481	-0.935	6.299
6	597.57	5	0.412	1.701	-0.632	6.393
7	827.92	6	0.500	2.000	-0.367	6.719
8	794.53	7	0.588	2.426	-0.121	6.678
9	911.38	8	0.675	3.081	0.118	6.815
10	1171.77	9	0.763	4.222	0.365	7.066
11	1165.09	10	0.851	6.706	0.643	7.061
12	1415.47	11	0.939	16.286	1.026	7.255
13						

Figure 3.18: Preparing Design A for Weibull's Analysis.

Next, α value is determined through the regression function and the gradient of regression function is the β parameter. A line plot was plotted with the data in Column E versus Column F through the simple linear regression function in Microsoft Excel software. Figure 3.19 illustrate the result of linear regression for Design A. In order to perform the linear regression function, Analysis ToolPak Add-In was loaded into Microsoft Excel. Then, Data Analysis was selected from Tools locates at menu bar. "Regression" that placed inside the Data Analysis is selected. Column F was selected as "Input Y Range" and column E was selected as "Input X Range". Microsoft Excel will perform the regression and place the output in a new worksheet as shown in Figure 3.19. Besides, the value of α is calculated through with the formula: =EXP(-B17/B18). Cell B17 indicates the y-intercept of the line fit plot for the regression function. The β parameter is equal to the cell B8 in Figure 3.19.

	A	B	C	D	E	F	G	H	I
1	SUMMARY OUTPUT								
2									
3	*Regression Statistics*								
4	Multiple R	0.980821767							
5	R Square	0.962011338							
6	Adjusted R Square	0.957790375							
7	Standard Error	0.23092622							
8	Observations	11							
9									
10	ANOVA								
11		*df*	*SS*	*MS*	*F*	*Significance F*			
12	Regression	1	12.153887	12.153887	227.912791	1.0668E-07			
13	Residual	9	0.479942273	0.053326919					
14	Total	10	12.63382927						
15									
16		*Coefficients*	*Standard Error*	*t Stat*	*P-value*	*Lower 95%*	*Upper 95%*	*Lower 95.0%*	*Upper 95.0%*
17	Intercept	-11.77435295	0.748287774	-15.7350599	7.44053E-08	-13.4670975	-10.08160841	-13.4670975	-10.08160841
18	ln(Design A)	1.738466646	0.115154791	15.09678082	1.0668E-07	1.47796841	1.998964882	1.47796841	1.998964882
19	beta	1.738466646							
20	alpha	873.7881857							
21									
22	RESIDUAL OUTPUT								
23									
24	*Observation*	*ln(ln(1/(1-Media*	*Residuals*						
25	1	-2.475960019	-0.282810789						
26	2	-2.292794277	0.469466552						
27	3	-1.203293612	-0.10496499						
28	4	-0.823346724	-0.112144599						
29	5	-0.660564348	0.028523233						
30	6	-0.093749571	-0.27276335						
31	7	-0.165301507	0.044320566						
32	8	0.073218067	0.044814303						
33	9	0.510119818	-0.145225637						
34	10	0.500185696	0.143238065						
35	11	0.838598278	0.187546646						
36									

Figure 3.19: Results of Linear Regression for Design A.

The reliability plot for base shear data was plotted using parameter such of β and α. Figure 3.20 illustrate Weibull's reliability calculator for Design A that perform in Excel. The value of α and β from Figure 3.19 was copied and paste into cell B3 and Cell B2 respectively. In Column D, the base shear value from 0 to 3100 was entered with increments of 1000. Survival probability was calculated in Column E with the formula: =WEIBULL(D2, B1, B2, TRUE) at cell E2. In Column F, the reliability of the Design A was calculated through the formula: =1-E2 at cell F2. Next, copy the row 2 at Column E and F to the row 33. A reliability plot was plotted for Column F versus Column D.

	A	B	C	D	E	F
1	Beta or shape parameter	1.738466646		Base Shear (N)	Survival Probability	Reliability
2	Alpha or characteristic life	873.7881857		0	0.0000	1.0000
3				100.00	0.0228	0.9772
4				200.00	0.0741	0.9259
5				300.00	0.1444	0.8556
6				400.00	0.2267	0.7733
7				500.00	0.3154	0.6846
8				600.00	0.4056	0.5944
9				700.00	0.4934	0.5066
10				800.00	0.5759	0.4241
11				900.00	0.6510	0.3490
12				1000.00	0.7176	0.2824
13				1100.00	0.7751	0.2249
14				1200.00	0.8238	0.1762
15				1300.00	0.8640	0.1360
16				1400.00	0.8966	0.1034
17				1500.00	0.9226	0.0774
18				1600.00	0.9429	0.0571
19				1700.00	0.9584	0.0416
20				1800.00	0.9702	0.0298
21				1900.00	0.9789	0.0211
22				2000.00	0.9853	0.0147
23				2100.00	0.9899	0.0101
24				2200.00	0.9931	0.0069
25				2300.00	0.9954	0.0046
26				2400.00	0.9969	0.0031
27				2500.00	0.9980	0.0020
28				2600.00	0.9987	0.0013
29				2700.00	0.9992	0.0008
30				2800.00	0.9995	0.0005
31				2900.00	0.9997	0.0003
32				3000.00	0.9998	0.0002
33				3100.00	0.9999	0.0001

Figure 3.20: Weibull Reliability Calculator for Design A

Lastly, the structural damage reliability analysis for base shear under different sets of PGA was completed with the structural performance level indices IO, LS and CP and structural condition. The reliability index for IO, LS and CP are 0.80, 0.50 and 0.17 respectively. A reliability curve is plotted for the structural reliability analysis.

3.10 Summary

An overview of the methodology and work plan is discussed in this chapter. The 1 bay 1 frame 3 storey is scaled down with factor 1:8 to fit in the size of the shaking table provided in advanced civil lab UTAR campus. The construction of the scaled model includes the preparation of reinforcement and plywood formwork, the proportion of concrete mix by trial mix, the concrete casting of model and the curing and compressive test of cylinder specimens. The model with and without the inverted V-braced damper is tested on the shaking table test under eleven different sets of PGA. Weibull's Reliability Method is used to obtain the structural damage reliability through Microsoft Excel software. The test result for both conditions will be presented and discussed in the next chapter.

CHAPTER 4

RESULTS AND DISCUSSION

4.1 Introduction

In this experiment, the scaled model with and without inverted V-braced damper was tested by the shaking table under eleven different inputs of PGA. The input value of PGA are 0.1 g, 0.16 g, 0.2 g, 0.3 g, 0.4 g, 0.5 g, 0.6 g, 0.7 g, 0.8 g, 0.9 g and 1.0g. The experiment data obtained from the shaking table test are the acceleration and displacement at each floor of the model under different value of PGA. In this chapter, the spectral acceleration, inter-storey drift, seismic energy dissipation and structural damage reliability will be discussed and compared for the model with and without inverted V-braced damper.

4.2 Spectral Acceleration

Spectral acceleration is the acceleration experienced by the building which differs from the peak acceleration experienced at the ground level. Spectral acceleration is useful for the structural engineer to estimate the seismic load impose on the building. In this experiment, the spectral acceleration is obtained through the installed accelerometer on each floor. Both model spectral acceleration at each floor under eleven different sets of PGA will be discussed and compared in this section.

4.2.1 Model without Inverted V-Braced Damper

Figure 4.1 shows the graph of storey versus acceleration for each different sets of PGA from 0.1 g to 1.0 g. Figure 4.2 illustrate the histogram of acceleration versus PGA for each storey. Both Figure 4.1 and Figure 4.2 illustrate the acceleration pattern for the model *without* inverted V-braced damper at each storey. Based on the graph, the spectral acceleration will increase when the input PGA is increased. The spectral acceleration at the roof floor is the highest as compared to 1st floor and 2nd floor. This is true because the mass taken by first, second and third storey to return are dissimilar. Higher seismic forces will be imposed at the higher storey of building due to greater acceleration at a

particular storey. The highest spectral acceleration for the model without inverted V- braced damper is 7.859 m^2/s which located at the roof floor where model experiences 1.0 g. However, 2^{nd} floor has the lowest spectral acceleration among other stories except for the PGA 0.16 g where experience 0.874 m^2/s slightly higher than 1^{st} floor having 0.863 m^2/s of spectral acceleration. Base on Figure 4.1, the model experience a minor ground motion (minor earthquake) at and before 0.4 g and shows a similar curved trend. The large curvature of the line present from PGA 0.5 g to 1.0 g indicates large ground motion (major earthquake) induced at model.

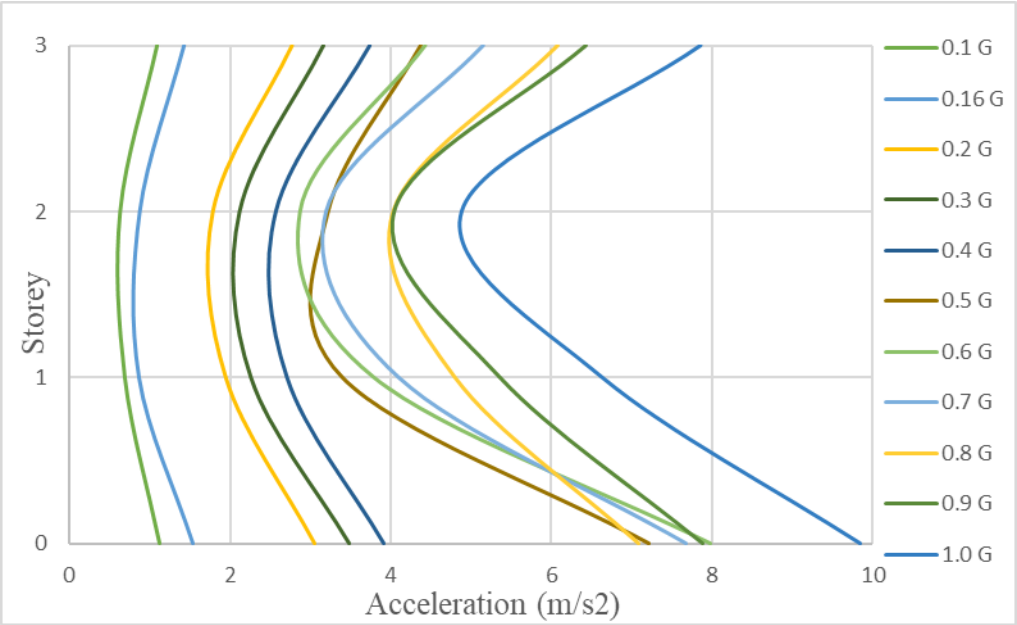

Figure 4.1: Graph of Storey Against Maximum Responded Acceleration with PGA 0.1g, 0.16g, 0.2g, 0.3g, 0.4g, 0.5g, 0.6g, 0.7g, 0.8g, 0.9g and 1.0g for Model without Inverted V-Braced Damper.

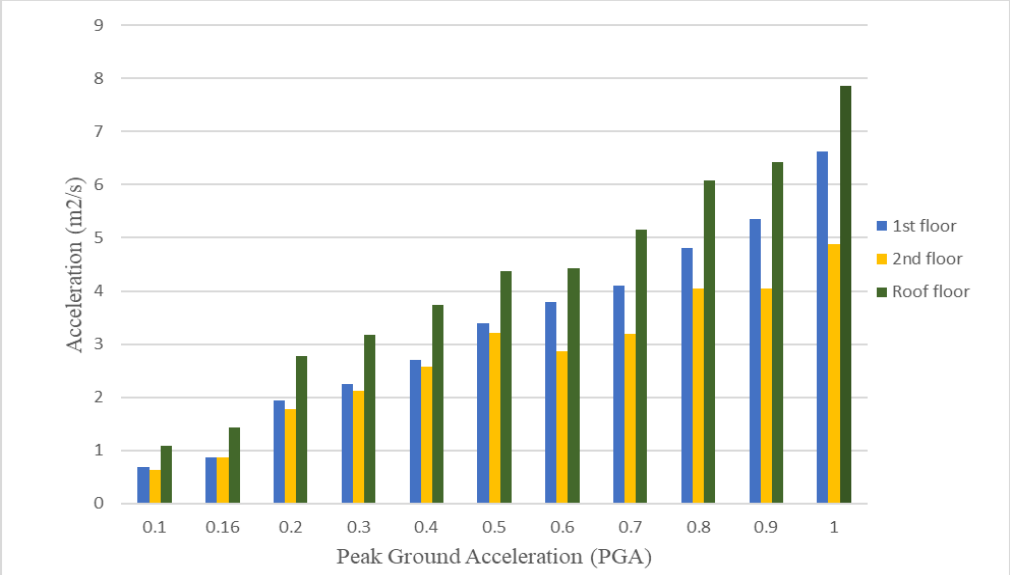

Figure 4.2: Histogram of Maximum Responded Acceleration Against Eleven Sets of PGA at 1st Floor, 2nd Floor and Roof Floor for Model without Inverted V-Braced Damper.

4.2.2 Model with Inverted V-Braced Damper

Figure 4.3 shows the graph of storey versus acceleration for each different sets of PGA from 0.1 g to 1.0 g. Figure 4.4 illustrate the histogram of acceleration versus PGA for each storey. Both Figure 4.3 and Figure 4.4 illustrate the acceleration pattern for the model *with* inverted V-braced damper at each storey. Based on the pattern of the graph, the spectral acceleration will increase when the input PGA is increased. The spectral acceleration at the roof floor is the highest as compared to 1st floor and 2nd floor. This is true because the mass taken by first, second and third storey to return are dissimilar. Higher seismic forces will be imposed at the higher storey of building that due to the greater acceleration at a particular storey. The highest spectral acceleration for the model with inverted V-braced damper is 8.088 m^2/s which located at the roof floor where model experiences 1.0g. However, 2nd floor has the lowest spectral acceleration among other stories in every set of PGA. Base on Figure 4.3, PGA 0.1 g, 0.16 g, 0.3 g, 0.5 g, 0.6 g, 0.7 g, 0.9 g and 1.0 g share similar curved trend from ground floor to roof floor which is single curvature of line where PGA 0.2 g, 0.4 g and 0.8 g show double curvature of line. Besides, the degree of curvature of PGA 0.1 g, 0.16 g and 0.3 g illustrates in Figure 4.3 indicates the minor difference of spectral acceleration between 1st floor, 2nd floor and roof floor.

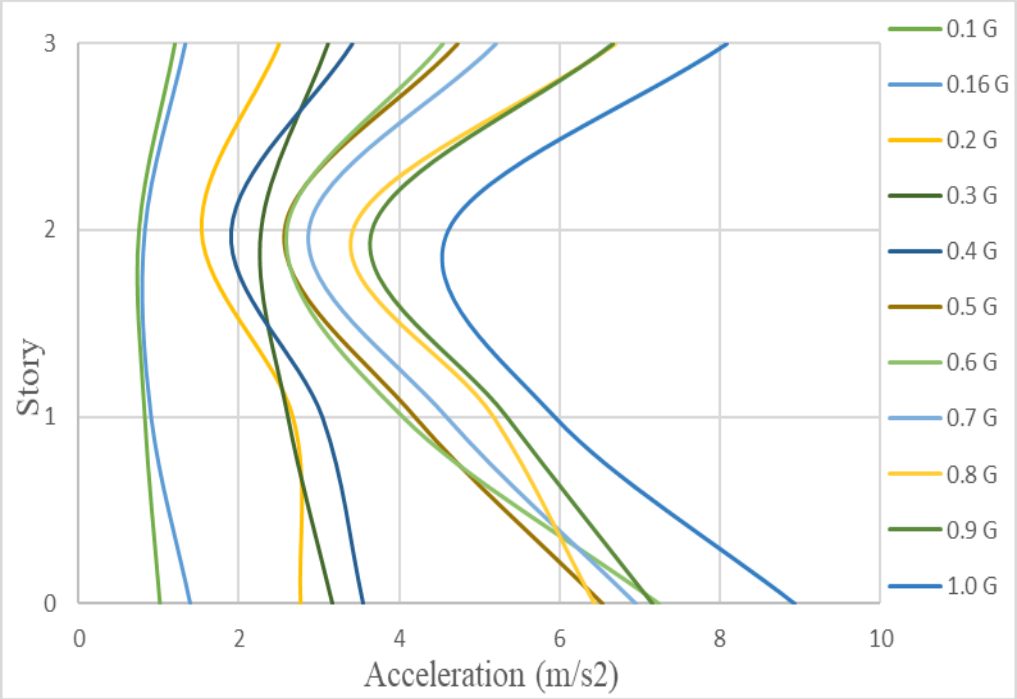

Figure 4.3: Graph of Storey Against Maximum Responded Acceleration with PGA 0.1g, 0.16g, 0.2g, 0.3g, 0.4g, 0.5g, 0.6g, 0.7g, 0.8g, 0.9g and 1.0g for Model with Inverted V-Braced Damper.

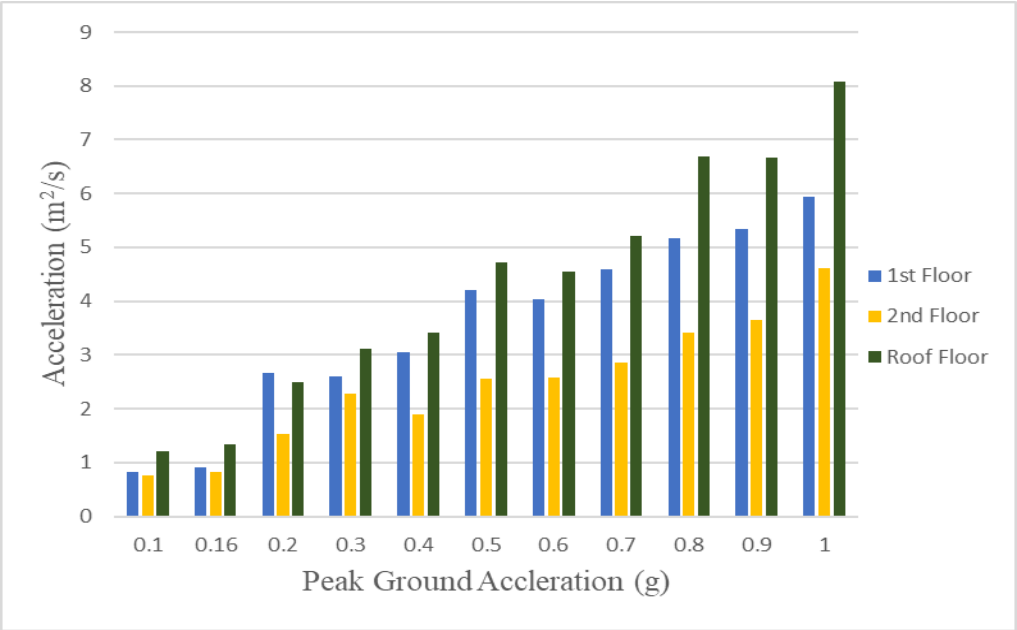

Figure 4.4: Histogram of Maximum Responded Acceleration Against Eleven Sets of PGA at 1st Floor, 2nd Floor and Roof Floor for Model without Inverted V-Braced Damper.

4.2.3 Spectral Acceleration Comparison

Roof spectral acceleration is chosen for comparison as the roof spectral acceleration gives the highest acceleration and highest seismic load as compared to 1st and 2nd floor. Figure 4.5 shows the histogram of model with and without inverted V-braced damper roof spectral acceleration against eleven different sets of PGA. The roof spectral acceleration is reduced at PGA 0.16 g, 0.2 g, 0.3 g and 0.4 g for the model equipped with inverted V-braced damper. The highest roof spectral acceleration reduction is up to 9.66% when experience 0.2 g of PGA. The reduction of roof spectral acceleration indicates the inverted V-braced viscous damper dissipates the seismic energy efficiently. The seismic energy is absorbed by the damper through the moving piston of compressible fluid inside. However, the spectral acceleration for PGA 0.1 g, 0.5 g, 0.6 g, 0.7 g, 0. 8 g, 0.9 g and 1.0 g are slightly higher at the model with viscous damper.

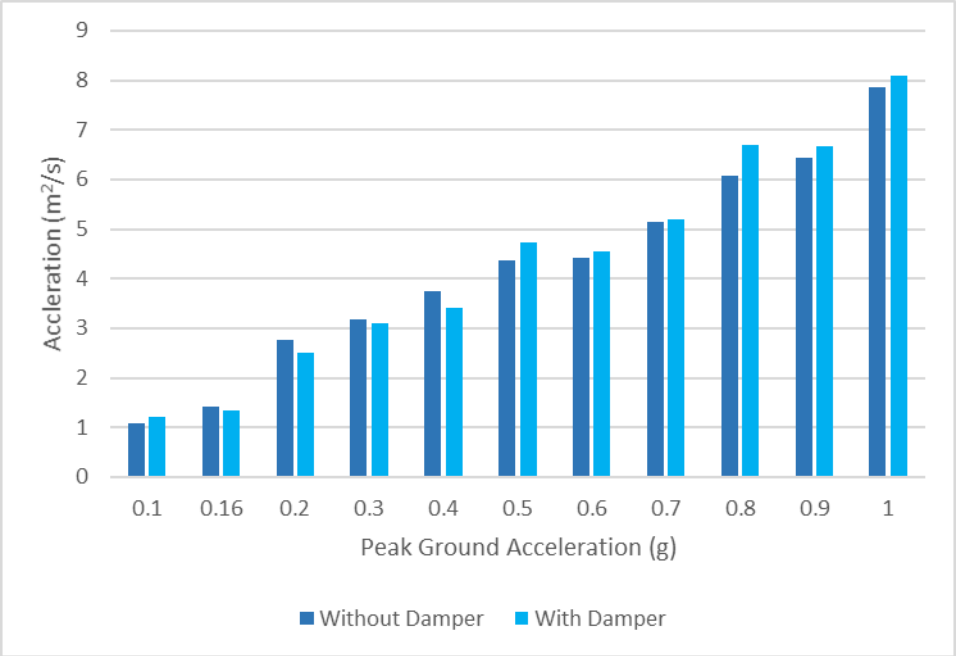

Figure 4.5: Histogram of Roof Spectral Acceleration Against Eleven Sets of PGA for Comparison Model with and without Inverted V-Braced Damper.

4.3 Inter-storey Drift

Drift is defined as the total horizontal displacement at the roof of the building where inter-storey drift is the difference in horizontal deflection between the top and bottom floor. Inter-storey drift is useful to determine the floor level damage. In this experiment, total 4 LVDT were installed on the scaled model at ground floor, 1st floor, 2nd floor and roof floor. However, the ground floor displacement is the shaking table displacement in each different cyclic loading. The maximum displacement on each floor was captured by the LVDT and plot into graph. Inter-storey also calculated and plot into graph for better visualisation. Then, both model inter-storey drift at each floor under eleven different sets of PGA are discussed and compared in this section.

4.3.1 Model without Inverted V-Braced Damper

Figure 4.6 and Figure 4.7 illustrate the maximum responded displacement and inter-storey drift at each level under eleven different sets of PGA. The displacement on each floor increased as the PGA value increased. Based on Figure 4.6, the maximum drift happens at the 2nd floor for all eleven sets of PGA. The maximum drift for the model without inverted-v braced damper is 23.65 mm at 2nd floor when experience 1.0 g of PGA. The lowest drift happens where model experiences 0.1 g of PGA at 1st floor which is 6.014 mm. The curved line show in Figure 4.6 indicates the mode shape of the building. The model experiences double curvature of mode shape when experience PGA lower than 0.9 g. The line turns to single curvature when model experience at 1.0 g of PGA. Apart from that, the inter-storey drift at 1st storey is the highest as compared to 2nd and 3rd storey. The inter-storey drift also increases as the PGA increased. The maximum inter-story drift happens at the 1st floor of model experience 1.0 g which is 21.66 mm. The maximum inter-storey drift indicates the particular storey is lack of stiffness and undergo largest deformation change. Therefore, 1st storey is more vulnerable to damage during ground motion when compare to other storey.

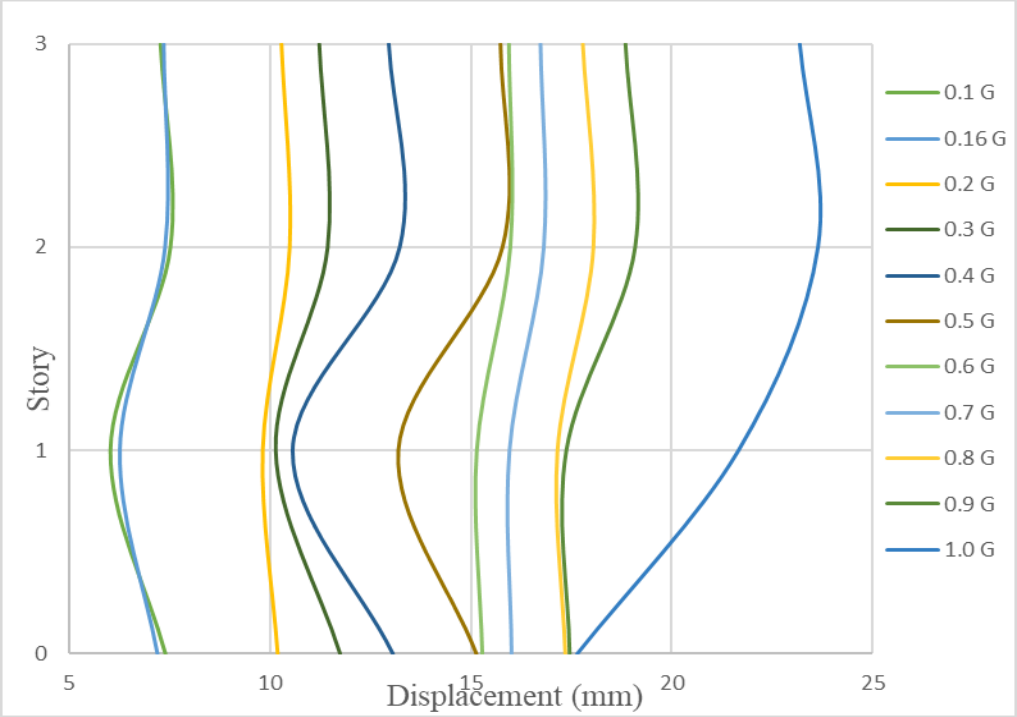

Figure 4.6: Graph of Storey Against Maximum Responded Displacement with PGA 0.1g, 0.16g, 0.2g, 0.3g, 0.4g, 0.5g, 0.6g, 0.7g, 0.8g, 0.9g and 1.0g for Model without Inverted V-Braced Damper.

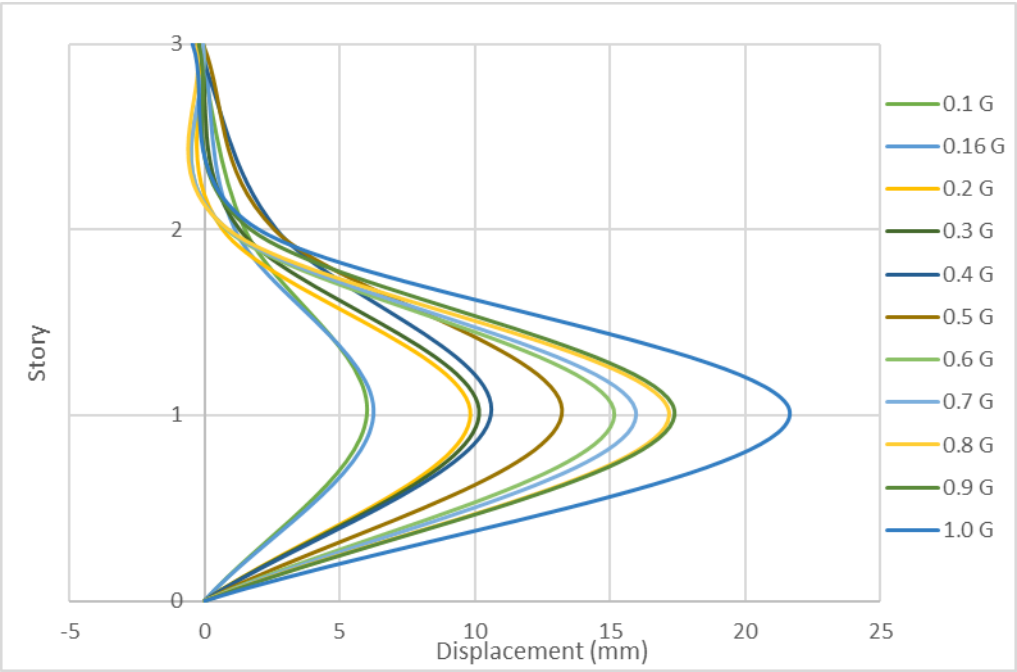

Figure 4.7: Graph of Storey Against Inter-Storey Drift with PGA 0.1g, 0.16g, 0.2g, 0.3g, 0.4g, 0.5g, 0.6g, 0.7g, 0.8g, 0.9g and 1.0g for Model without Inverted V-Braced Damper.

4.3.2 Model with Inverted V-Braced Damper

Figure 4.8 and Figure 4.9 illustrate the maximum responded displacement and inter-storey drift at each level under eleven different sets of PGA. The displacement on each floor increased as the PGA value increased except for PGA 0.16 g. Based on Figure 4.8, the maximum drift happens at the 2nd floor for all the sets of PGA except 0.1 g and 0.2 g PGA. The maximum drift for the model with inverted V-braced damper is 22.555 mm at 2nd floor when experience 1.0 g of PGA. The lowest drift happens where model experiences 0.16 g of PGA at 1st floor which is 7.3042 mm. The curved line shown in Figure 4.8 indicates the mode shape of the building. The model experiences single curvature of line when experiencing all eleven sets of PGA. Apart from that, the inter-storey drift at 1st storey is the highest as compared to 2nd and 3rd storey. The inter-storey drift also increases as the PGA increased. The maximum inter-story drift happens at the 1st floor of model experience 1.0 g which is 22.026 mm. The maximum inter-storey drift indicates the particular storey is lack of stiffness and undergo largest deformation change. Therefore, 1st storey is more vulnerable to damage during ground motion when compared to other storeys.

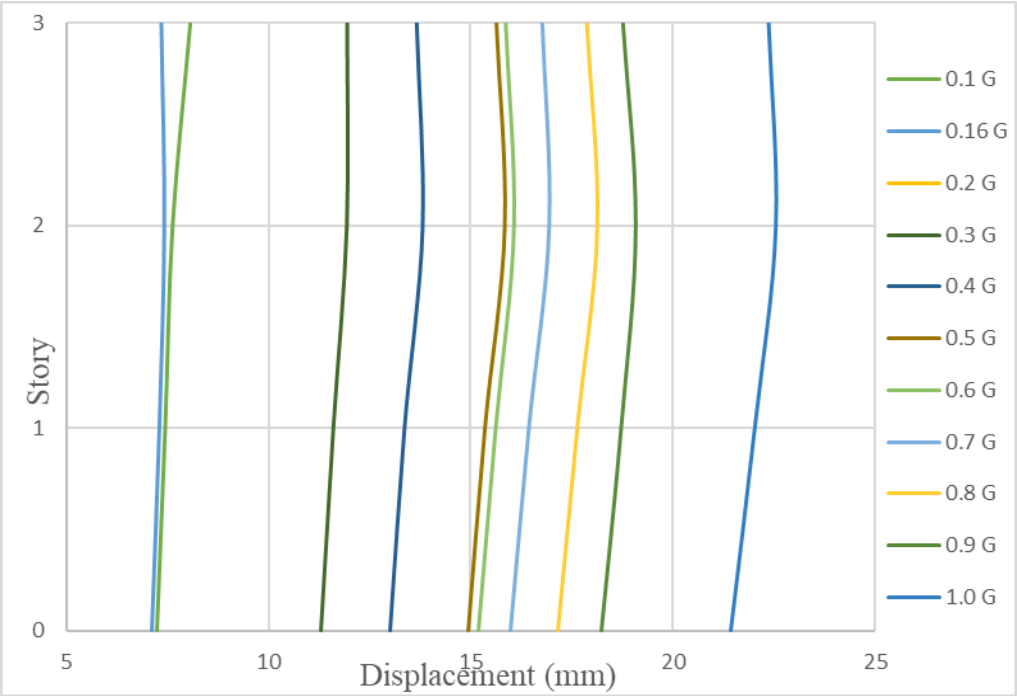

Figure 4.8: Graph of Storey Against Maximum Responded Displacement with PGA 0.1g, 0.16g, 0.2g, 0.3g, 0.4g, 0.5g, 0.6g, 0.7g, 0.8g, 0.9g and 1.0g for Model with Inverted V-Braced Damper

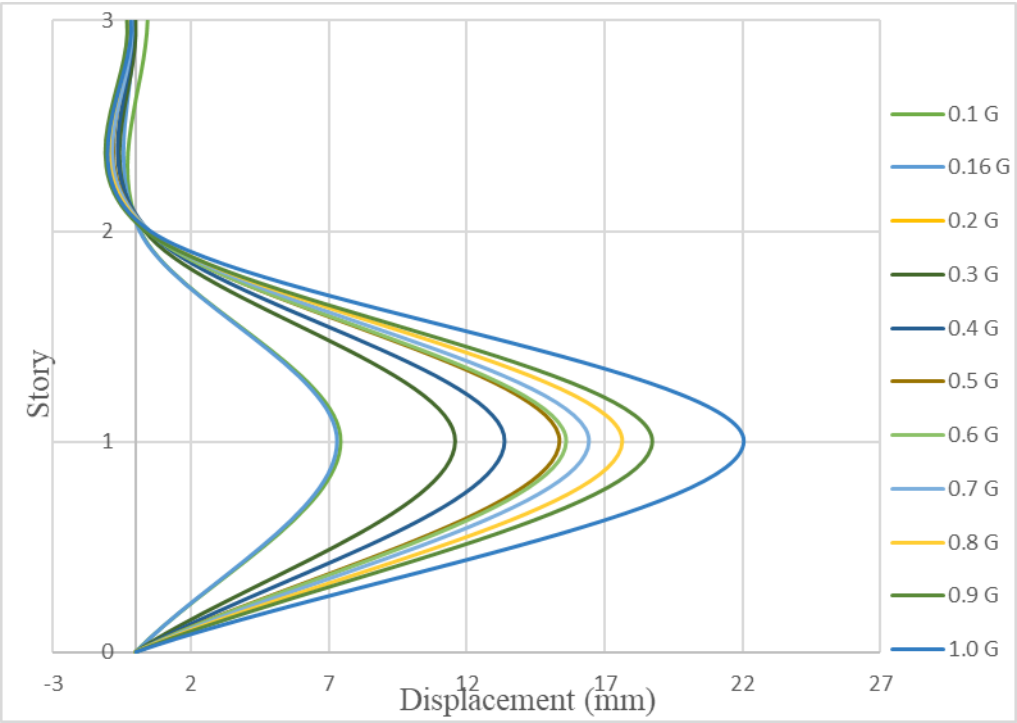

Figure 4.9: Graph of Storey Against Inter-Storey Drift with PGA 0.1g, 0.16g, 0.2g, 0.3g, 0.4g, 0.5g, 0.6g, 0.7g, 0.8g, 0.9g and 1.0g for Model with Inverted V-Braced Damper.

4.3.3 Comparison of Inter-Storey Drift

The displacement of the model will increase when the PGA increased. The maximum drift always happens on the 2nd floor in both model with and without inverted V-braced damper. The viscous damper shows slight improvement in reducing the displacement of the model. For example, the 2nd floor drift decrease from 23.65 mm to 22.555 mm when experience 1.0 g PGA in both model. The viscous damper will absorb and dissipate the seismic energy through the viscous fluid. Therefore, less seismic force is applied to the model and cause less deflection of model. Moreover, the deflection pattern of model without inverted V-damper had changed from double curvature to single curvature when equipped with viscous damper. Only single concentrated load point is formed at the single curvature. Therefore, less deflection occurs in the overall model. Besides, model with inverted V-damper also shows improvement in inter-storey drift. The inter-storey drift at 2nd storey is reduced in all eleven different sets of PGA. The maximum inter-storey drift reduction at 2nd storey is 2.207 mm where model experiences 0.4 g of PGA. However, the inter-storey drift at 1st and 3rd storey show no and slightly improvement when equipped with inverted V-braced damper. The maximum inter-storey drift at both models is at 1st storey which more vulnerable to earthquake.

4.4 Seismic Energy Dissipation

Seismic energy dissipation is the amount of seismic energy dissipated by the structure during shaking table test with different sets of PGA ranging from 0.1 g to 1.0 g. In this section, early stage (PGA 0.1 g and PGA 0.2 g), mid stage (PGA 0.5 g and PGA 0.6 g) and later stage (PGA 0.8 g and PGA 0.9 g) are classified for the comparison of seismic energy dissipation at various stages. The seismic energy dissipation is calculated through hysteresis curves for model with and without inverted V-braced. The hysteresis curves that select for analysis is at the 3rd storey due to a higher base shear is obtained. The area within the hysteresis curve for both models is calculated through the AutoCAD software. The seismic energy dissipation for model with and without inverted V-braced are discussed and compared in this section.

4.4.1 Model without Inverted V-Braced Damper

Figure 4.10 illustrates the hysteresis curve for the model without inverted V-braced damper for PGA of 0.1g, 0.2g, 0.5g, 0.6g, 0.8g and 0.9g. Figure 4.11 illustrates the global seismic energy dissipation curve of the model without inverted V-braced damper. The curve shows the higher the PGA experience by model, the higher the seismic energy dissipation.

In the early stage, the seismic energy dissipations from model are 0.59 kNmm and 3.02 kNmm. The seismic energy dissipation at early stage is low due to the higher stiffness of model at initial stage to limit any movement caused by shaking table. In the mid stage, model has seismic energy dissipation of 9.94 kNmm and 10.52 kNmm. The seismic energy dissipation is almost 3.5 times large as compare to PGA 0.2 g at initial stage. The increment of seismic energy dissipation indicates the crack formation at model such as diagonal crack. In later stage, 13.70 kN mm and 15.03 kNmm of seismic energy dissipated away from the model. The seismic dissipation energy of later stage is largest as compared to other stages due to the area under hysteresis curve is the largest. The high seismic energy dissipation of model at later stage allows some plastic hinge form at model without structural failure. This indicates occupant stay within the structure has more time to escape without failure of structural

component such as column and beam. Therefore, occupants are safe when structure experience later stage (PGA 0.8 g and PGA 0.9 g) of earthquake event.

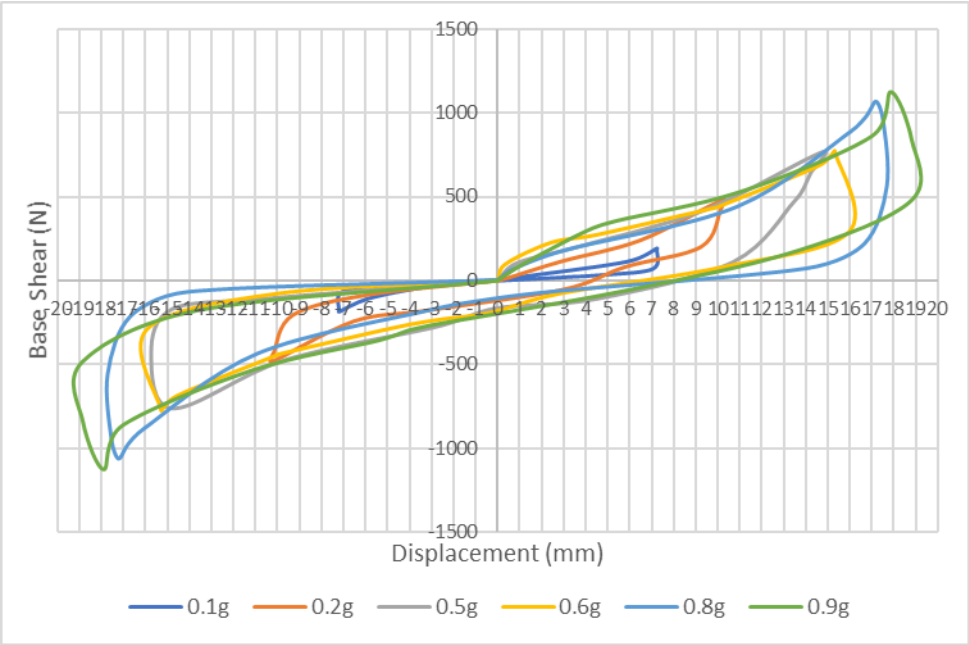

Figure 4.10: Hysteresis Curve for Model without Inverted V-Braced Damper

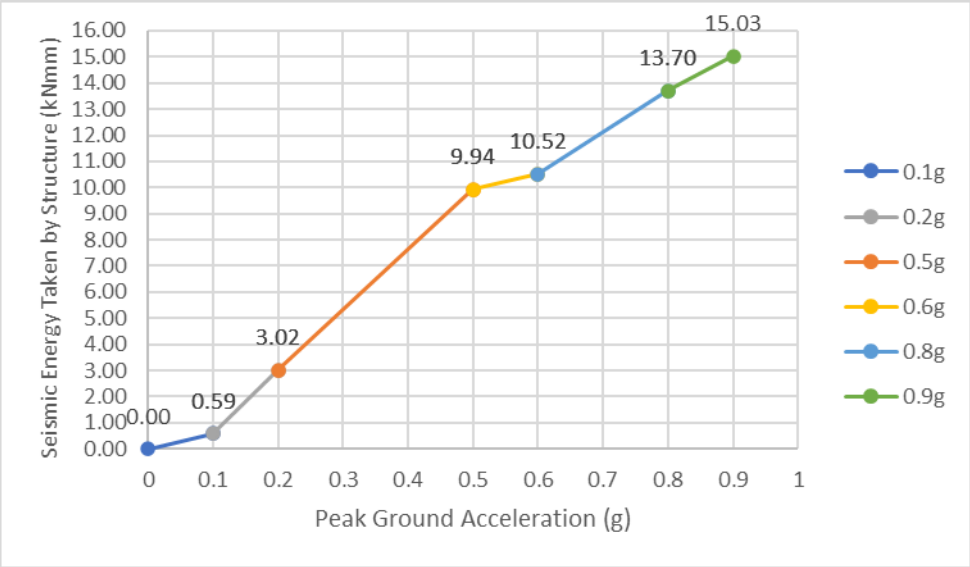

Figure 4.11: Global Seismic Energy Dissipation Curve for Model without Inverted V-Braced Damper at Different Stages.

4.4.2 Model With Inverted V-Braced Damper

Figure 4.12 illustrates the hysteresis curve for the model without inverted V-braced damper for PGA of 0.1g, 0.2g, 0.5g, 0.6g, 0.8g and 0.9g. Figure 4.13 illustrates the global seismic energy dissipation curve of the model without inverted V-braced damper. The curve shows the higher the PGA experience by model, the higher the seismic energy dissipation.

In the early stage, the seismic energy dissipation from model is 1.17 kNmm and 3.06 kNmm. The seismic energy dissipation at early stage is low due to the higher stiffness of model at initial stage to limit any movement caused by shaking table. In the mid stage, model has seismic energy dissipation of 10.10 kNmm and 13.19 kNmm. The increment of seismic energy dissipation indicates the crack formation at model such as diagonal crack. In later stage, 19.04 kN mm and 20.63 kNmm of seismic energy dissipated away from the model. The seismic dissipation energy of later stage is largest as compared to other stages due to the area under hysteresis curve is the largest. The high seismic energy dissipation of model at later stage allows some plastic hinge form at model without structural failure. This indicates occupant stay within the structure has more time to escape without failure of structural component such as column and beam. Therefore, occupants are safe when structure experience later stage (PGA 0.8 g and PGA 0.9 g) of earthquake event.

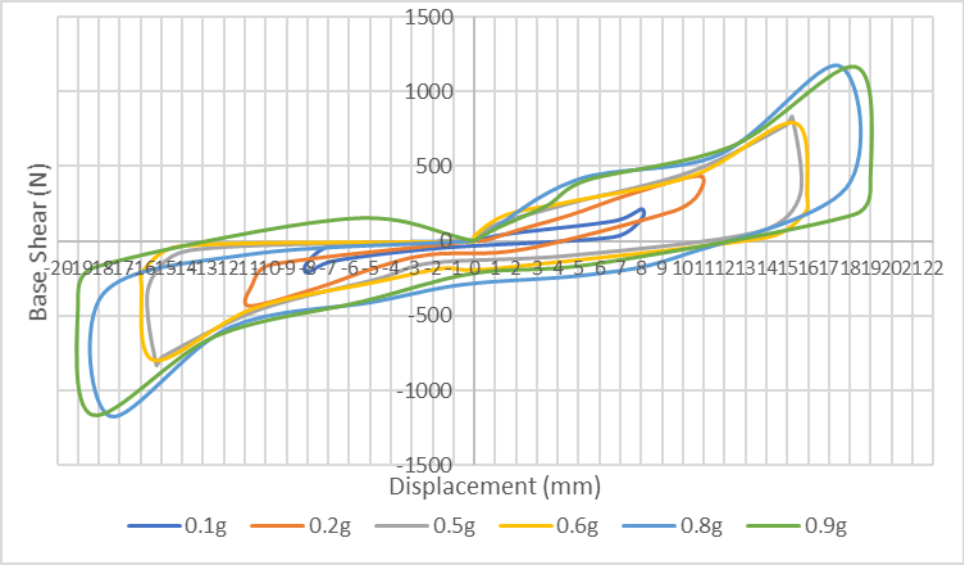

Figure 4.12: Hysteresis Curve for Model with Inverted V-Braced Damper

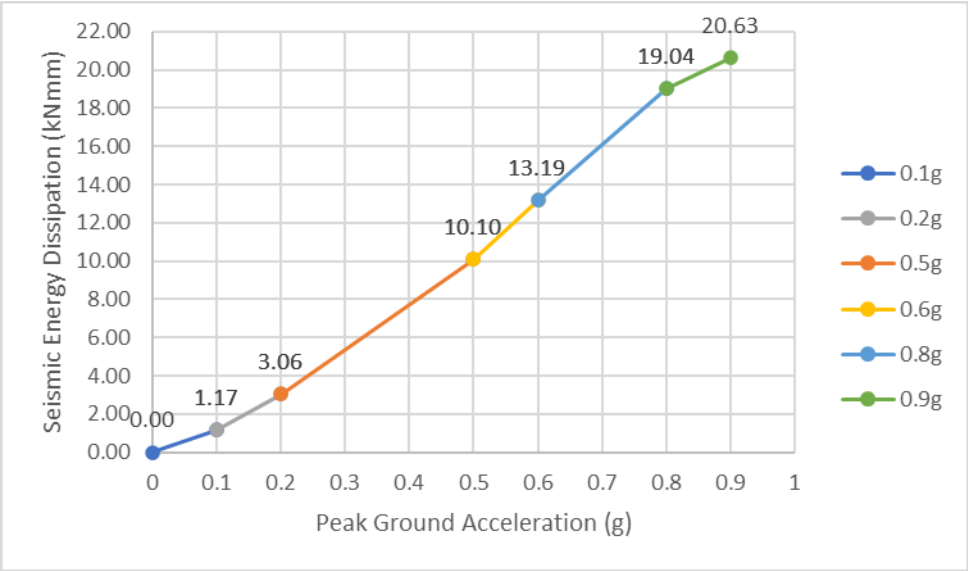

Figure 4.13: Global Seismic Energy Dissipation Curve for Model with Inverted V-Braced Damper at Different Stages.

4.4.3 Increment of Seismic Energy Dissipation

Figure 4.14 illustrates the two global seismic curve for model with and without inverted V-braced damper. In the early stage, the curve shows model equip with inverted V-braced damper has higher seismic energy dissipation. The seismic energy dissipation increment by viscous damper under PGA 0.1 g and PGA 0.2 g are 0.58 kNmm and 0.04 kNmm respectively. However, the seismic energy dissipation increment is low at early stage due to high stiffness of model at initial stage that inactivates the function of viscous damper. In the mid stage, the seismic energy dissipation increment of PGA 0.5 g and PGA 0.6 g are 0.16 g and 2.67 g respectively. Large ground acceleration by shaking table activates the viscous damper to dissipate the seismic energy and crack formation usually happened at the mid stage. Besides, the seismic energy dissipation increment is higher at the later stage. The seismic energy dissipation increment for PGA 0.8 g and PGA 0.9 g are 5.34 kNmm and 5.60 kNmm respectively. The great seismic energy dissipation by the model with inverted V-braced damper indicates high seismic energy is dissipated by viscous damper to lessen the formation of plastic hinge at later stage. Therefore, viscous damper prevents structural component failure and structure collapse by lower down the seismic energy experience at model. Table 4.1 illustrates the summary of seismic energy dissipation increment.

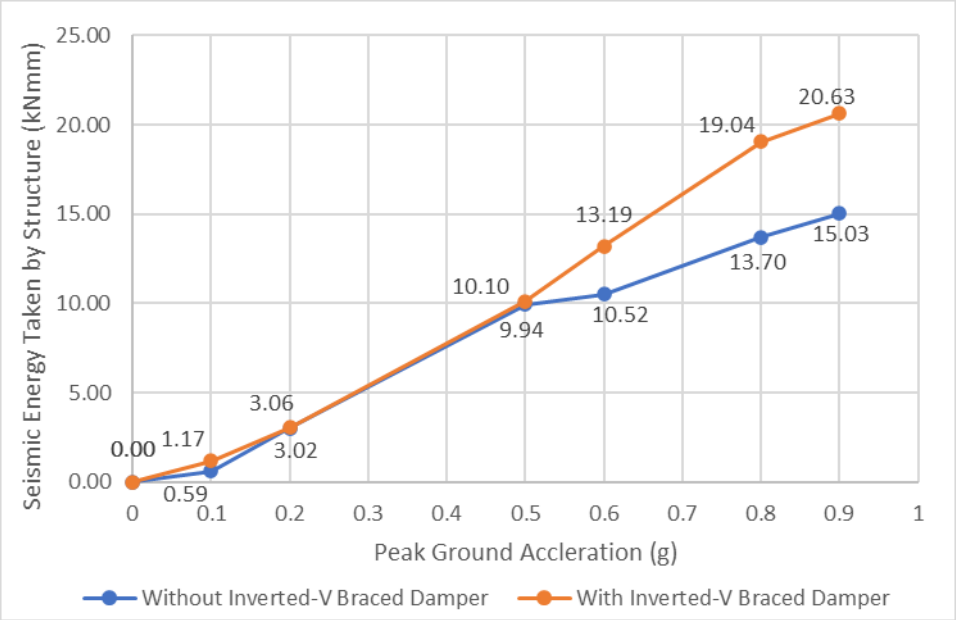

Figure 4.14: Comparison of Global Seismic Energy Dissipation Curve

Table 4.1: Summary of Seismic Energy Dissipation Increment

PGA	Seismic Energy Dissipation, kNmm		Seismic Energy Dissipation Increment (kNmm)
	Without Inverted V-Braced Damper	With Inverted V-Braced Damper	
0.1g	0.59	1.17	0.58
0.2g	3.02	3.06	0.04
0.5g	9.94	10.10	0.16
0.6g	10.52	13.19	2.67
0.8g	13.70	19.04	5.34
0.9g	15.03	20.63	5.60

4.5 Structural Damage Reliability

Weibull's reliability method is used to obtain the structural damage reliability for 1 bay 1 frame 3 storey model with and without inverted V-braced damper. The structural element selected to determine the structural damage reliability in both cases is base shear. Base shear is the summation of products of the model mass and roof spectral acceleration. Roof spectral acceleration is the highest acceleration experience by model at each PGA which will give the highest base shear according to Newton's second law, F = ma. The roof spectral acceleration for both cases was obtained through the shaking table test with 11 different sets of PGA ranging from 0.1g to 1.0g. Microsoft Excel software was used to perform Weibull's reliability analysis by using the base shear data. The structural damage reliability for both cases was discussed and compared in this section.

4.5.1 Model Without Inverted V-Braced Damper

Table 4.2: Base Shear for Model without Inverted V-Braced Damper

PGA (g)	Base Shear (N)
0.1	190.29
0.16	250.38
0.2	484.06
0.3	554.17
0.4	654.32
0.5	764.49
0.6	774.50
0.7	901.36
0.8	1064.94
0.9	1125.03
1.0	1375.41

Table 4.2 illustrates 11 sets of tested base shear data for the model without inverted V-braced damper. Table 4.3 shows the table prepared for the Weibull Analysis. The base shear data from Table 4.2 was grouped into first column (Design A) of Table 4.3 in ascending order with its own rank. 11 ranks

are available in Table 4.3. Firstly, median ranks were calculated by using Equation 4.1. Median ranks approximation is a method to lower down errors and bias in the distribution. Next, the median ranks data conversion was performed through Equation 4.2. Then, a Weibull distribution plot was plotted by Equation 4.3 against conversion of design (A) by Equation 4.4.

$$MR = \frac{(rank-0.3)}{(\sum rank+0.4)} \tag{4.1}$$

$$Conversion = \frac{1}{1-MR} \tag{4.1}$$

$$Conversion = In\left(In\left(\frac{1}{1-MR}\right)\right) \tag{4.2}$$

$$Conversion = In\,(Design\ A) \tag{4.3}$$

Table 4.3: Preparing Model without Inverted V-Braced Damper Data for Weibull Analysis.

Design A (N)	Rank	Median Ranks	1/(1-Median Rank)	In (In(1/(1-Median Rank)))	In(Design A)
190.29	1	0.061	1.065	-2.759	5.249
250.38	2	0.149	1.175	-1.823	5.523
484.06	3	0.237	1.310	-1.308	6.182
554.17	4	0.325	1.481	-0.935	6.317
654.32	5	0.412	1.701	-0.632	6.484
764.49	6	0.500	2.000	-0.367	6.639
774.50	7	0.588	2.426	-0.121	6.652
901.36	8	0.675	3.081	0.118	6.804
1064.94	9	0.763	4.222	0.365	6.971
1125.03	10	0.851	6.706	0.643	7.026
1375.41	11	0.939	16.286	1.026	7.227

Figure 4.15 shows the line fit plot for the ln(ln(1/(1-Median Rank))) versus In(Design A) under regression function in Microsoft Excel software. The purpose of plotting the line fit plot is to obtain the gradient (Weibull slope) which is the shape parameter or known as beta, β. Beta helps to indicate the behaviour of the Weibull distribution in term of failure rate. Beta is used to indicate the damage reliability of model with or without inverted V-braced damper in this project. The gradient obtains through the regression function by excel for the base shear is 1.80. (William, 2007) stated $\beta>1.0$ indicates an increasing failure rate which product was wearing out naturally. The beta 1.80>1.0 indicate the model without inverted V-braced damper will fail under fatigue due to the cyclic loading during shaking table test.

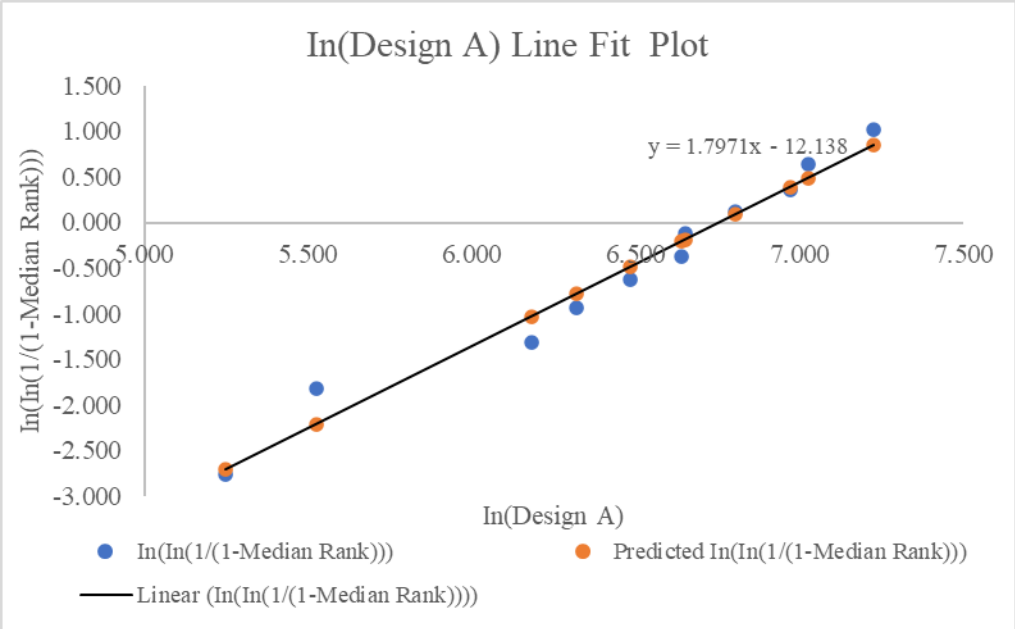

Figure 4.15: Line Fit Plot for Model without Inverted V-Braced Damper

Furthermore, scale parameter or characteristic of life, α is another important parameter required for Weibull's reliability plot. According to Figure 4.15, the intercept coefficient and ln(Design A) coefficient obtain from regression function are -12.14 and 1.80 respectively. Then, alpha, α is calculated based on Equation 4.5. The calculated scale parameter, α is 857.66. Equation 4.6 shows the reliability equation that uses for Weibull's reliability plot.

$$\alpha = EXP\left(\frac{-\,Intercept\ Coefficient\ t}{In\ (Design\ A\ Coeffiecint\ t)}\right) \tag{4.4}$$

$$R(t) = e^{-\left(\frac{x}{\alpha}\right)^{\beta}} \tag{4.5}$$

Figure 4.16 illustrates the reliability plot for the base shear of model without inverted V-braced damper. The x-axis of the plot is the base shear where the y-axis is the reliability index. Base shear x=0 indicates the model experience zero ground acceleration and the model is fully operation with the reliability index, R=1.0. The reliability plot curved shows in Figure 4.16 indicates the reliability index decreased as the base shear increased. The reliability curved is divided into three indices and three zone. Operation zone has the structural reliability in between 0.8 and 1.0. Index Immediate Occupancy (IO) in the operational zone has 0.8 structural reliability indicates 80% functional of structure under 371 N of base shear. Besides, the damage control zone has structural reliability of 0.50 which is the index Life Safety (LS). 50% structure is survived under 700N of base shear during ground motion. Moreover, limited safety zone is placed between index LS and index Collapse Prevention (CP). CP has the reliability index of 0.17 equivalent to 83% of failure of the structure under 1180N of base shear.

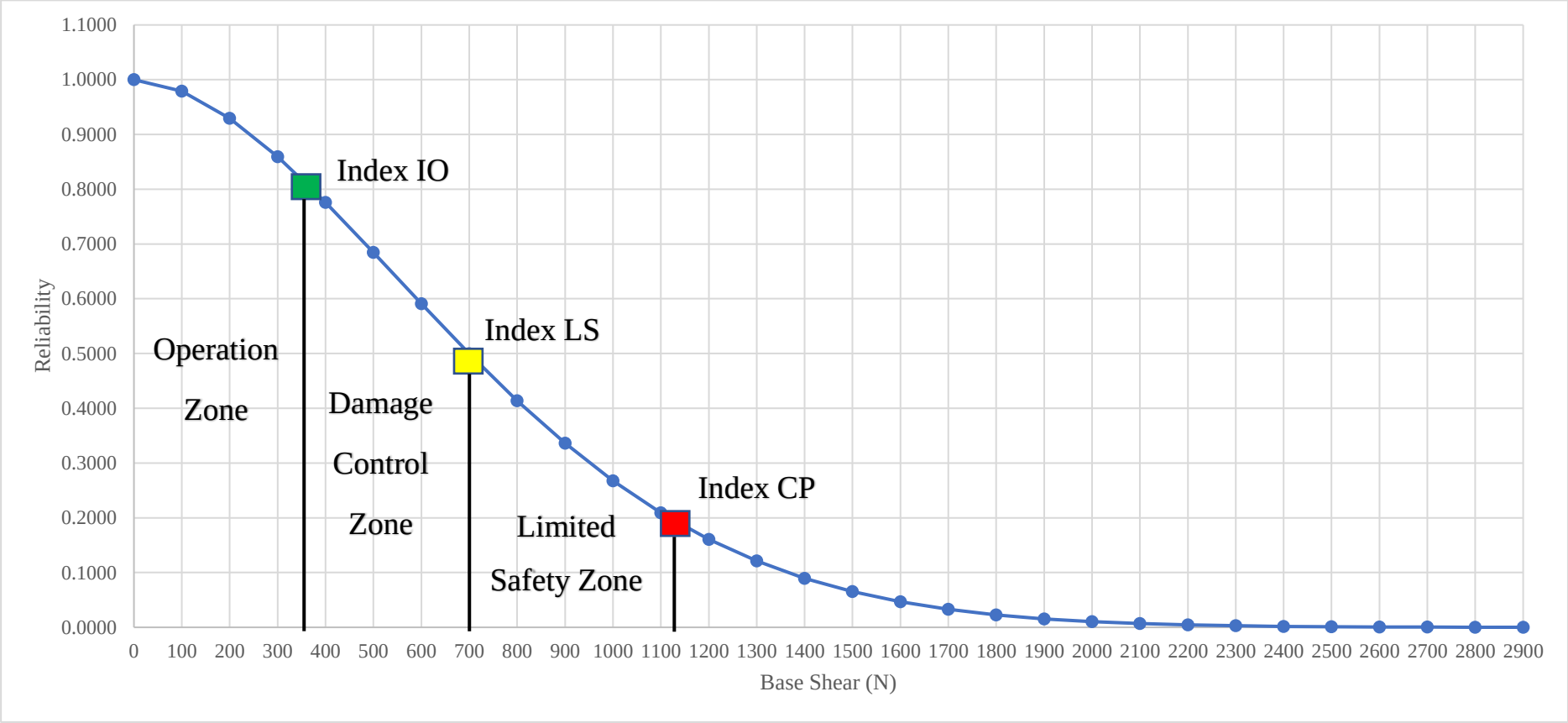

Figure 4.16: Reliability Plot for Model without Inverted V-Braced Damper

Table 4.4: Summary of the Structural Damage Reliability Model without Inverted V-Braced Damper.

PGA (g)	Base Shear (N)	Reliability index	Structural Condition	Structural Performance level
0.1	190.29	0.94	94% Functional	IO
0.16	250.38	0.84	84% Functional	IO
0.2	484.06	0.70	70% Functional	LS
0.3	554.17	0.63	63% Functional	LS
0.4	654.32	0.54	54% Functional	LS
0.5	764.49	0.44	56% Failed	CP
0.6	774.50	0.43	57% Failed	CP
0.7	901.36	0.34	66% Failed	CP
0.8	1064.94	0.23	77% Failed	CP
0.9	1125.03	0.20	80% Failed	CP
1	1375.41	0.10	90% Failed	-

Table 4.4 shows the reliability index of base shear of the model without inverted V-braced damper under eleven different sets of PGA value. The reliability index of the base shear also calculated by the reliability Equation 4.6. The model under 0.1g and 0.16g of PGA have the reliability of 0.94 and 0.84 respectively. The reliability values indicate the model is under the operational zone with IO structural performance level. The model is under the elastic zone where did not undergo permanent drift. Besides, model under 0.2g, 0.3g and 0.4g of PGA has the structural condition of 70%, 63% and 53% functional. The model under this category is in the damage control zone with reliability index LS. Part of stiffness and strength are left in all stories of model and some permanent drift occurs at the model.

The model structural reliability in between 0.2 to 0.5 has experience 0.5g to 0.9g of PGA. The model in the limited safety zone has a failure rate over 50%. The model at this zone with index CP indicates the model experiences extensive damage and large permanent lateral drifts. Besides, 90% failure has occurred where the model experience 1.0g of PGA. The reliability index has beyond the index CP and indicates the collapse of model.

4.5.2 Model with Inverted V-Braced Damper

Table 4.5: Base Shear for Model without Inverted V-Braced Damper

PGA (g)	Base Shear (N)
0.1	210.32
0.16	233.69
0.2	437.33
0.3	544.15
0.4	597.57
0.5	827.92
0.6	794.53
0.7	911.38
0.8	1171.77
0.9	1165.09
1	1415.47

Table 4.5 illustrates 11 sets of tested base shear data for the model equipped with inverted V-braced damper. Table 4.6 shows the table prepared for the Weibull Analysis. The base shear data from Table 4.5 was grouped into first column (Design A) of Table 4.6 in ascending order with its own rank. 11 ranks are available in Table 4.6. Firstly, median ranks were calculated by using Equation 4.1. Next, the median ranks data conversion was performed through Equation 4.2. Then, a Weibull distribution plot was plotted by Equation 4.3 against conversion of design (A) by Equation 4.4.

Table 4.6: Preparing Model with Inverted V-Braced Damper Data for Weibull Analysis.

Design A (N)	Rank	Median Ranks	1/(1-Median Rank)	In(In(1/(1-Median Rank)))	In(Design A)
210.32	1	0.061	1.065	-2.759	5.349
233.69	2	0.149	1.175	-1.823	5.454
437.33	3	0.237	1.310	-1.308	6.081
544.15	4	0.325	1.481	-0.935	6.299
597.57	5	0.412	1.701	-0.632	6.393
827.92	6	0.500	2.000	-0.367	6.719
794.53	7	0.588	2.426	-0.121	6.678
911.38	8	0.675	3.081	0.118	6.815
1171.77	9	0.763	4.222	0.365	7.066
1165.09	10	0.851	6.706	0.643	7.061
1415.47	11	0.939	16.286	1.026	7.255

Figure 4.17 shows the line fit plot for the ln(ln(1/(1-Median Rank))) versus In(Design A) under regression function in Microsoft Excel software. The gradient obtains through the regression function by excel for the base shear is 1.74. (William, 2007) stated $\beta > 1.0$ indicates an increasing failure rate which product was wearing out naturally. The beta 1.73>1.0 indicate the model without inverted V-braced damper will fail under fatigue due to the cyclic loading during shaking table test.

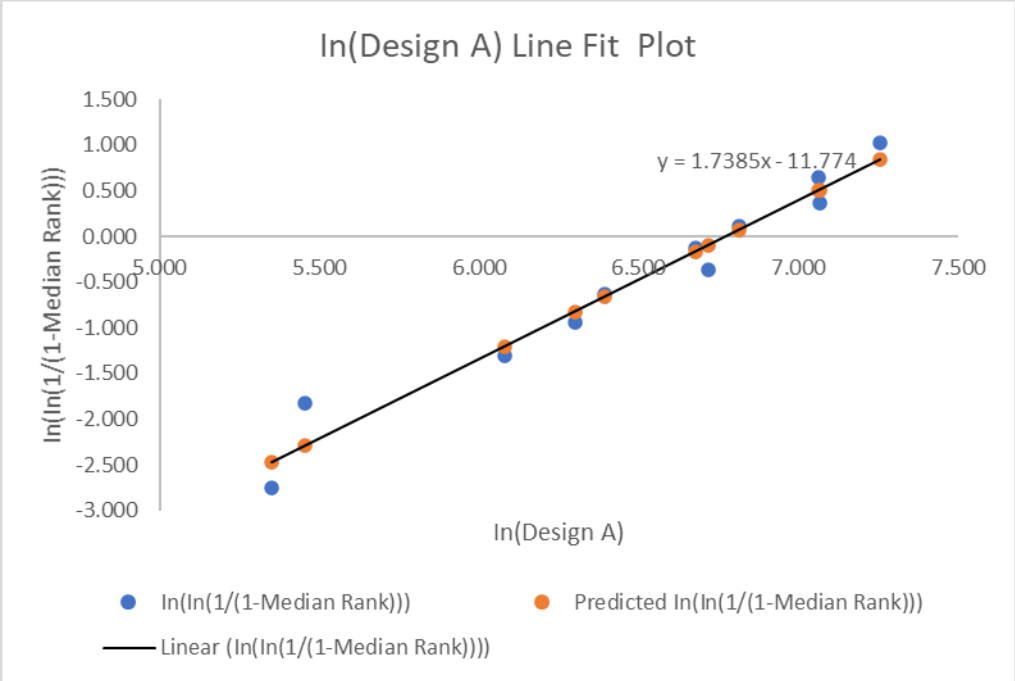

Figure 4.17: Line Fit Plot for Model with Inverted V-Braced Damper

Apart from that, scale parameter or characteristic of life, α is another important parameter required for Weibull's reliability plot. According to Figure 4.17, the intercept coefficient and ln(Design A) coefficient obtain from regression function are -11.77 and 1.74 respectively. Then, alpha, α is calculated based on Equation 4.5. The calculated scale parameter, α is 873.79.

Figure 4.18 illustrates the reliability plot for the base shear of model with inverted V-braced damper. Base shear x=0 indicates the model experience zero ground acceleration and the model is fully operation with the reliability index, R=1.0. The reliability plot curved shows in Figure 4.18 indicates as the base shear increased, reliability index decrease. The reliability curved is divided into three indices and three zone. Operation zone has structural reliability in between 0.8 and 1.0. Index Immediate Occupancy (IO) in the operational zone has 0.8 structural reliability indicates 80% functional of structure under 368 N of base shear. Besides, the damage control zone has structural reliability of 0.50 which is the index Life Safety (LS). 50% structure is survived under 700N of base shear during ground motion. Moreover, limited safety zone is placed between index LS and index Collapse Prevention (CP). CP has the reliability index of 0.17 equivalent to 83% of failure of the structure under 1215N of base shear.

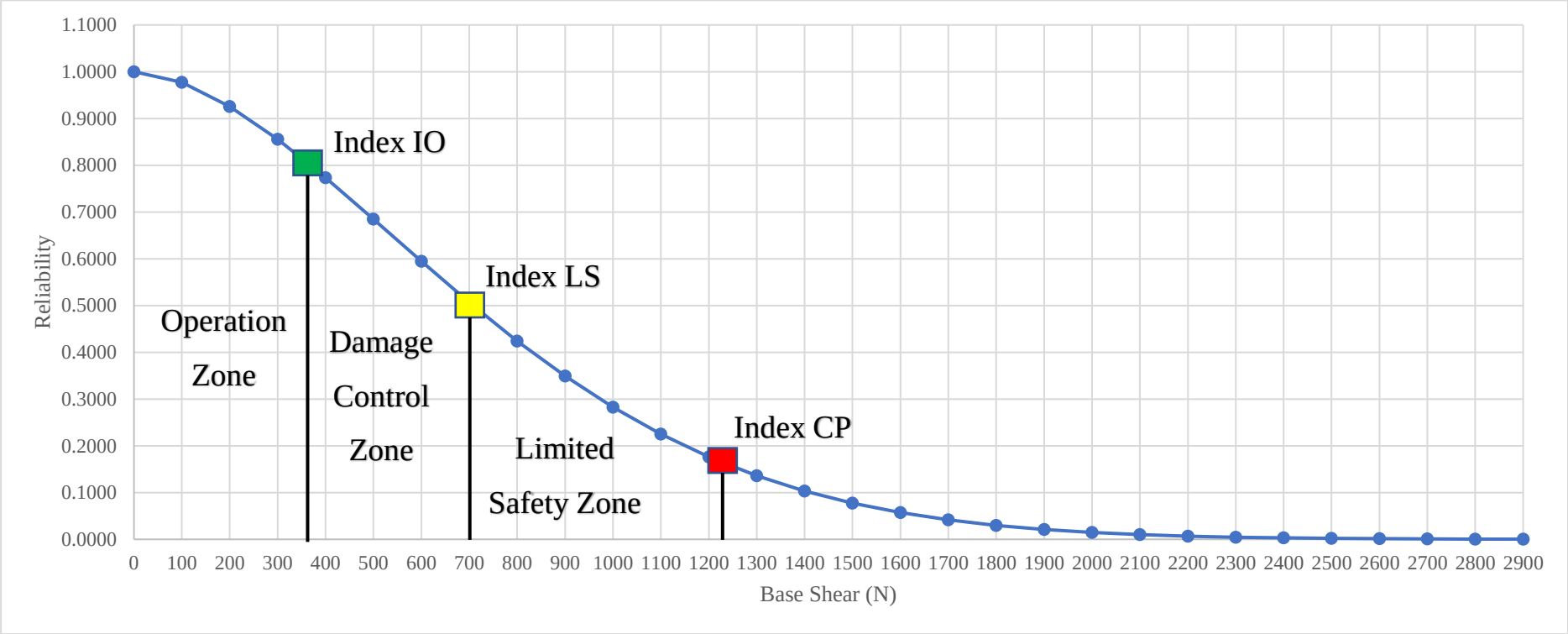

Figure 4.18: Reliability Plot for Model with Inverted V-Braced Damper

Table 4.7: Summary of the Structural Damage Reliability Model with Inverted V-Braced Damper.

PGA (g)	Base Shear (N)	Reliability Index	Structural Condition	Structural Performance Level
0.1	210.32	0.92	92% Functional	IO
0.16	233.69	0.90	90% Functional	IO
0.2	437.33	0.74	74% Functional	LS
0.3	544.15	0.64	64% Functional	LS
0.4	597.57	0.60	60% Functional	LS
0.5	827.92	0.40	60% Failed	CP
0.6	794.53	0.43	57% Failed	CP
0.7	911.38	0.34	66% Failed	CP
0.8	1171.77	0.19	81% Failed	CP
0.9	1165.09	0.19	81% Failed	CP
1.0	1415.47	0.10	90% Failed	-

Table 4.7 shows the reliability index of base shear of the model with inverted V-braced damper under eleven different sets of PGA value. The reliability index of the base shear also calculated by Equation 4.6. The model under 0.1g and 0.16g of PGA have the reliability of 0.92 and 0.90 respectively. The reliability values indicate the model is under the operational zone with index IO. The model did not undergo permanent drift and retains its structural stiffness. Besides, model under 0.2g, 0.3g and 0.4g of PGA has the structural condition of 74%, 64% and 60% functional. The model under this category is in the damage control zone with reliability index LS. Some permanent drifts and minor damages occur at the model.

The model experience 0.5g to 0.9g of PGA has the structural reliability in between 0.2 to 0.5. The model in the limited safety zone has the failure rate over 50% but less than 83%. The model at this zone with index CP indicates the model experiences extensive damage and large permanent lateral drifts. Besides, 90% failure has occurred where the model experience 1.0g of PGA. The reliability index has beyond the index CP and indicates the collapse of model.

4.5.3 Comparison of Structural Damage Reliability

The beta value for both cases is greater than one indicates both models under increasing failure rate. Besides, the structural reliability is dropped when model experiences higher PGA due to higher base shear induced in both cases. The structural performance for both model with and without inverted V-braced damper experience 0.1 g and 0.16 g of PGA is immediate occupancy. Some improvement of the reliability index for the model equipped with inverted V-braced damper that experiences 0.16 g, 0.2 g, 0.3 g and 0.4 g of PGA can be noticed. The structural reliability of PGA 0.16g, PGA 0.2g, PGA 0.3g and PGA 0.4g improve from 0.84 to 0.90, 0.70 to 0.74, 0.63 to 0.64 and 0.54 to 0.60 respectively. The improvement of reliability index indicates model with inverted V-braced damper can have a higher percent of structure functionality when experiencing the same PGA as compared to model without inverted V-braced damper. Moreover, the percentage of base shear improvement with different structural performance level is important for computation. The base shear at index IO drops 0.81% and 0% improvement at index LS. However, the base shear at index CP improved with 2.97% from 1180 N to 1215N. The base shear improvement at index CP indicates model can withstand higher base shear during earthquake before collapse. In short, structural damage reliability analysis is to analyse the reliability and damage of reinforced concrete building when experiencing different intensity of ground motion. The 1 bay 1 frame 3 storey reinforced concrete model with and without inverted V-braced damper under PGA 0.1 g and PGA 0.6 g with no damage to the model; PGA 0.2 g, PGA 0.3 g and PGA 0.4 g with minor damage to the model; PGA 0.5 g, PGA 0.6 g, PGA 0.7 g, PGA 0.8 g and PGA 0.9 g with extensive damage to the model; PGA 1.0 g with model collapse.

4.6 Summary of Results and Discussion

In summary, 1 bay 1 frame 3 storey reinforced concrete building with and without inverted V-braced damper that undergoes shaking table test under eleven different sets of PGA is analysed and compared in this chapter. The analysis result and discussion are divided into four main sections. The first section discusses the spectral acceleration of the model at each floor. The difference in spectral acceleration is explained by various mass to return at each floor. The highest spectral acceleration always acquires at the roof floor. Inter-storey drift is discussed and compared in the next section under different sets of PGA. The inter-storey drift is analysed by computing differences in lateral displacement between top and bottom floor. The maximum inter-storey always indicates the particular storey undergo the largest deformation due to lack of stiffness. Then, seismic energy dissipation of model with and without inverted V-braced is discussed and compared in the next section. The seismic energy dissipation is obtained through the area of hysteresis loop under three stages which is initial stage, mid stage and later stage. The finding under this section is to understand the seismic energy dissipation increment by the viscous damper. Structural damage reliability analysis is presented in the last section of the result and discussion chapter. Weibull's Reliability Analysis is used to perform the reliability index. The outcome of the analysis is to comprehend the reliability index, damages and structural performance level of the model with and without inverted V-braced damper under various sets of PGA.

CHAPTER 5

CONCLUSIONS AND RECOMMENDATIONS

5.1 Conclusions

The research is concluded with the accomplishment of three research aims and objectives. The first objective of the research is to construct a 1 bay 1 frame 3 storey reinforced concrete structure in laboratory. A 1 bay 1 frame 3 storey scaled down model is constructed according to the C&S and architecture drawings. The model is scaled with a factor 1:8 to fit the 2m x 2m of shaking table. The dimension of the scaled model is 1500mm x 750mm x 750mm and the mass is 175kg. The reinforced concrete scaled model is constructed with 3 mm steel reinforcement, 1mm steel wire shear links and concrete grade of 30 N/mm^2 for 28days. Trial mix and compression strength test are performed to determine a suitable concrete mixture that achieves concrete grade of $30N/mm^2$. The concrete mixture used to construct the scaled model is OPC, water, fine sand, fine aggregate and plasticiser. The fine sand and fine aggregates are 100 µm and 5nm respectively to fit the spacing of the reinforcement. Plywood formwork is used to shape the scaled model with accurate dimension during concrete casting.

The second objective is to apply suitable levels of dynamic loads for the structure with and without inverted V-bracing dampers. The 1 bay 1 frame 3 storey scaled model with and without inverted V-brace damper underwent earthquake simulation by shaking table test with different levels of dynamic loads. The shaking table test is in one-directional. The installed inverted V-braced dampers are parallel to the shaking direction. The dynamic loads are in simple cycle motion with eleven different sets of PGA. The PGA values are 0.1g , 0.16g, 0.2g, 0.3g, 0.4g, 0.5g, 0.6g, 0.7g, 0.8g, 0.9g and 1.0g.

The third objective is to assess structural reliability based on the structural behaviour, spectral accelerations and seismic energy dissipation curve for both with and without inverted V-braced damper structure. The three objectives can be outlined relate to the results and discussion. Firstly, the spectral acceleration is obtained through the accelerometer placed at each floor

of the model during shaking table test. The spectral acceleration at each floor of model with and without inverted V-braced dampers under eleven different sets can be concluded with

i. The spectral acceleration increases as the PGA increases in both model.
ii. The maximum spectral acceleration always happens at the roof floor as compared to 1st floor and 2nd floor in both model regardless the PGA values. The mass taken by first, second and third storey to return are dissimilar.
iii. The maximum spectral acceleration for model with and without inverted V-braced damper is 8.088 m^2/s and 7.859 m^2/s respectively in the case of both model experience PGA 1.0 g at roof floor.
iv. The roof spectral acceleration of model with inverted V-braced damper is reduced at PGA of 0.16 g, 0.2 g, 0.3 g and 0.4 g. A maximum 9.66% of spectral acceleration reduction happens when model experience 0.2 g of PGA.
v. The roof spectral acceleration at PGA 0.1 g, 0.5 g, 0.6 g, 0.7 g, 0.8 g, 0.9 g and 1.0 g are slightly higher at the model with inverted V-braced damper.

Next, seismic energy dissipation is the amount of seismic energy dissipated by structure during earthquake simulation. Three stages are categorised for comparison seismic energy dissipation at various stage. The stages are early stage (PGA 0.1 g and PGA 0.2 g), mid stage (PGA 0.5 g and PGA 0.6 g) and later stage (PGA 0.8 g and PGA 0.9 g). The seismic energy dissipation is calculated through the area of hysteresis curve at 3rd storey. The seismic energy dissipation for model with and without inverted V-braced can be concluded with

i. The seismic energy dissipation increases as the PGA increase in both model.
ii. The highest seismic energy dissipation of model with and without inverted V-braced damper is 20.63 kNmm and 15.03

kNmm respectively in the case of both model experience PGA 0.9 g.

iii. The seismic dissipation energy increment by model with inverted V-braced damper compare to model without inverted V-braced damper at early stage is low because of great stiffness of model at initial stage. The seismic dissipation energy increment at mid stage is increase slightly due to the activation of viscous damper to dissipate seismic energy from the structure. Later stage have the highest seismic energy dissipation increment with 5.34 kNmm and 5.60 kNmm at PGA 0.8 g and 0.9 g respectively. The high seismic energy dissipation increment shows viscous dampers have dissipated the seismic energy efficiently from model.

Lastly, Weibull's reliability method is used to assess the structural reliability analysis. Microsoft Excel software is used to perform Weibull's reliability analysis by using the base shear data obtain through spectral acceleration at roof floor. The structural damage reliability for model with and without inverted V-braced model can be concluded with

i. The beta value of mode with and without inverted V-braced damper are 1.73 and 1.80 respectively which more than 1.0 indicate the model under increasing failure rate.

ii. The reliability plot illustrates the reliability index decrease with the base shear increases for both model.

iii. The reliability index improves at the model with inverted V-braced damper that experiences PGA of 0.16 g, 0.2 g, 0.3 g and 0.4 g. The improvement represents the model with inverted V-braced dampers have higher structure functionality when experience PGA of 0.16 g, 0.2 g, 0.3 g and 0.4 g as compare to model without inverted V-braced damper.

iv. Base shear at index CP improved with 2.97% which indicates model with inverted V-braced damper can withstand higher base shear before collapse.

v. The structural performance level of both model experience PGA of 0.1 g and 0.16 g is IO where no damage at the model. The structural performance level of both mode experience PGA of 0.2 g, 0.3 g and 0.4 g is LS where minor damage happens at model. The structural performance level of both mode experience PGA of 0.5 g, 0.6 g, 0.7 g, 0.8 g and 0.9 g is CP where extensive damage happens to the model. Both model experience PGA 1.0 g have beyond the CP level which indicates collapse of model.

5.2 Recommendations for future work

In this research, some recommendation and future improvement for dynamic load energy dissipation of low-rise reinforced concrete building with and without inverted V-braced damper are stated as follows.

i. The dynamic load energy dissipation of low-rise reinforced concrete building with and without inverted V-braced damper can be carried out by structural analysis software such as MidasGen, SAP2000 and SCIA Engineer. Thus, a comparison and new conclusion can be drawn based on the experimental test and structural analysis software.

ii. A bi-directional earthquake simulation by shaking table test shall be performed in the future to create a more realistic earthquake ground motion to the structure.

iii. The seismic energy dissipation can be further carried out for mid-rise and high-rise reinforce concrete building to study the behaviour of building under different sets of PGA.

iv. Adopting other earthquake resistance system and devices on the model to analyse the structure seismic energy dissipation. Thus, a comparison and new conclusion can be made for the seismic

energy dissipation efficiency by other earthquake resistance system and devices. For examples, X-bracing, base isolation, friction damper, bricks wall and shear wall the recommended.

REFERENCES

Adiyanto, M.I. and Majid, T.A., 2014. Seismic design of two storey reinforced concrete building in Malaysia with low class ductility. *Journal of Engineering Science and Technology*, *9*(1), pp.27-46.

Agrawal, A.K. and Amjadian, M., 2016. Seismic component devices. In *Innovative bridge design handbook* (pp. 531-553). Butterworth-Heinemann.

Anderson, J.C. and Naeim, F., 2012. *Basic structural dynamics*. John Wiley & Sons.

Applied Technology Council (ATC)., 2020. Building Safety and Earthquakes: Earthquake Forces in Building. *The Path to Quality Seismic Design and Construction.* [online]. Available at <https://www.atcouncil.org/pdfs/bp1b.pdf> [Accessed 11 August 2020]

Arnold, C., 2006. Designing for earthquakes: A manual for architects. Mimari Tasarımda Deprem, Fema, 454.

Australian Bureau of Statistic, 2019. *Building Activity, Australia, Dec 2018.* [online]. Available at < https://www.abs.gov.au/ausstats/abs@.nsf/Lookup/8752.0Feature+Article1Dec%202018>. [Accessed 22 August 2020]

British Geological Survey, 2020. *Plate tectonics.* [online]. Available at<https://www.bgs.ac.uk/discoveringGeology/hazards/earthquakes/plateTectonics.html>[Accessed 15 August 2020].

Center For Excellence in Disaster Management & Humanitarian Asistance, (2016). *Malaysia Disaster Management Reference Handbook.* [online]. Available at <https://reliefweb.int/sites/reliefweb.int/files/resources/disaster-mgmt-ref-hdbk-Malaysia.pdf.pdf> [Accessed 2 August 2020]

Corporation, R. (2015) 'ReliaSoft's Life Data Analysis'.

Damtech Earthquake Protection., 2015. Diagonal bracing. *Damtech Earthquake Protection,* [online] Available at: <https://www.damptech.com/diagponal-bracing> [Accessed 27 February 2021].

Daniell, J.E., Schaefer, A.M. and Wenzel, F., 2017. Losses associated with secondary effects in earthquakes. *Frontiers in Built Environment*, *3*, p.30.

Dhande, S.N., Suryawanshi, Y.R. and Patil, P.S., 2015. Industrial Building Design on Seismic Issues.

Federal Emergency Management Agency., 1996. *FEMA 273 NEHRP Guidelines for the seismic rehabilitation of building*. Washington, D.C: Building Safety Seismic Council.

FHWA, 2010. Earthquake-resistant design concepts–An introduction to the NEHRP recommended seismic provisions for new buildings and other structures. *FEMA P-749/2009 Edition*.

Ghobarah, A., 2004. On drift limits associated with different damage levels. In International workshop on performance-based seismic design (Vol. 28). Dept. of Civil Engineering, McMaster University.

Hamburger, R.O. and Gumpertz, S., 2009. Facts for steel buildings: Earthquakes and seismic design. *American Institute of Steel Construction*Building

Hilti, 2020. *Dynamic loads and Application.* [online]. Available at <https://www.construmatica.com/archivos/46568/manual_calculo_dinamico.pdf> [Accessed 10 August 2020]

Kappos, A., 2014. *Earthquake resistant concrete structures*. CRC Press.

Kukuplaut.com, 2018. *How safe is Malaysia from Natural Disasters?* [online]. Available at <https://kukuplaut.com/how-safe-is-malaysia-from-natural-disasters/#:~:text=Malaysia%20is%20not%20earthquake%2Dfree,no%20major%20earthquakes%20in%20Malaysia.&text=However%2C%20Malaysia%20is%20now%20an,the%20coast%20of%20West%20Malaysia.> [Accessed 2 August 2020]

Lin, W., and Yoda, T., 2017. Loads and Load Distribution. *Bridge Engineering*, pp 71-83.

Lorant, G., 2012. Seismic design principles. *National Institute of Building Sciences. Available [online]*, pp.01-10.

Matthew, J. S. 2000. Reliability-Based Seismic Performance Evaluation of Steel Frame Buildings using Nonlinear Static Analysis Methods. University Of California, Los Angeles.

Miranda, E., 1996. Assessment of the seismic vulnerability of existing buildings. In *11th World Conference on Earthquake Engineering*.

Murty, C.V.R., Goswami, R., Vijayanarayanan, A.R. and Mehta, V.V., 2012. Some concepts in earthquake behaviour of buildings. *Gujarat State Disaster Management Authority, Government of Gujarat*.

National Research Council. 2003. *Preventing Earthquake Disasters: The Grand Challenge in Earthquake Engineering: A Research Agenda for the Network for Earthquake Engineering Simulation (NEES)*. Washington, DC: The National Academies Press.

Ozturk, M. and Ogutcu, T.F., 2018. An Experimental Study on the Strengthening of RC Frames with Soft Storey Irregularities with Different Types of Steel Diagonals. *Periodica Polytechnica Civil Engineering*, *62*(4), pp.1067-1075.

Patil, Pravin & Sonar, Ishwar. (2018). *RCC STRUCTURE WITH DIFFERENT BRACING CONFIGURATION ON SEISMIC ISSUES.*

R. E. Bichell, 2016. *Where The Biggest Earthquake Ever Recorded Hit Chile, It Rocked The World.* [online] NPR.org. Available at < https://www.npr.org/2016/08/29/490239181/when-the-biggest-earthquake-ever-recorded-hit-chile-it-rocked-the-world> [Accessed 14 August 2020].

Rajasekaran, S., 2009. *Structural dynamics of earthquake engineering: theory and application using MATHEMATICA and MATLAB*. Elsevier.

Saatcioglu M., 2013 Structural Mitigation. In: Bobrowsky P.T. (eds) Encyclopedia of Natural Hazards. Encyclopedia of Earth Sciences Series. Springer, Dordrecht. https://doi.org/10.1007/978-1-4020-4399-4_334

Saatcioglu, M. 2013. Structural Damage Caused by Earthquakes. *Encyclopedia of Earth Sciences Series*, 947–959. doi:10.1007/978-1-4020-4399-4_346

Saruddin, S.N.A. and Nazri, F.M., 2015. Fragility curves for low-and mid-rise buildings in Malaysia. *Procedia Engineering*, *125*, pp.873-878.

Sen, T.K., 2009. *Fundamentals of seismic loading on structures*. John Wiley & Sons.

Tongkul, F., 2016. The 2015 Ranau Earthquake: cause and impact. *Sabah Society Journal*, 32, pp.1-28.

U.S Geological Survey (USGS), 2020. *20 Largest Earthquake in the World.* [online]. Available at < https://www.usgs.gov/natural-hazards/earthquake-hazards/science/20-largest-earthquakes-world?qt-science_center_objects=0#qt-science_center_objects> [Accessed 14 August 2020].

Weibull.com., 2021. Characteristics of the Weibull Distribution. [online]. Available at < Weibull Distribution: Characteristics of the Weibull Distribution> [Accessed 28 February 2021].

William, D. (2007). *Using Microsoft Excel for Weibull Analysis*. 290 Airpark Blvd. Chico, CA 95973: Quality Digest Publisher.

Yön, B., Sayın, E. and Onat, O., 2017. Earthquake and structural damages. *Earthquakes-Tectonics, Hazard and Risk Mitigation*, pp.319-339.

Yuen, M. K., 2017. Safer buildings in the works. *The Star online*, [online] 12 February. Available at https://www.thestar.com.my/news/nation/2017/02/12/safer-buildings-in-the-works-safer-buildings-in-the-works-a-new-design-code-for-buildings-in-malaysi/> [Accessed 2 August 2020]

Zhou, Y., Chen, P., Wang, C., Zhang, L. and Lu, L., 2018. Seismic performance evaluation of tall, multitower reinforced concrete buildings with large bottom podiums. *Structural Concrete*, *19*(6), pp.1591-1607.

APPENDICES

APPENDIX A: Acceleration and Displacement Graph of Model with and without Inverted V-Braced Damper under Eleven Different Sets of PGA.

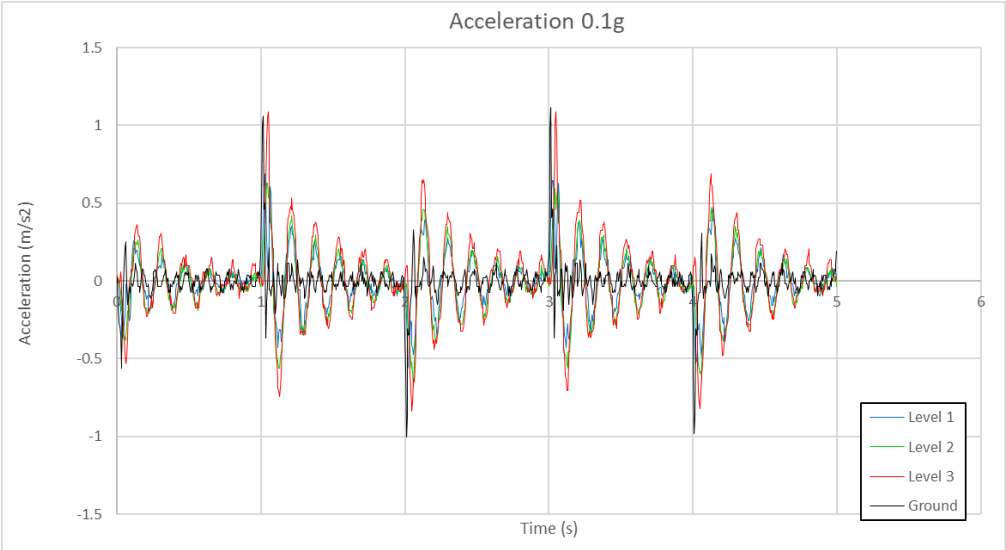

Figure A-1: Acceleration of Model without Inverted V-braced Damper at PGA 0.1g.

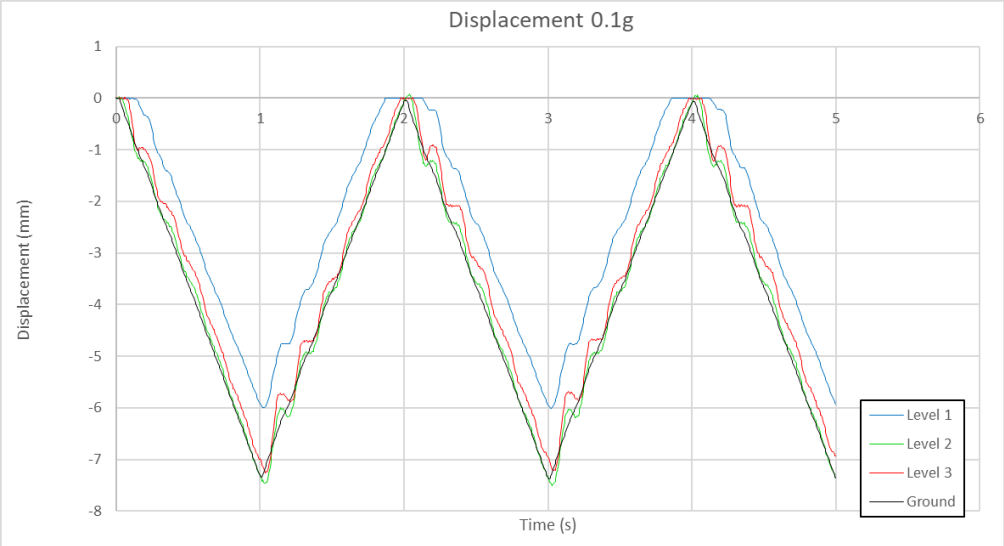

Figure A-1: Displacement of Model without Inverted V-braced Damper at PGA 0.1g.

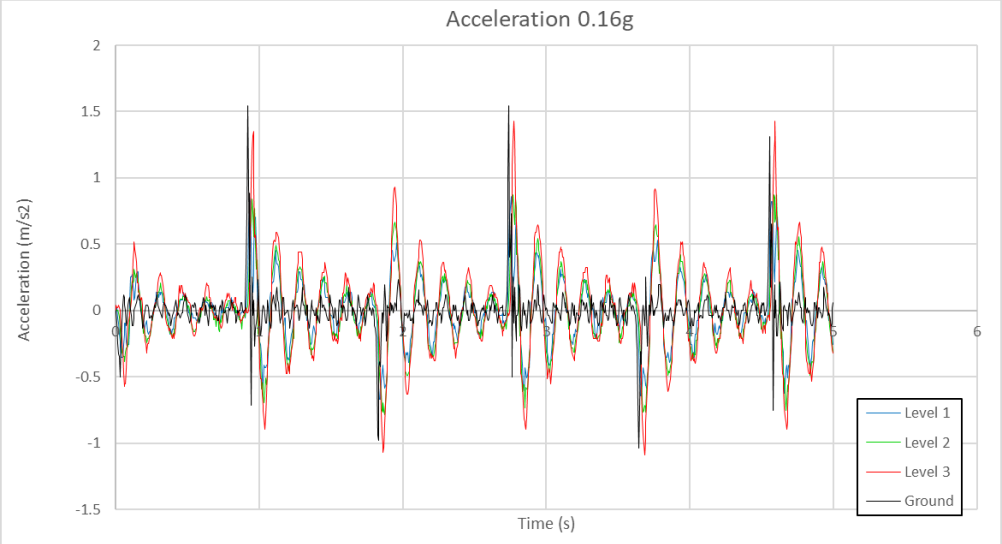

Figure A-3: Acceleration of Model without Inverted V-braced Damper at PGA 0.16g.

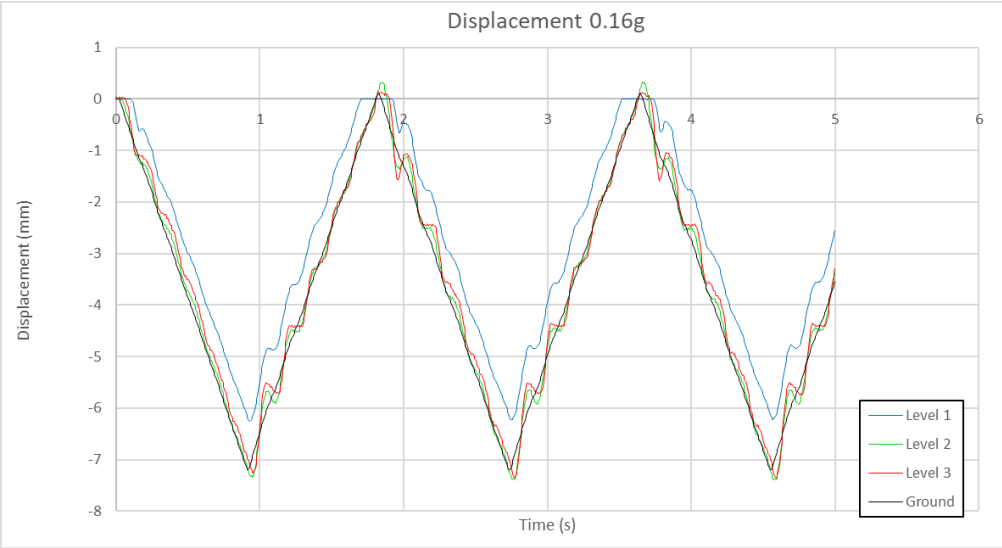

Figure A-4: Displacement of Model without Inverted V-braced Damper at PGA 0.1g.

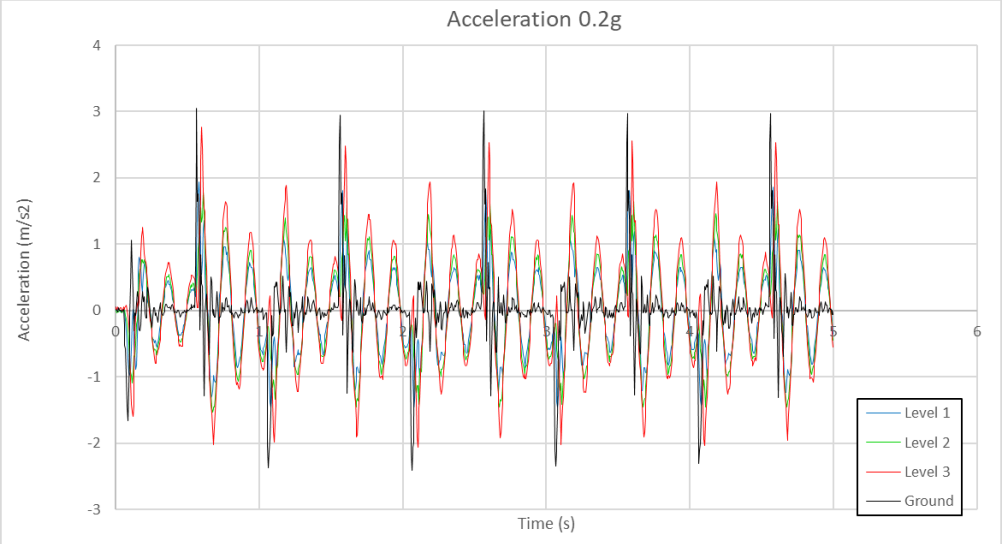

Figure A-5: Acceleration of Model without Inverted V-braced Damper at PGA 0.2g.

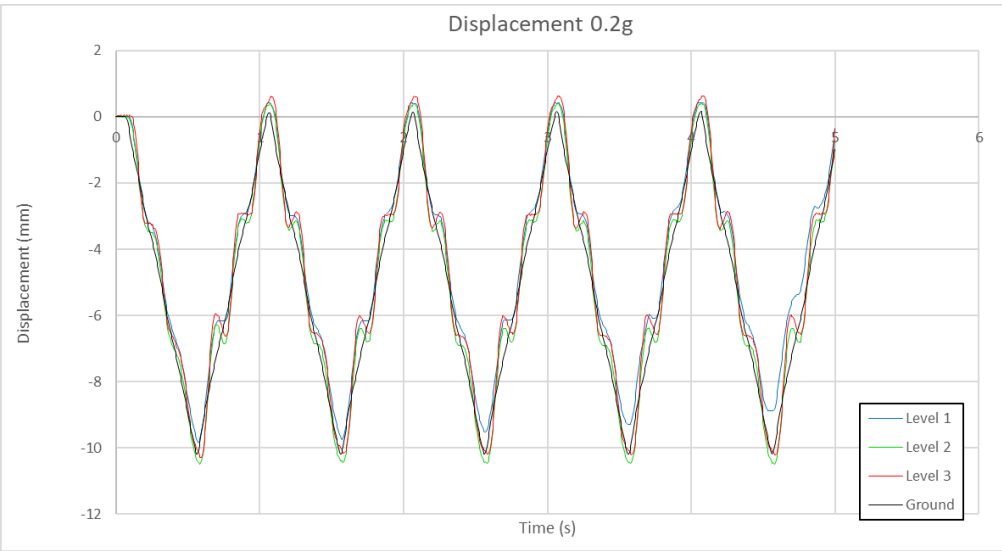

Figure A-6: Displacement of Model without Inverted V-braced Damper at PGA 0.2g.

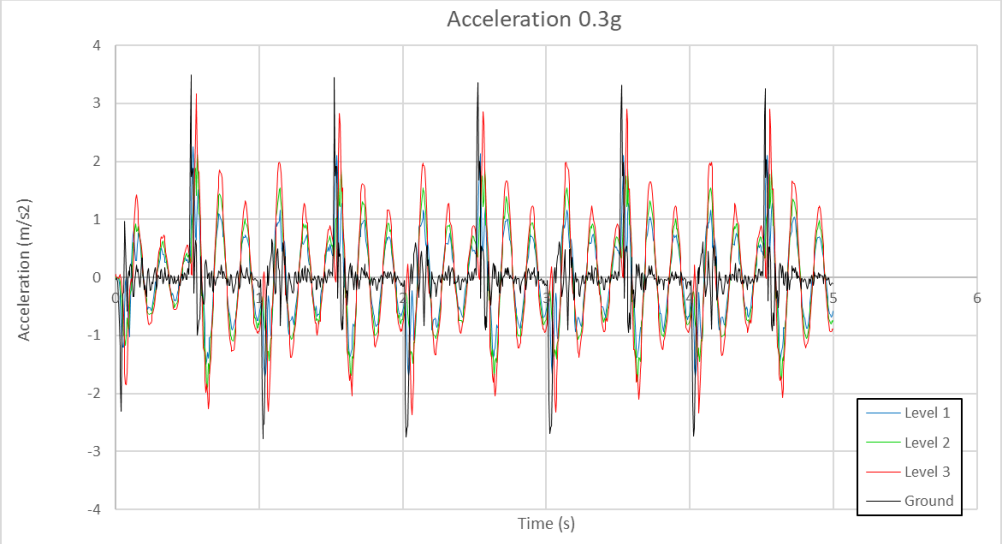

Figure A-7: Acceleration of Model without Inverted V-braced Damper at PGA 0.3g.

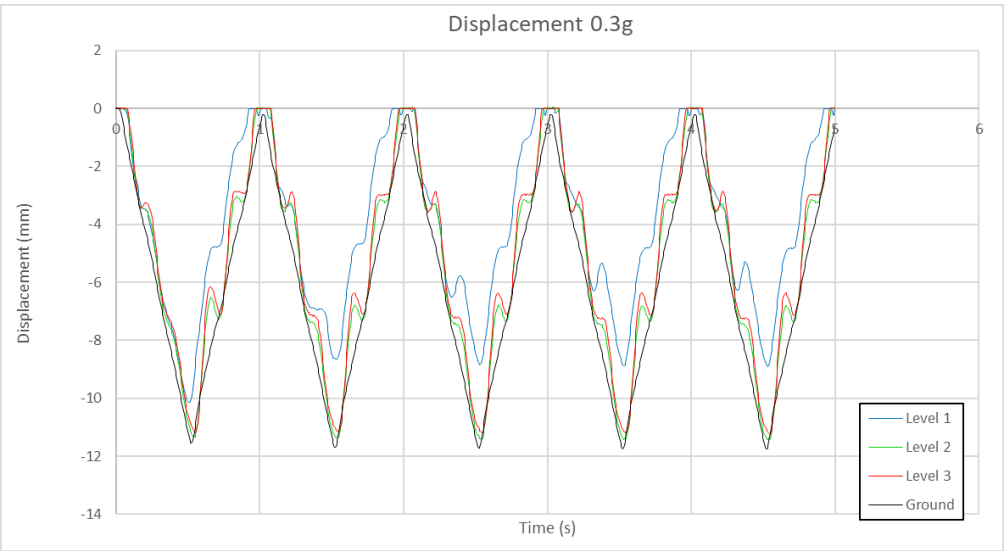

Figure A-8: Displacement of Model without Inverted V-braced Damper at PGA 0.3g.

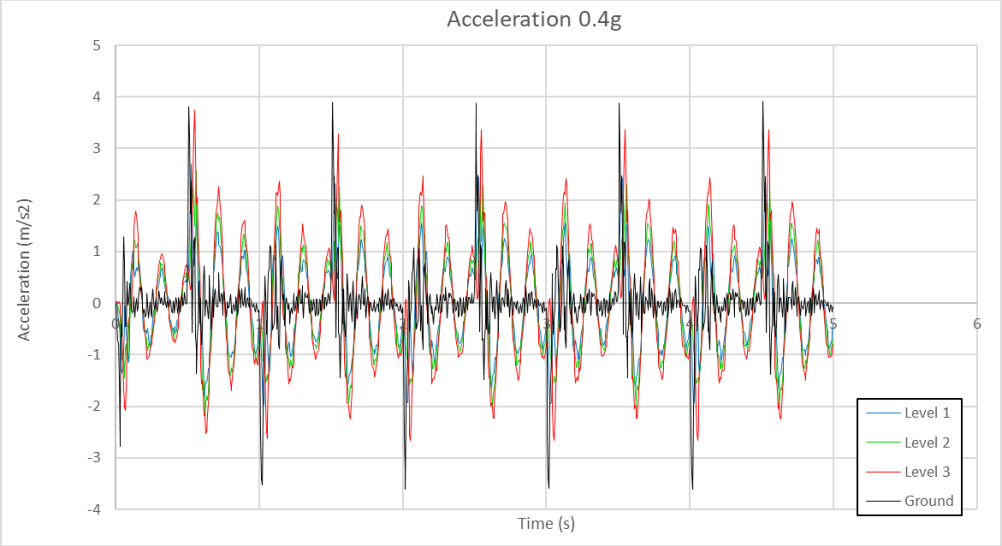

Figure A-9: Acceleration of Model without Inverted V-braced Damper at PGA 0.4g.

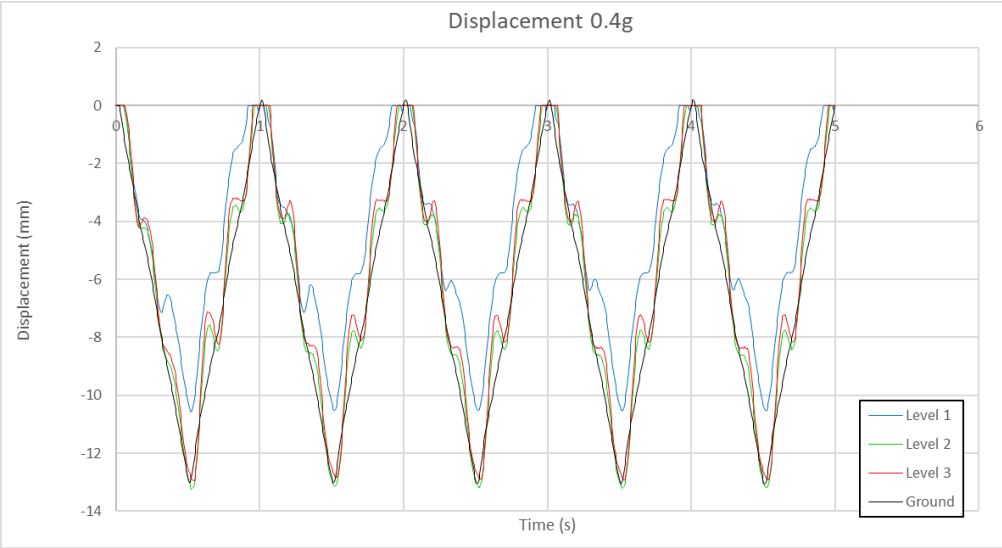

Figure A-10: Displacement of Model without Inverted V-braced Damper at PGA 0.4g.

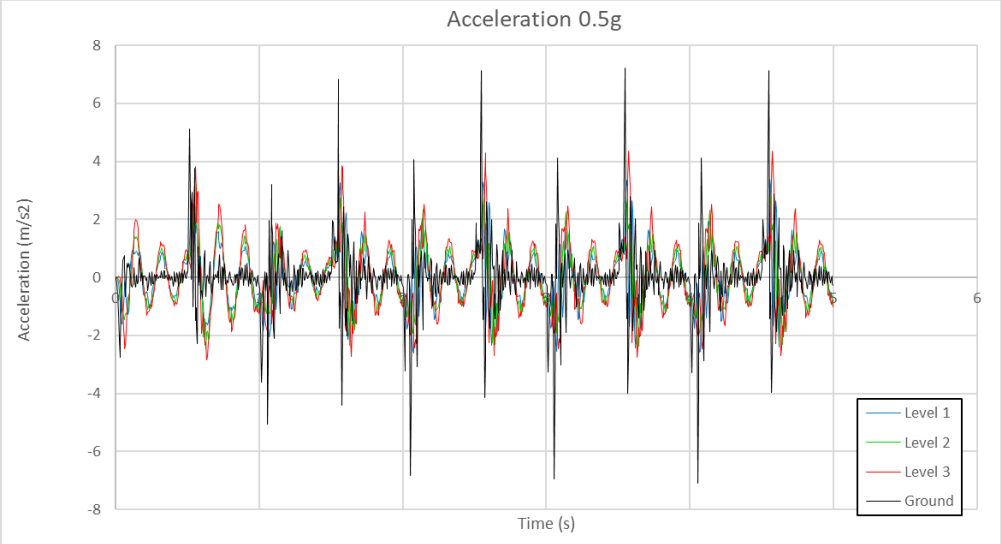

Figure A-11: Acceleration of Model without Inverted V-braced Damper at PGA 0.5g.

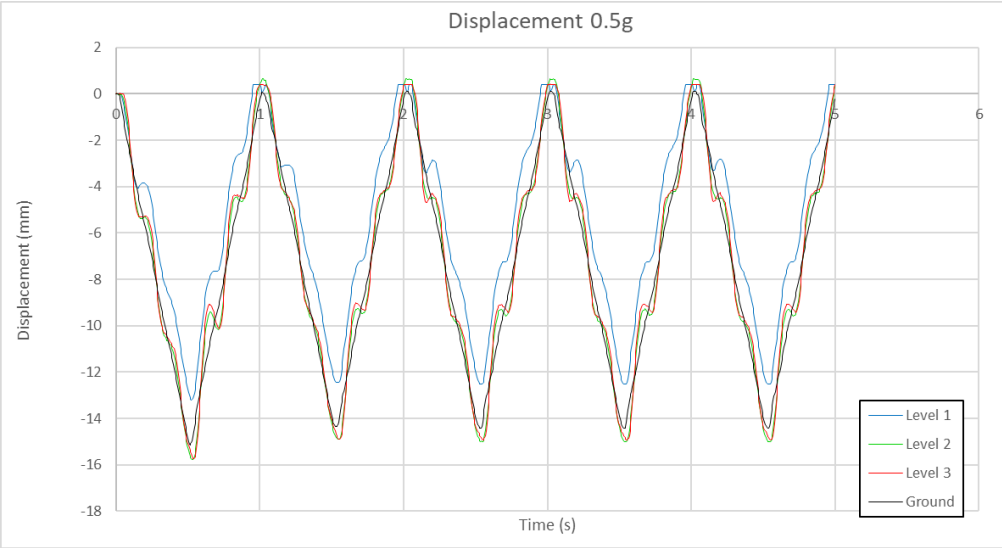

Figure A-12: Displacement of Model without Inverted V-braced Damper at PGA 0.5g.

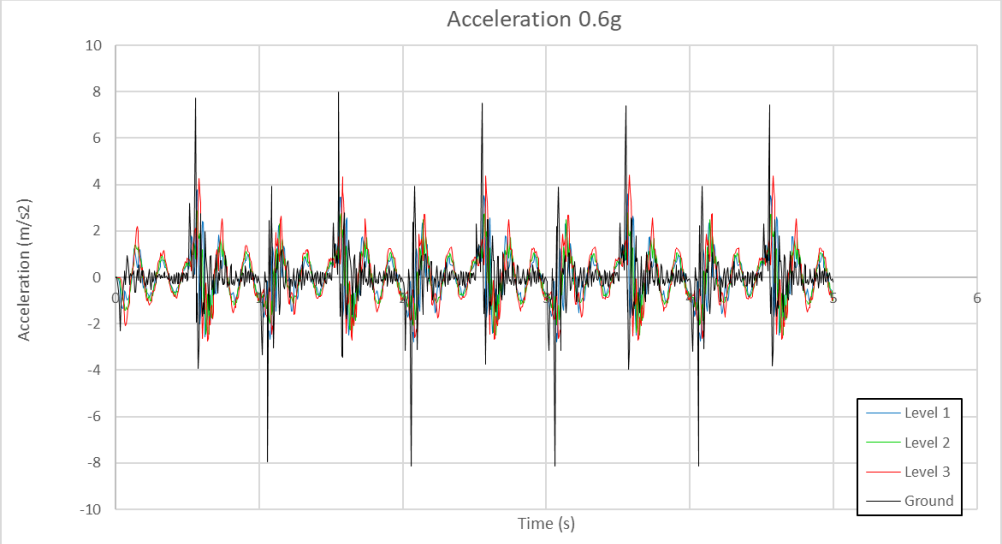

Figure A-13: Acceleration of Model without Inverted V-braced Damper at PGA 0.6g.

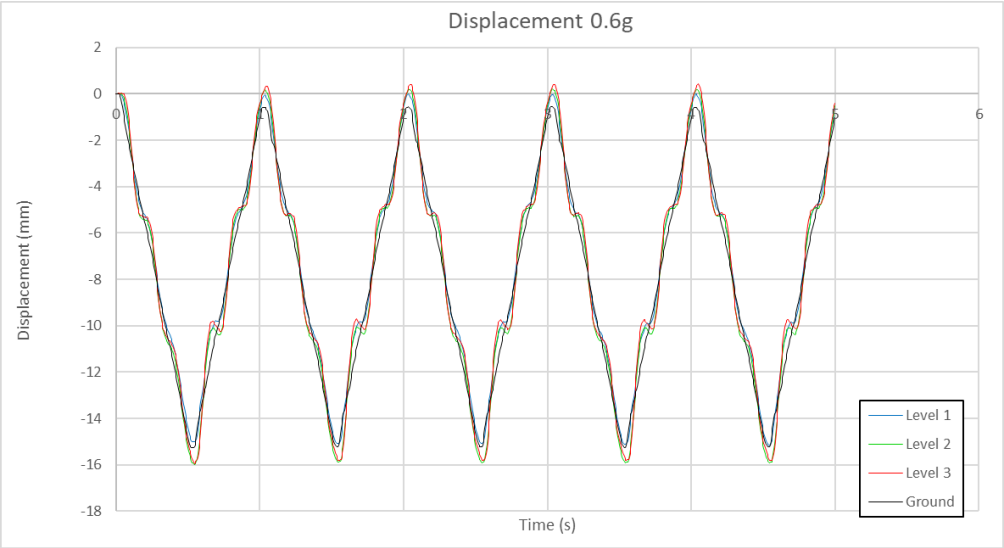

Figure A-14: Displacement of Model without Inverted V-braced Damper at PGA 0.6g.

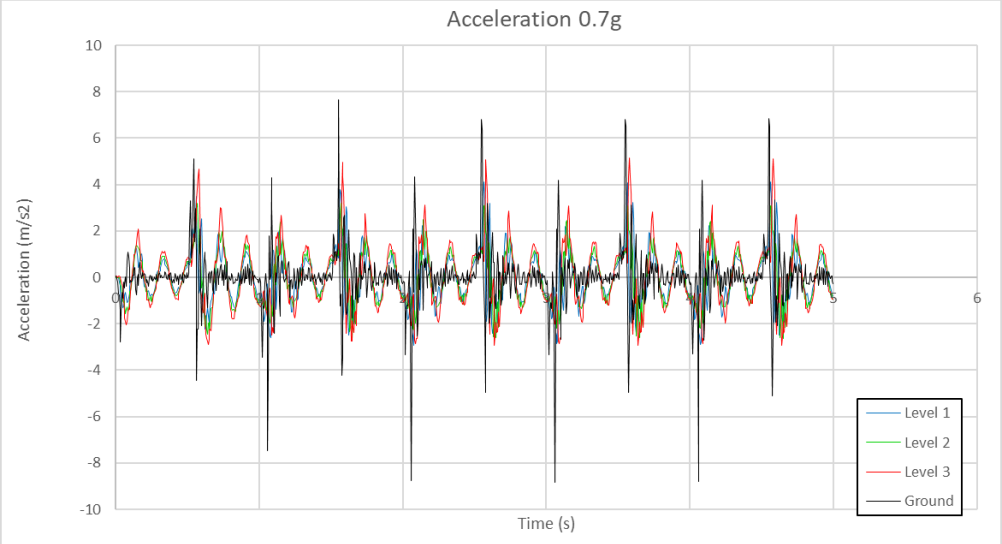

Figure A-15: Acceleration of Model without Inverted V-braced Damper at PGA 0.7g.

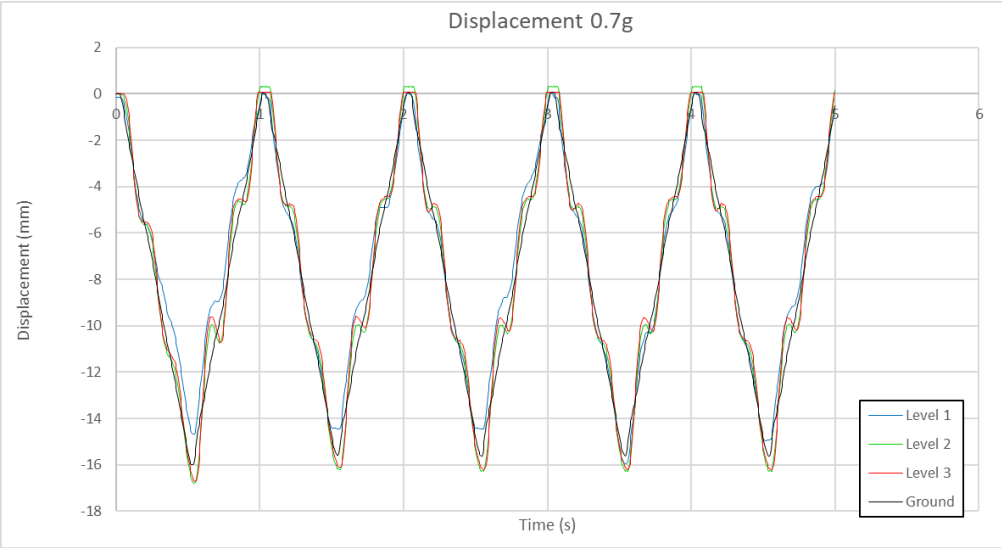

Figure A-16: Displacement of Model without Inverted V-braced Damper at PGA 0.7g.

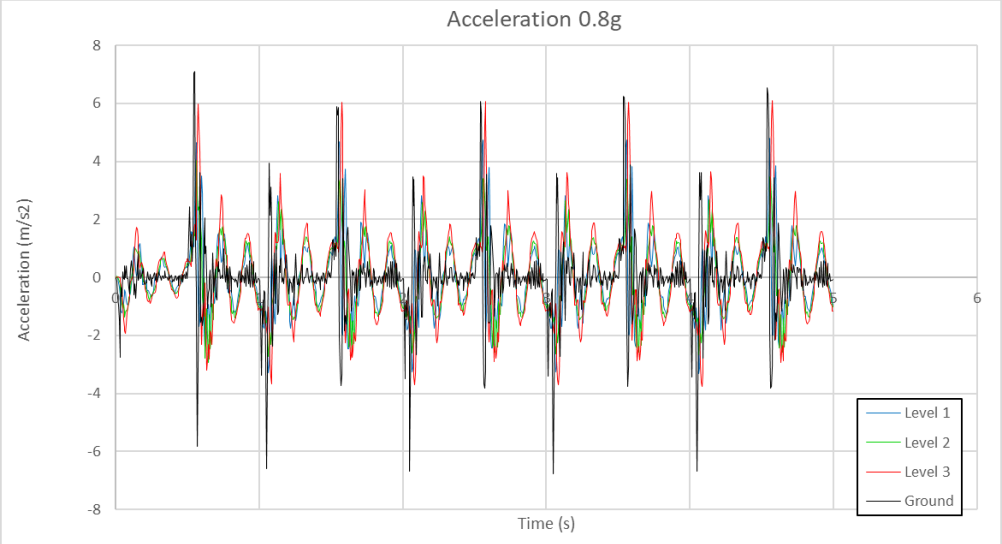

Figure A-17: Acceleration of Model without Inverted V-braced Damper at PGA 0.8g.

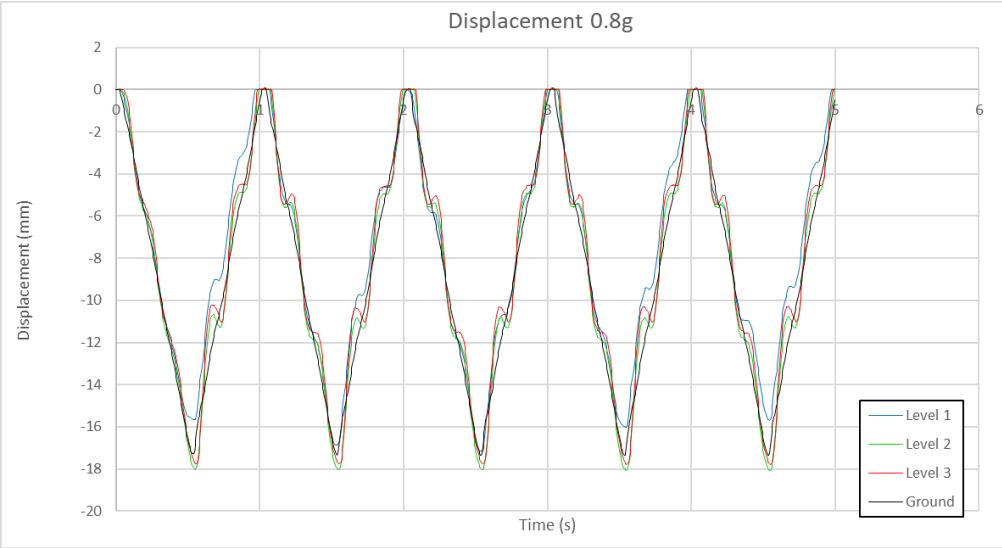

Figure A-18: Displacement of Model without Inverted V-braced Damper at PGA 0.8g.

5

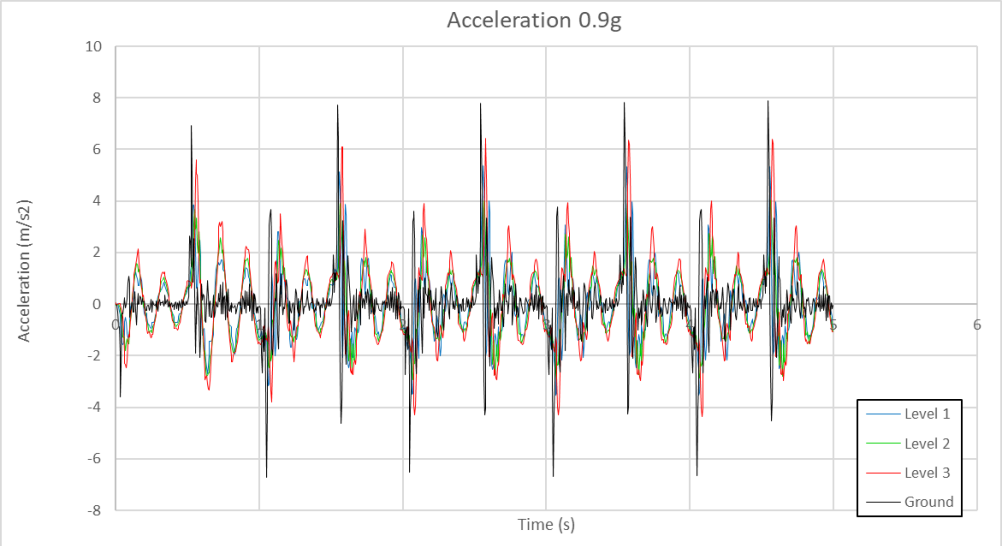

Figure A-19: Acceleration of Model without Inverted V-braced Damper at PGA 0.9g.

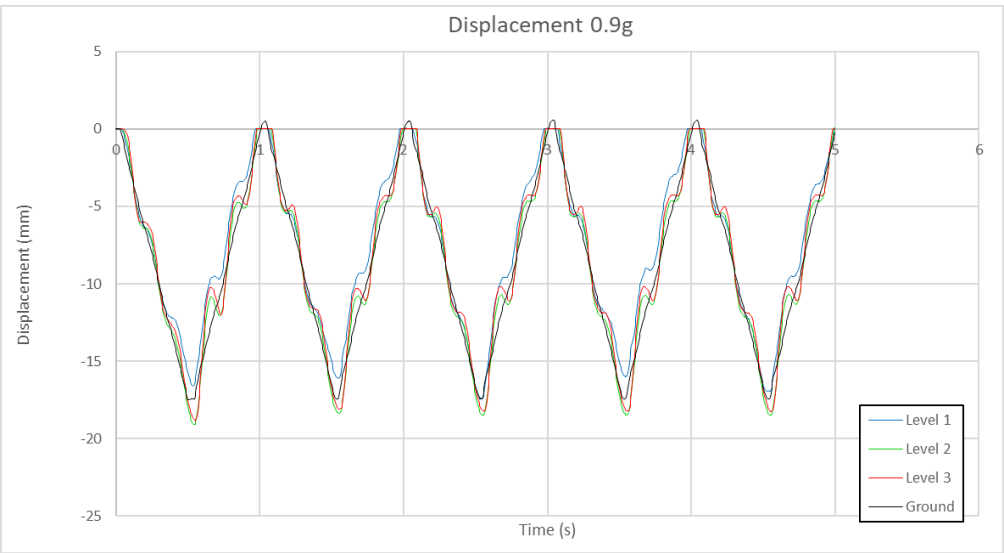

Figure A-20: Displacement of Model without Inverted V-braced Damper at PGA 0.9g.

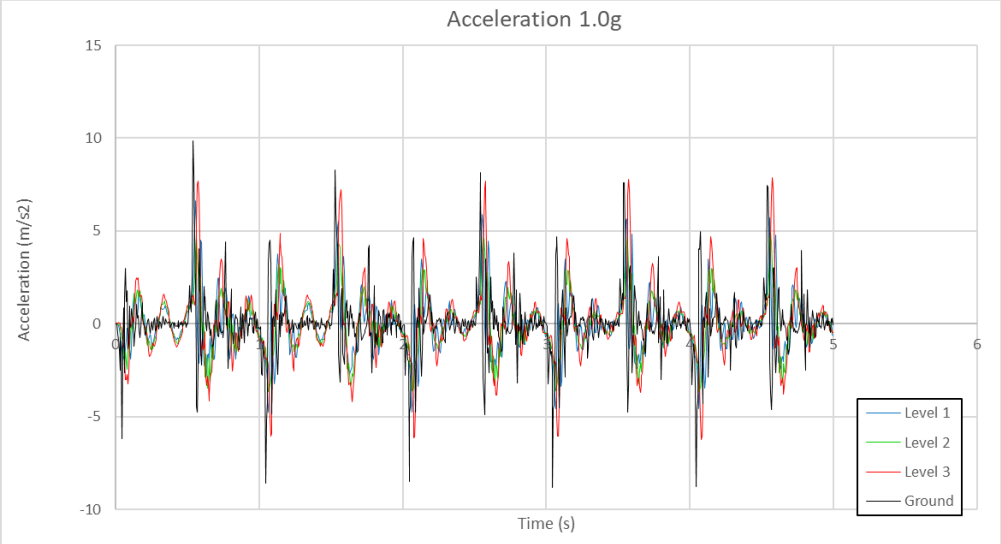

Figure A-21: Acceleration of Model without Inverted V-braced Damper at PGA 1.0g.

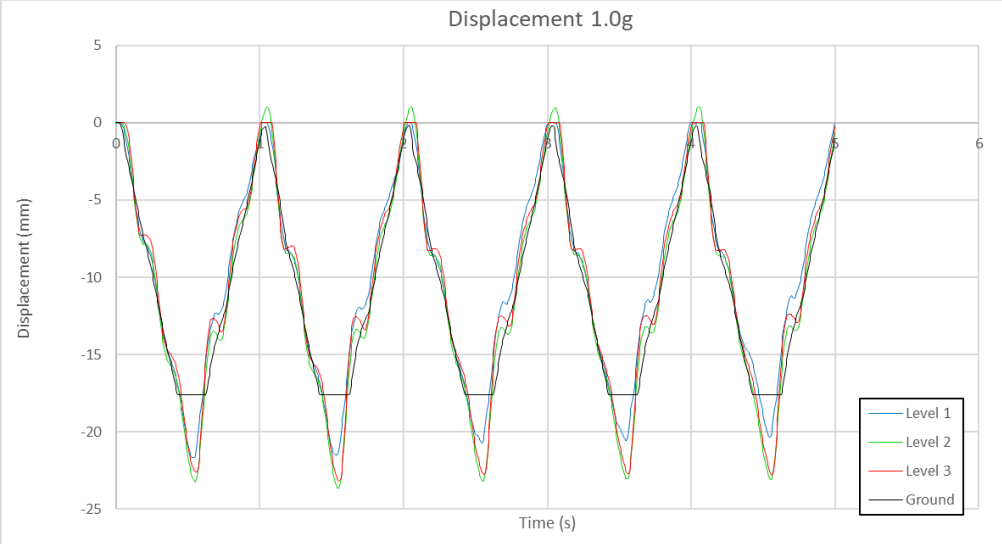

Figure A-22: Displacement of Model without Inverted V-braced Damper at PGA 1.0g.

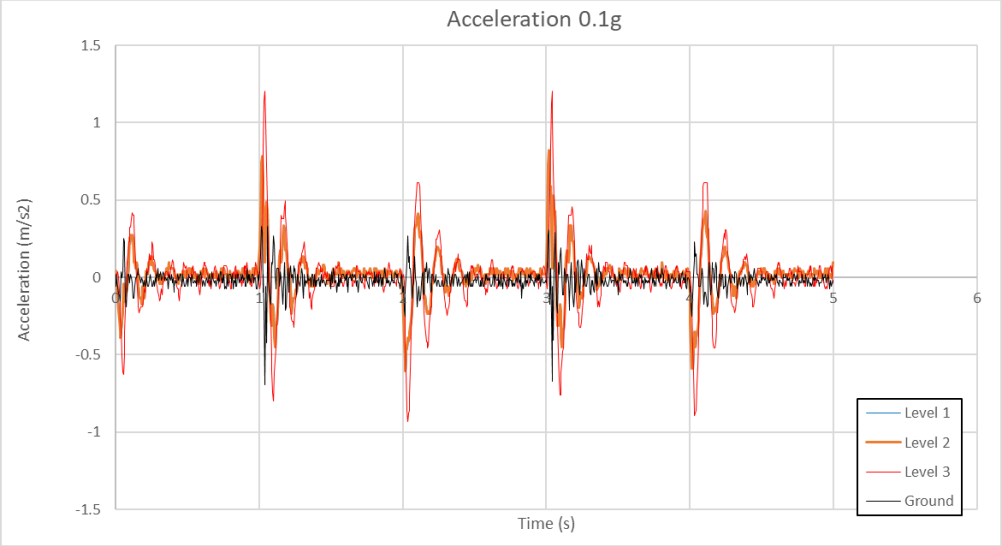

Figure A-23: Acceleration of Model with Inverted V-braced Damper at PGA 0.1g.

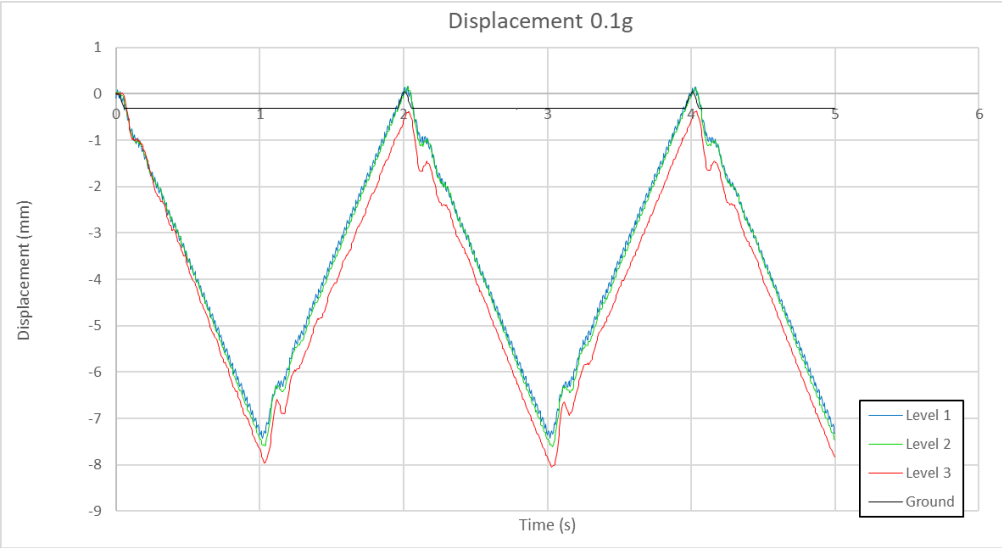

Figure A-24: Displacement of Model with Inverted V-braced Damper at PGA 0.1g.

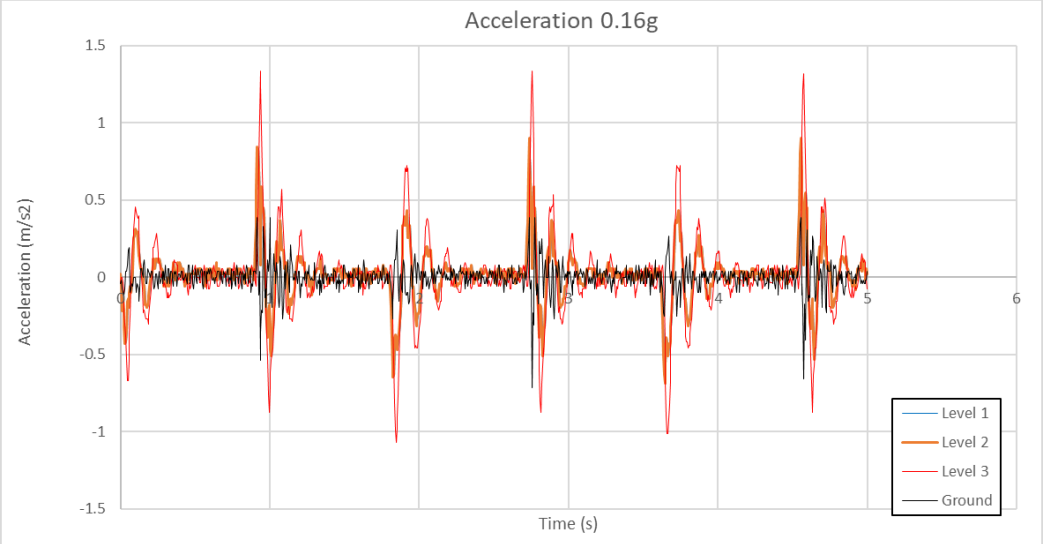

Figure A-25: Acceleration of Model with Inverted V-braced Damper at PGA 0.16g.

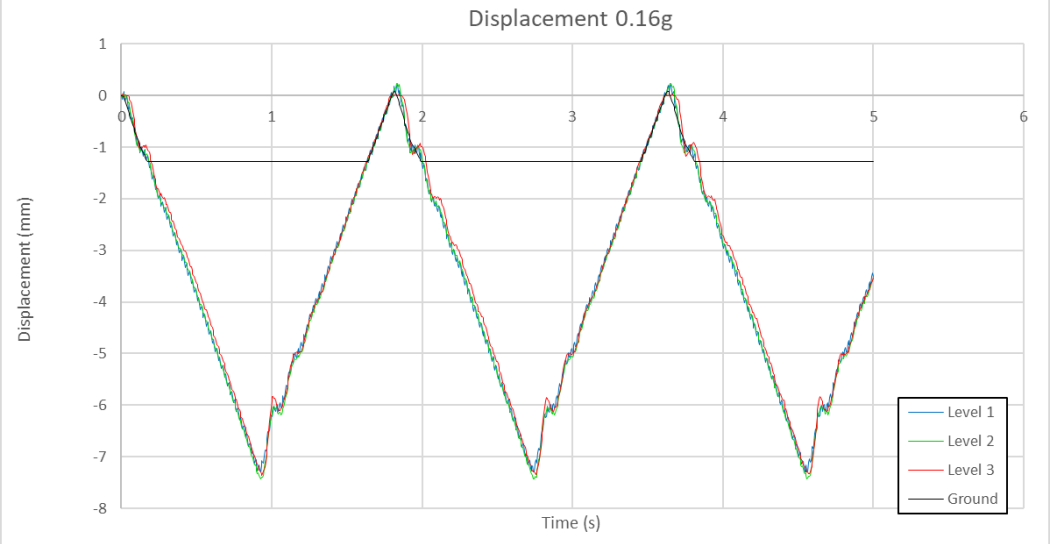

Figure A-26: Displacement of Model with Inverted V-braced Damper at PGA 0.16g.

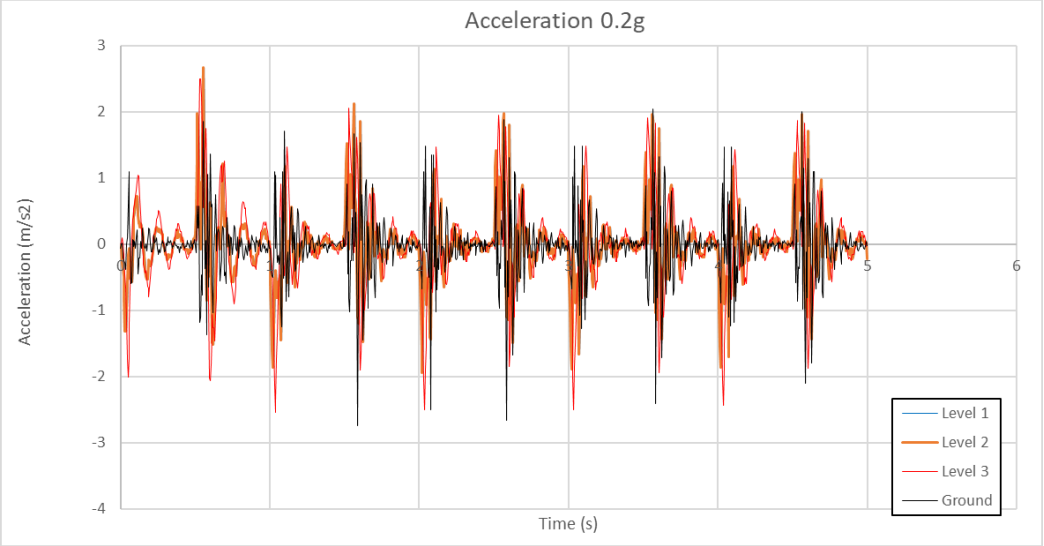

Figure A-27: Acceleration of Model with Inverted V-braced Damper at PGA 0.2g.

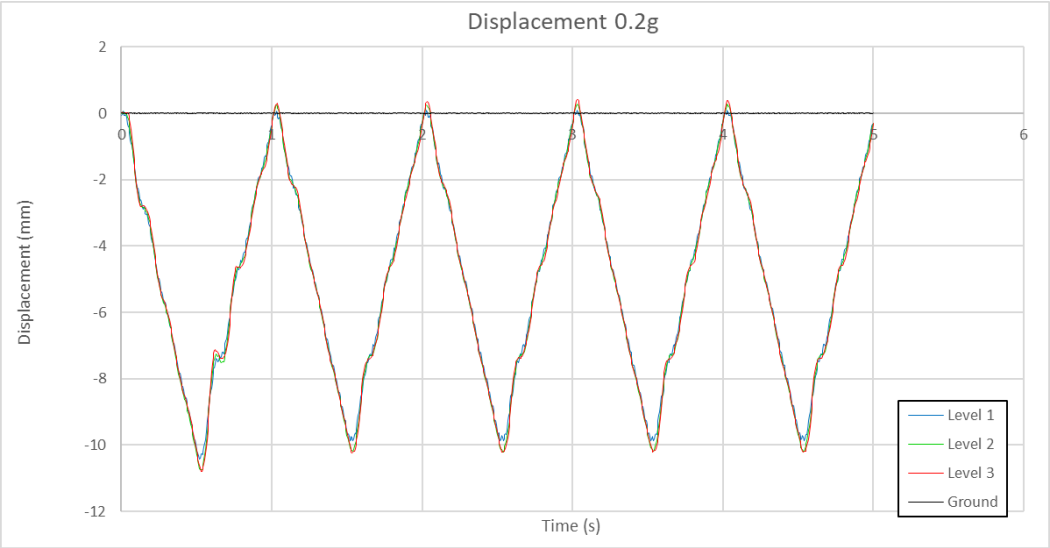

Figure A-28: Displacement of Model with Inverted V-braced Damper at PGA 0.2g.

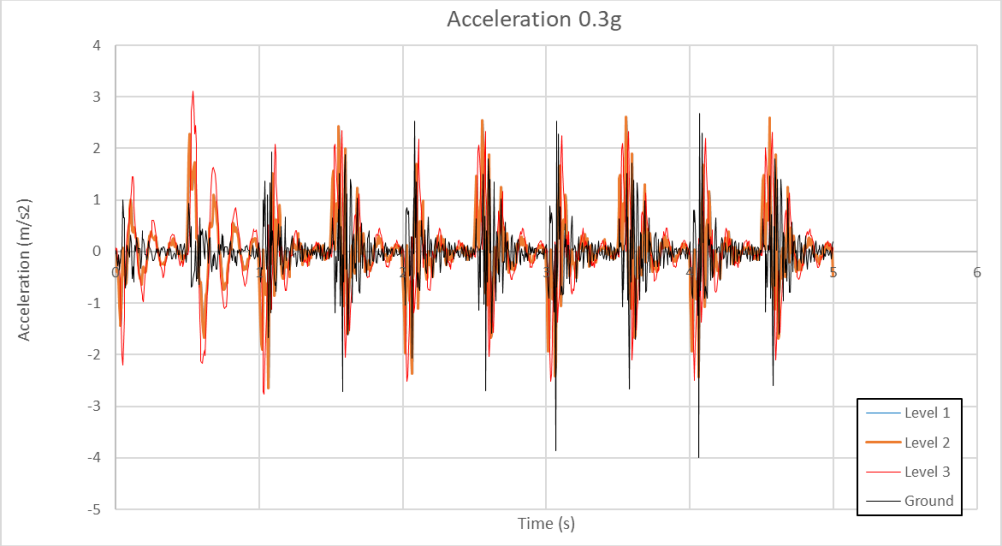

Figure A-29: Acceleration of Model with Inverted V-braced Damper at PGA 0.3g.

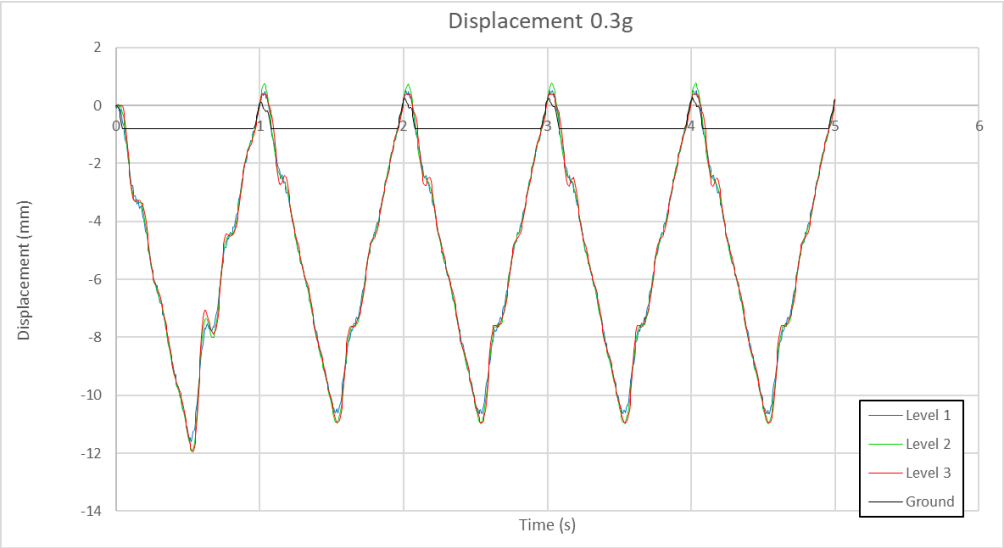

Figure A-30: Displacement of Model with Inverted V-braced Damper at PGA 0.3g.

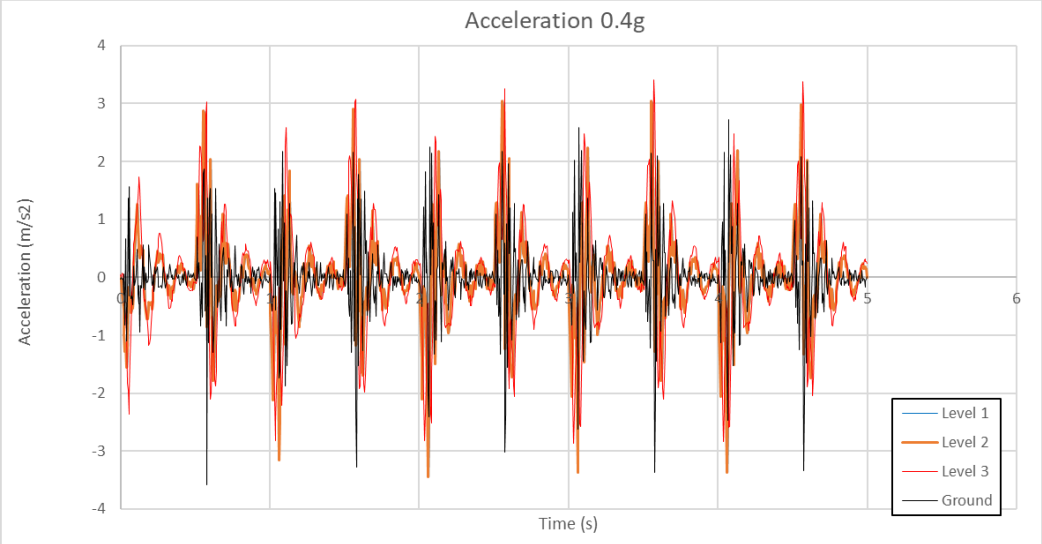

Figure A-31: Acceleration of Model with Inverted V-braced Damper at PGA 0.4g.

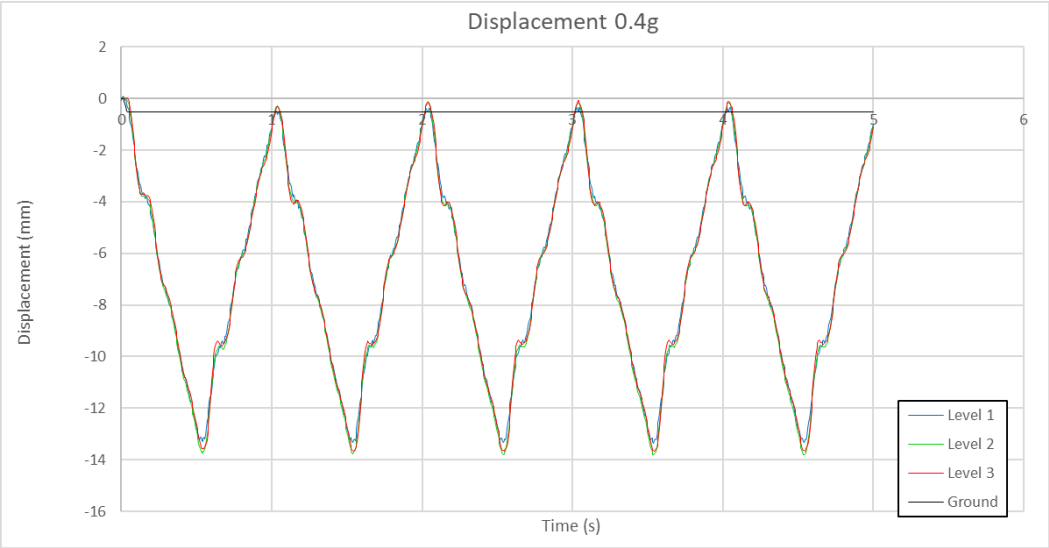

Figure A-32: Displacement of Model with Inverted V-braced Damper at PGA 0.4g.

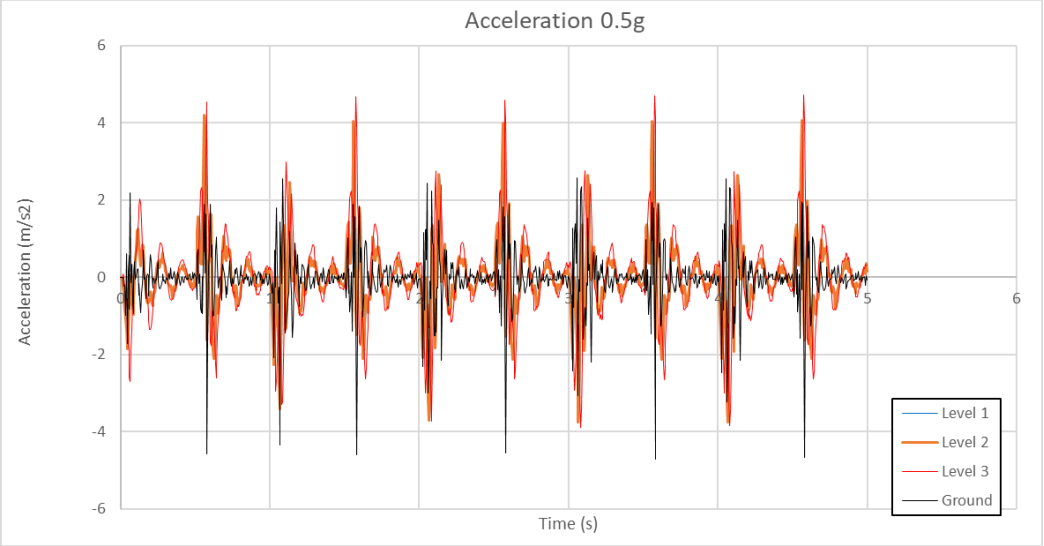

Figure A-33: Acceleration of Model with Inverted V-braced Damper at PGA 0.5g.

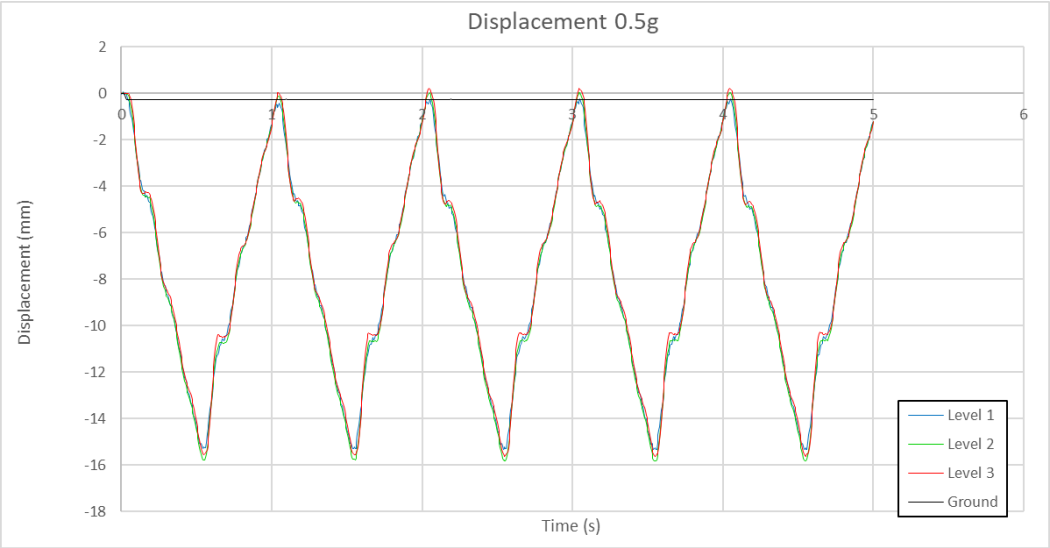

Figure A-34: Displacement of Model with Inverted V-braced Damper at PGA 0.5g.

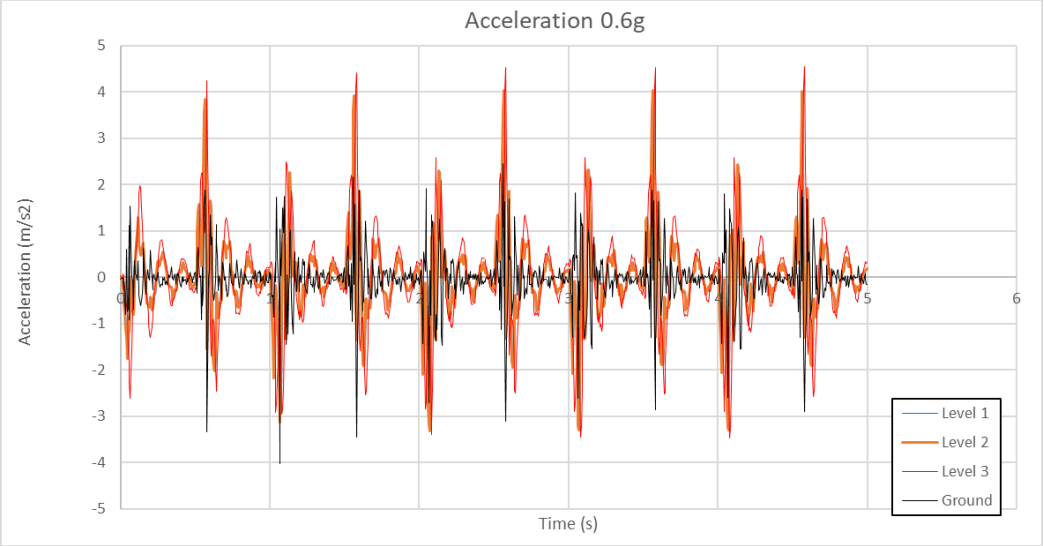

Figure A-35: Acceleration of Model with Inverted V-braced Damper at PGA 0.6g.

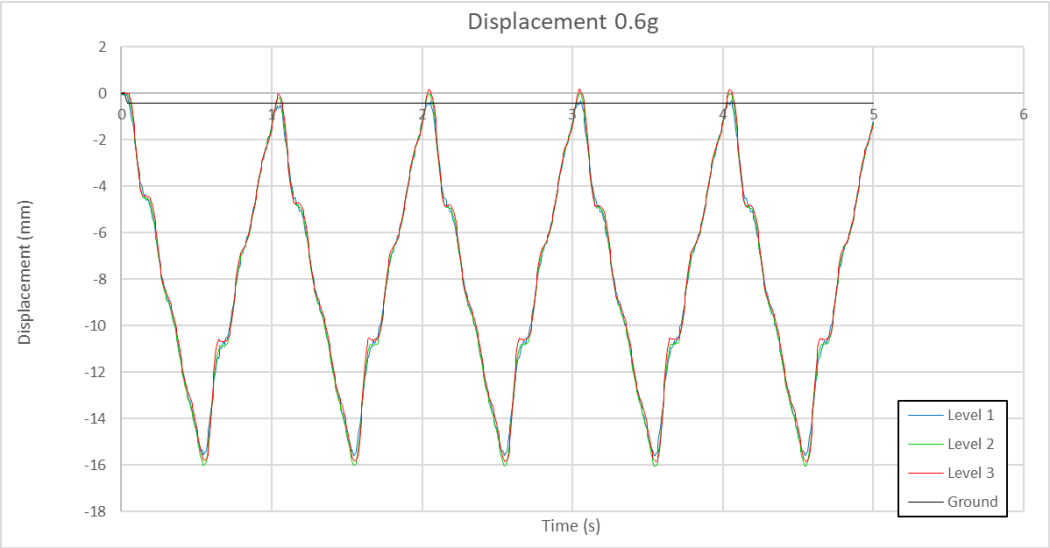

Figure A-36: Displacement of Model with Inverted V-braced Damper at PGA 0.6g.

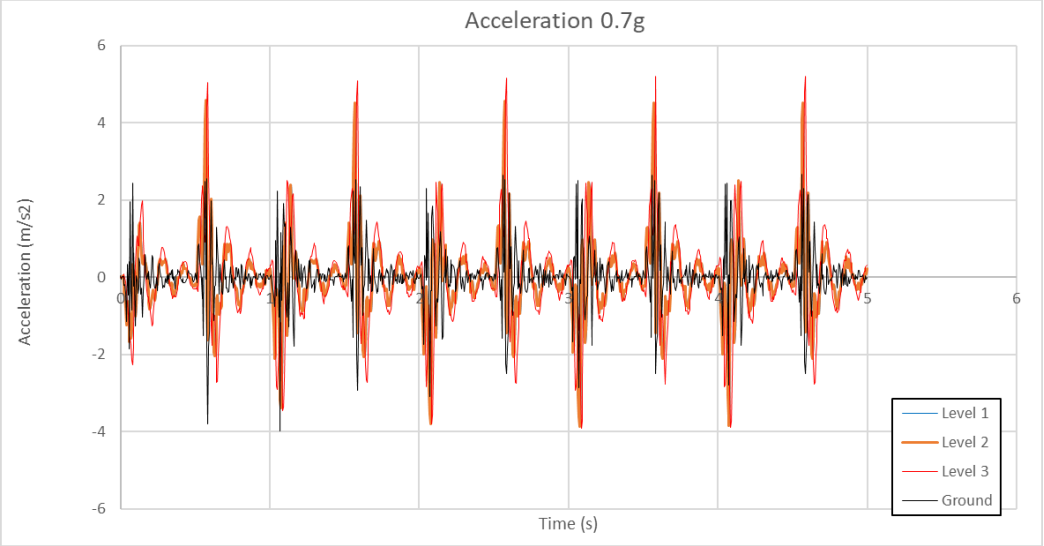

Figure A-37: Acceleration of Model with Inverted V-braced Damper at PGA 0.7g.

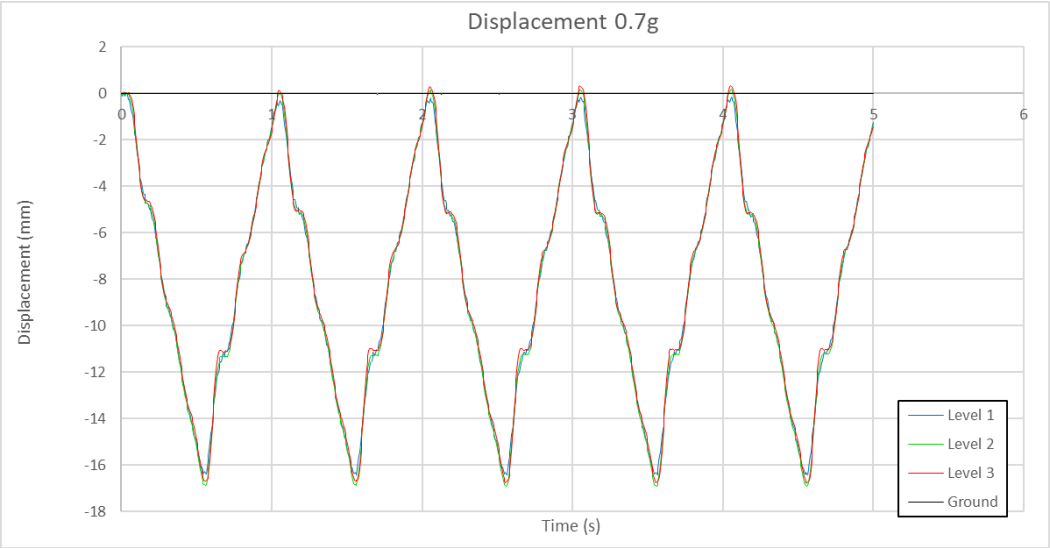

Figure A-38: Displacement of Model with Inverted V-braced Damper at PGA 0.7g.

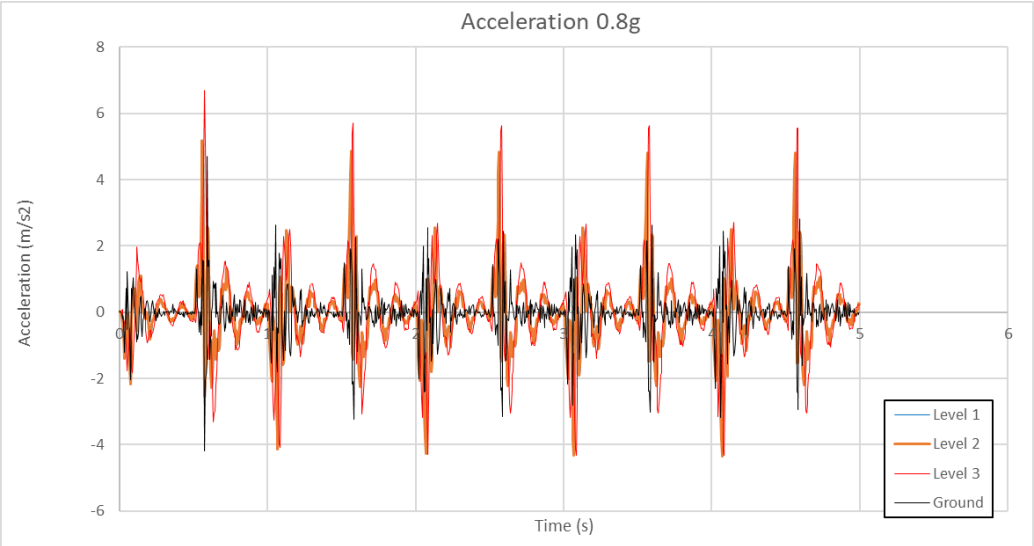

Figure A-39: Acceleration of Model with Inverted V-braced Damper at PGA 0.8g.

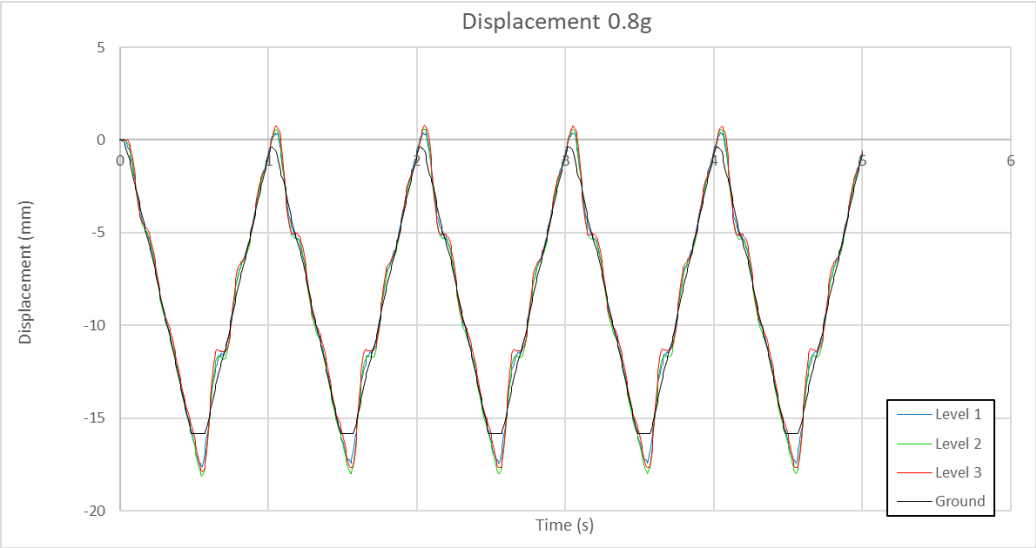

Figure A-40: Displacement of Model with Inverted V-braced Damper at PGA 0.8g.

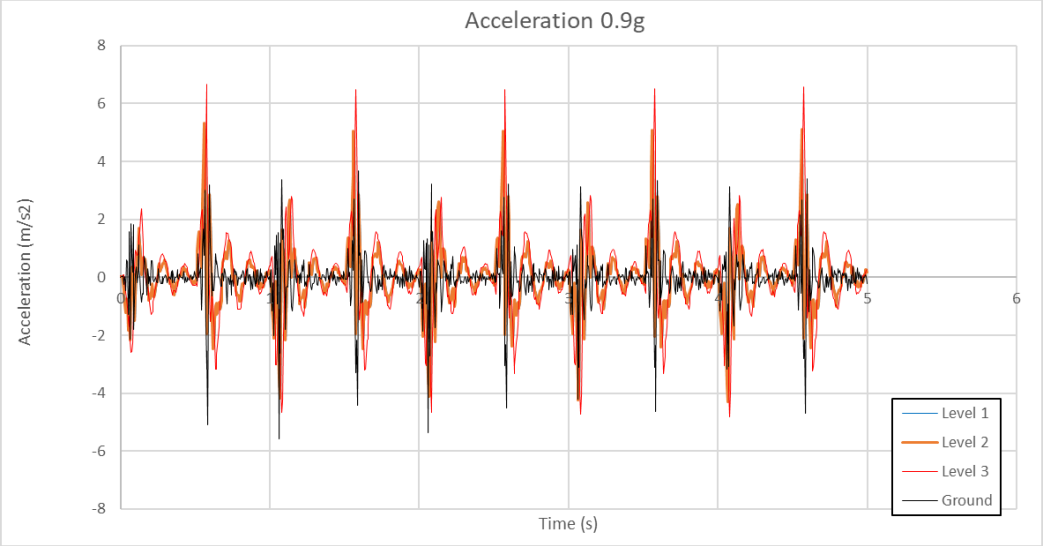

Figure A-41: Acceleration of Model with Inverted V-braced Damper at PGA 0.9g.

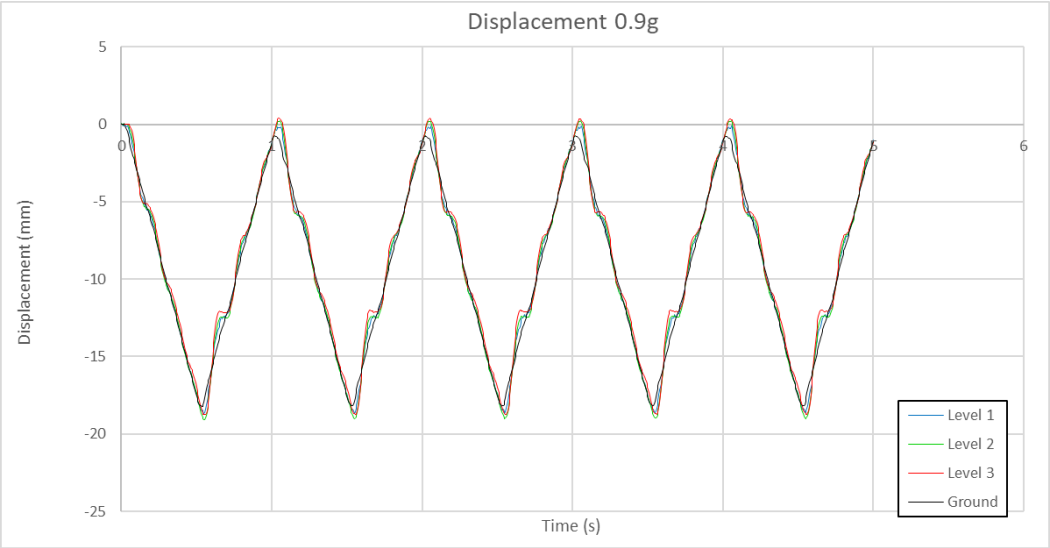

Figure A-42: Displacement of Model with Inverted V-braced Damper at PGA 0.9g.

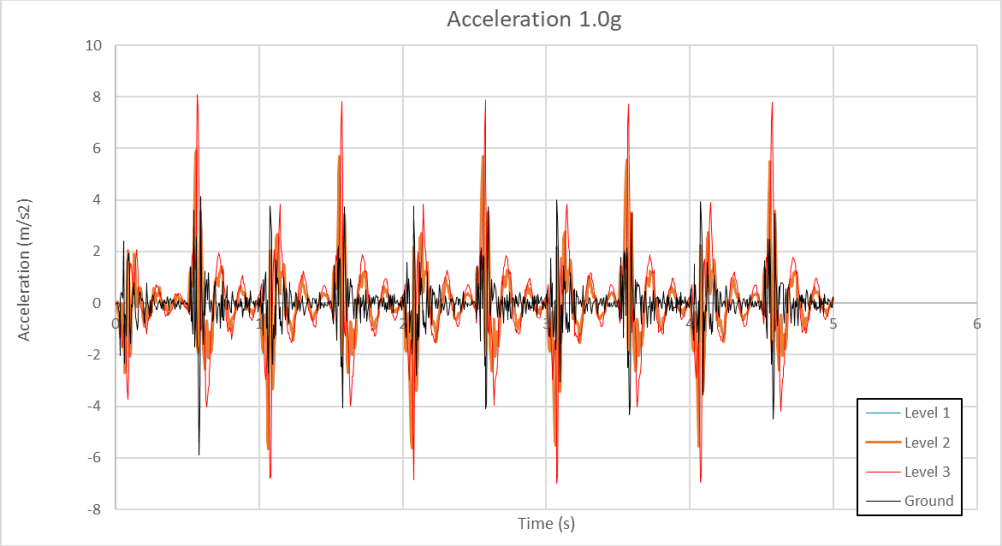

Figure A-43: Acceleration of Model with Inverted V-braced Damper at PGA 1.0g.

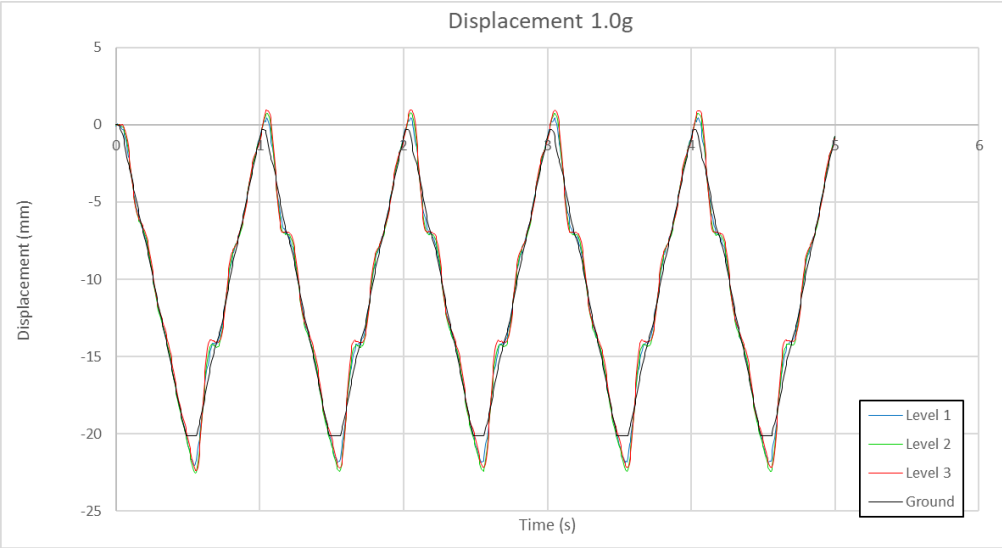

Figure A-44: Displacement of Model with Inverted V-braced Damper at PGA 1.0g.

APPENDIX B: Tables

Appendix B1: Compressive Strength of Cylinder Specimens in 7 days

	Compressive Strength (MPa)			
Floor	Cylinder A	Cylinder B	Cylinder C	Average
1st Storey	29.64	30.33	25.78	28.58
2nd Storey	30.72	32.29	24.85	29.29
3rd Storey	29.68	30.47	25.38	28.51